Fall 2019

Studies on the Mechanism and Application of Steam Thermography

Raymond Gerard Belliveau III

STUDIES ON THE MECHANISM AND APPLICATION OF STEAM THERMOGRAPHY

By

Raymond Gerard Belliveau III

Bachelor of Science
University of South Carolina – Aiken, 2012

Submitted in Partial Fulfillment of the Requirements

for the Degree of Doctor of Philosophy in

Chemistry

College of Arts and Sciences

University of South Carolina

2019

Accepted by:

Michael L. Myrick, Major Professor

Stephen L. Morgan, Chairman, Examining Committee

John L. Ferry, Committee Member

Jamil A. Khan, Committee Member

Cheryl L. Addy, Vice Provost and Dean of the Graduate School

ACKNOWLEDGEMENTS

There are a number of people who have been influential to my career as a chemist that I would like to acknowledge. Back in undergrad, Dr. Monty Fetterolf gave me my first real shot doing research. The first time we opened a monochromator, it impressed on me a love for instrumentation that has persisted to this day. Dr. Nandeo Choony was kind enough to let me assist him in the teaching lab, beginning a love for teaching that has also persisted (for better or worse). After undergrad, I worked under Jim Dewey, who taught me how to get my hands dirty taking apart and fixing mass spectrometers. Working in that GC-MS lab, I gained an important appreciation for the distinction between a Bachelor's degree and a PhD for a young chemist in modern times.

So, I set off for grad school. I could not have known then what I was in for throughout my graduate career, but I was lucky enough to find in Dr. Michael Myrick someone that would give me an environment to succeed despite so many things in my life that tried to prevent that. I truly believe I would not be writing the acknowledgements to my dissertation if I had had anyone else as a research advisor. I cannot overstate my gratitude to him for giving me the singular constant in my life for the past several years.

I would like to thank my peers in the Myrick lab, especially Cameron Rekully and Stefan Faulkner for all the intellectually stimulating debates such as 'Is a hot dog a sandwich?' My thanks go to Stephanie DeJong and Shawna Tazik for the tons of

practical grad student advice. And to Caitlyn English for reminding me how much we grow in our time as graduate students.

Lastly, I will acknowledge my parents, Joyce and Raymond, for some very hard lessons that shaped me into a person that cannot accept a failure to change the world around me.

ABSTRACT

The detection of blood on fabrics for forensic purposes is a widely studied topic in forensic science, and to that end, effort in this laboratory has been devoted to developing a thermal imaging method called steam thermography. Steam thermography is a method used to enhance chemical contrast in thermographic images by exposing a surface to water vapor during imaging. The exposure of water vapor to the surface generates heat, and can differentially increase the thermographically measured apparent temperature of imaged surfaces. This can result in thermographic contrast between surfaces with different chemical properties. Previously reported proposed mechanisms to describe the chemical contrast enhancement of dried blood stains on fabric during a steam thermography measurement include a radiant heat transfer which warms the blood and fabric differentially, a convective transfer of heat from the water vapor to the blood stains and fabric which result in a differential heating, the deposition of condensed airborne water droplets which results in a differential change in apparent temperature, a differential condensation of liquid water on the sample surface, a change in thermal emissivities of the bloodstain and fabric such that the difference in the emissive power of the surfaces increases, and lastly, a differential adsorption of the water vapor. The studies reported in this manuscript address the potential mechanisms of the enhanced chemical contrast observed during a steam thermography measurement, and in doing so provide evidence that the adsorption of water vapor is the primary (and in specifically designed

experiments, the only) mechanism of the enhancement. Thermographic contrast enhancement for dried blood on acrylic, nylon, cotton, and polyester fabrics is demonstrated, along with measurements describing the change in emissivity as each of the fabrics and dried blood on acrylic fabric are exposed to varying amounts of humidity. The degree of contrast enhancement between dried blood stains on the above mentioned fabric substrates and the blank fabrics is also reported for the exposure of the samples to eight other solvent vapors during thermal imaging. Additionally, the effect to a steam thermography measurement of the silanization of a bloodstained cotton fabric using trimethylmethoxysilane is described.

TABLE OF CONTENTS

LIST OF TABLES

LIST OF FIGURES

CHAPTER 1: INTRODUCTION

This manuscript focuses on several studies on the mechanism of steam thermography, a thermographic imaging method used to create or enhance chemical contrast during imaging, and the application of the method. Beginning with the knowledge base discussed in this chapter, measurements are described in Chapters 2 to 5 that aim to understand the contributions of various potential mechanisms of the chemical contrast enhancement observed during a steam thermography measurement. Lastly, Chapter 6 documents the application of steam thermography for the detection of dried blood on fabrics.

The first chapter reviews information important to the understanding of infrared thermography. It also provides a mathematical treatment of the radiance a thermal imaging camera measures, how that measurement is processed into a data file, and how that data file is processed into a form useful for analysis. Samples used in the thermographic measurements in this work are discussed. An overview of the potential mechanisms of the chemical contrast enhancement during a steam thermography measurement is given, and last is an outline of Chapters 2 through 6.

1.1 Infrared Thermography: Theory

Infrared thermography is an imaging method that uses the detection of infrared light as a method of measuring the temperature of a surface. As an object warms, the spectral radiance, $L_{T,\lambda}^{BB}$, increases according to Planck's law:

$$L_{T,\lambda}^{BB} = \frac{2hc^2}{\lambda^5\left(e^{\frac{hc}{\lambda k_b T}} - 1\right)} \tag{1.1}$$

Where h is the Planck constant, c is the speed of light in a vacuum, T is the temperature of the object, λ is the wavelength of light, and k_b is the Boltzmann constant. This describes the radiance of a perfect blackbody (superscript BB), but for a real-body this would be modified by the spectral emissivity. The emissivity (ε) of a surface is a key factor in a thermography measurement, another being the reflectivity (r). For an optically dense surface, the two sum to unity. During a thermography measurement, these two factors determine the relative amounts of light measured due to the observed surface's thermal emission, and of light reflected from the surface. Only the fraction of the measured light emitted by the surface is directly related to the surface's temperature.

The radiation measured by the camera from a surface is modeled as coming from four distinct sources, shown in Figure 1.1. The first two sources are direct emission from the sample (path A) and window (path B) to the camera. The next two sources are reflections of room (or baffle) thermal emission back to the camera from the sample (path C) and from the window (path D). It is assumed that the angle dependence of the measured signal is negligible over the small angle subtended by the sample and reference areas used in the signal intensity averaging. It is further assumed that the room/baffle thermal radiation can be treated as a blackbody radiator at ambient temperature, and that the contribution of the air itself is negligible.

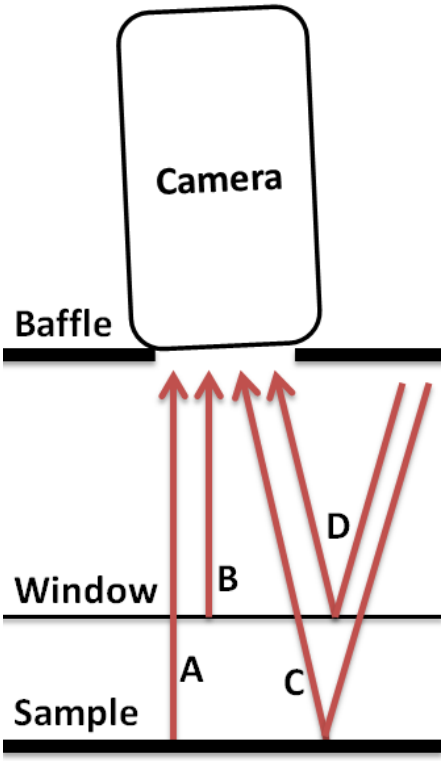

Figure 1.1. Diagram of the sources of signal intensity measured by the camera. A) Radiation emitted from the sample, which passes through the window before reaching the camera. B) Radiation emitted from the window that reaches the camera. C) Radiation emitted from the surrounding environment, which passes through the window, reflects off of the sample, passes through the window a second time, and then reaches the camera. D) Radiation emitted from the surrounding environment which is reflected off of the window, and reaches the camera. The camera itself is positioned slightly angled with respect to the sample surface in order to limit the specular reflection of the camera lens from being imaged directly over the measurement are of the sample.

While there are examples of the mathematical treatment of the sources of signal intensity in a thermographic measurement in literature, the specific case of the thermographic measurement of a surface in close proximity to an infrared window such that the reflectance of the sample-facing surface of the window is dominated by the sample emission has not been reported to date.[1,2] Therefore, in the following discussion, the spectral radiance reaching the camera along each path is discussed individually before combining and simplifying.

The radiation from the sample along path A is subject to a series of reflections from the window, back to the sample/reference, and then back to the window. This radiance from the surface emission and the series of multiple reflections at temperature T_s, and at each wavelength λ (spectral radiance) is given by:

$$L^{A}_{T_s,\lambda} = \frac{\varepsilon_{s,\lambda}\tau_{w,\lambda}L^{BB}_{T_s,\lambda}}{1 - r_{w,\lambda}r_{s,\lambda}} \tag{1.2}$$

Where $\varepsilon_{s,\lambda}$ is the emissivity of the imaged surface at wavelength λ, $\tau_{w,\lambda}$ is the transmittivity of a window at wavelength λ, $L^{BB}_{T_s,\lambda}$ is the spectral radiance at wavelength λ for a perfect blackbody radiator at the temperature of the imaged surface T_s, $r_{w,\lambda}$ is the spectral reflectivity of the window at wavelength λ, and $r_{s,\lambda}$is the spectral reflectivity of the imaged surface at wavelength λ. The reflection terms in the denominator account for multiple reflections, and are a small correction to the overall radiance (on the order of 1%). The $r_{s,\lambda}$value is taken as the reflectivity of the imaged surface in general. For specific cases it may be taken as the reflectivity of the sample or of the reference material even though some light from the sample will reflect from the reference material and vice versa.

The second source (path B in Figure 1.1) is radiance of the window material directly into the camera along with the series of multiple reflections from the window emission reflecting from the sample surface back to the window, and is given by:

$$L^{B}_{T_a,\lambda} = \varepsilon_{w,\lambda}L^{BB}_{T_a,\lambda}\left(\frac{1 - r_{w,\lambda}r_{s,\lambda} + r_{s,\lambda}\tau_{w,\lambda}}{1 - r_{w,\lambda}r_{s,\lambda}}\right) \tag{1.3}$$

Where $\varepsilon_{w,\lambda}$ is the emissivity of the window at wavelength λ, and $L_{T_a,\lambda}^{BB}$ is the spectral radiance at wavelength λ for a perfect blackbody radiator at ambient room temperature T_a. For the purposes of this calculation, the window temperature is approximated to be the same temperature as the room. This approximation is made because the temperature of the window material does not strongly influence our measurements due to its low absorption (*vide infra*) through the part of the thermal IR seen by the camera.

The third source (path C in Figure 1.1) is due to thermal radiance from the surroundings that passes through the window, reflects from the sample, and then either passes through the window a second time or continues to reflect from the window to the sample surface again before reaching the camera or being absorbed. The radiance observed by the camera due to these reflections is given by:

$$L_{T_a,\lambda}^{C} = \frac{\tau_{w,\lambda}{}^2 r_{s,\lambda} L_{T_a,\lambda}^{BB}}{1 - r_{w,\lambda} r_{s,\lambda}} \tag{1.4}$$

The reflectivity of a sample is never less than a few percent. Care is taken to ensure that the temperature of the surroundings is made as uniform as possible by the addition of a baffle and an intentional tilt of the thermal camera so that emission from the experimentalist, or the warm camera body, or other heated elements in the laboratory do not affect the measurements directly.

The fourth source of radiance is the reflection of the radiance of the surroundings from the window directly back to the camera (path D), and this signal intensity is given by:

$$L^{D}_{T_a,\lambda} = r_{w,\lambda} L^{BB}_{T_a,\lambda} \tag{1.5}$$

This reflection is specular, so objects in the surroundings at a different temperature could be imaged by the camera via this reflection. The camera lens itself is an object that can appear in the images by this mechanism because it peers at the sample through an aperture in the baffle; to avoid this sharp feature in thermographic images, the region of interest in the sample selected for measurement is chosen in a part of the sample where only the featureless baffle's direct reflection is visible.

The total spectral radiance ($L^{Tot}_{T_s,\lambda}$) reaching the camera for an imaged surface at a temperature T_s is the sum of the spectral radiance terms in Equations 1.2-1.5 above. $L^{Tot}_{T_s,\lambda}$ can be simplified and written as:

$$L^{Tot}_{T_s,\lambda} = \frac{\varepsilon_{s,\lambda}\tau_{w,\lambda}}{1 - r_{w,\lambda}r_{s,\lambda}} L^{BB}_{T_s,\lambda} + \left[1 - \frac{\varepsilon_{s,\lambda}\tau_{w,\lambda}}{1 - r_{w,\lambda}r_{s,\lambda}}\right] L^{BB}_{T_a,\lambda} \tag{1.6}$$

Integrals involving the spectral radiance will be required in the following steps, and in most cases we do not have quantitative estimates of the spectral reflectivity, emissivity or transmittivity parameters. We resort in this case to a graybody approximation – that the values are independent of wavelength over the "narrow" range of wavelengths observed by the thermal camera.[1] Under this assumption, the subscript λ values can be removed from many of the quantities:

$$L^{Tot}_{T_s,\lambda} = \frac{\varepsilon_s\tau_w}{1 - r_w r_s} L^{BB}_{T_s,\lambda} + \left[1 - \frac{\varepsilon_s\tau_w}{1 - r_w r_s}\right] L^{BB}_{T_a,\lambda} \tag{1.7}$$

The signal intensity reported by the camera is related to the radiance by the spectral responsivity of the camera (R_λ) plus an offset factor (C), where C represents the value that the camera would measure for an imaged surface at absolute zero. This relationship is given in equation 1.8:

$$I_{T_s,w}^{Tot} = \int_{\lambda_0}^{\lambda_\infty} L_{T_s,\lambda}^{Tot} R_\lambda + C \qquad (1.8)$$

Where $I_{T_s,w}^{Tot}$ is the measured total signal intensity for the imaged surface (superscript Tot) at the temperature of the imaged surface (subscript T_s) viewed through a window (subscript w). The total signal intensity reported by the camera while viewing a surface through the window is then given as:

$$I_{T_s,w}^{Tot} = \frac{\varepsilon_s \tau_w}{1 - r_w r_s} \int_{\lambda_0}^{\lambda_\infty} L_{T_s,\lambda}^{BB} R_\lambda \, d\lambda + \left[1 - \frac{\varepsilon_s \tau_w}{1 - r_w r_s}\right] \int_{\lambda_0}^{\lambda_\infty} L_{T_a,\lambda}^{BB} R_\lambda \, d\lambda + C \qquad (1.9)$$

Equation 1.9 describes the signal detected in every measurement made in this work by an infrared camera. In cases where no window is used, the equation is simplified, as τ_w would then equal 1 and r_w would equal 0. In the case of a perfect blackbody, the equation is similarly simplified, as ε_s would equal 1 and r_s would equal 0.

An object, black or 'real', will emit more light at all wavelengths at increasing temperatures. The peak wavelength (λ_{max}) of light emitted by an object at temperature T is given by Wein's displacement Law:

$$\lambda_{max} = \frac{b}{T} \qquad (1.10)$$

Where b is Wien's displacement constant. The peak wavelength for objects near ambient temperatures is approximately 10 μm.

1.2 Infrared Thermography: Methodology

An infrared thermographic measurement produces a thermogram – an image formed from thermal radiation incident on a detector. This can be produced by either a single detector scanning a scene to make an image from a series of measurements, or by an array of detectors making a measurement simultaneously. This array is called a focal plane array (FPA).[3] A common FPA-based thermal camera detector, and the detector type used in the cameras in this work, is the microbolometer.

The thermal imaging cameras used in this work are of the microbolometer FPA-type, which detect light in the long-wave infrared (LWIR) window, 8-12 μm. Microbolometer cameras use an uncooled array of micro-resistors which exhibit a change in electrical resistance when the detector material is heated by incident infrared radiation. This change in electrical resistance is measured as a change in the voltage of a current running through the resistor. This is then converted into a digital signal referred to in this manuscript as the signal intensity. By default, most thermal imagers then convert that signal into a temperature. This conversion is based on an assumed surface graybody emissivity, and consequently also based on the graybody reflectivity of the surface.[3] In this work, measurements are recorded as the digital signal intensity, without any temperature conversion. This data is saved into a binary (.bin) file, uncompressed, using an interface developed in-house in the LabVIEW 2013 programming environment (National Instruments, Austin, TX). Each binary file is processed into a three dimensional array with dimensions X and Y corresponding to the array of pixel intensities, and the Z

dimension corresponding to the order of the frames in time using MATLAB R2012b (The MathWorks, Inc., Natick, MA). Unless otherwise stated, each recording reported in this manuscript is performed at 30 frames per second. The Matlab program used for this processing step is called 'binarymovie' and can be found in Appendix A.

A signal intensity-temperature calibration was performed for this camera in December 2015 across a range of temperatures from 30 °C to 50 °C referenced against a blackbody calibration standard (Optronics Laboratories, Orlando, Fl, model OL 480). The data was fit using a linear regression (R^2 = 0.9996), with a slope of 227.54±1.44 intensity units per degree Celsius, and a y-intercept of 12674±58.4 intensity units.

1.3 Sample Fabrics

The work reported in this manuscript consists of measurements on four fabrics: a purple acrylic, a brown polyester, a green nylon, and a red cotton fabric. The fabrics used in this study have been the subject of several publications by this laboratory, and information about properties the fabrics and the fibers they are composed of are consolidated here in Table 1.1, including the dyes used for each fabric, along with references to publications in which a number of spectroscopic measurements on each fabric are reported by this research group.[4-15] Each fabric was commercially obtained undyed, and subsequently triple-dyed at North Carolina State University's Wilson College of Textiles in 2004.

Because the cotton and nylon fabrics are twills, they have two distinct faces. One of the faces has warp threads that are the most prominent, while the other is dominated by weft threads. In both cases, however, the two types of threads contribute to the exposed

surface. The warp-dominant side of the fabric was the face used in these measurements for both fabrics.

Table 1.1. Fabric and fiber properties of the four fabrics used in this study. Specific surface area and areal density measurements are reported in Reference 6. Thread count and cover factor are calculated based on optical microscopy of the fabrics. Fiber diameter and the linear density calculations are based on SEM measurements of the four fabrics (data not shown).

	Cotton	Acrylic	Nylon	Polyester
Specific Surface Area (m^2/g)	0.940	0.272	0.410	0.057
Fabric Areal Density (g/m^2)	257	296	346	121
Thread Count (warp x weft, per cm)	22x12	22x12	23x12	32x26
Cover Factor	0.99	0.99	0.70	0.82
Fiber Diameter (μm)	20	13	9	22
Fiber Linear Density (dtex)	4.84	1.55	0.79	5.25
Weave Structure	2/1 Twill	Plain	2/1 Twill	Plain
Dyes	Remazol Orange 3G-A Remazol BR Red 3BS Remazol Brilliant Violet 5R	Astrazon Golden Yellow GL-E Astrazon Red Violet 3RN Astrazon Blue FBL	Telon Yellow FG01 Nylanthrene Green CG Anthraquinone Blue B	Dianix Red E-FB Dianix Violet S-4R Dianix Yellow S-6G
Additional Data in References	4, 6-12, 14	4, 5, 6, 9, 10, 13-15	6, 10, 14	4, 6, 8-10, 14

In this manuscript, the acrylic fabric used in these measurements will be referred to as Acrylic 917, to differentiate it from any other acrylic fabric.

Acrylic fiber is a synthetic polymer fiber made from acrylonitrile, shown in Figure 1.2. While acrylic fibers are hydrophobic (adsorbing up to 2% moisture content by mass), the fiber does have a sorption site for water to hydrogen bond at the lone pair of the triple-bonded nitrogen.[16] The dipole moment in the nitrile group provides for a strong intermolecular attraction, and as a result, acrylic fibers are very strong.[17]

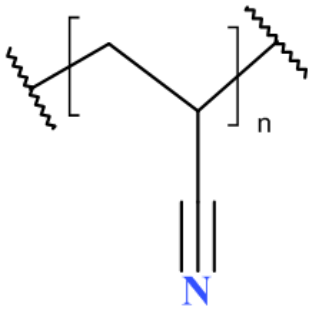

Figure 1.2. The polyacrylonitrile monomer. The exposed nitrile group acts as a potential bonding site during adsorption.

In this manuscript, the polyester fabric used in these measurements will be referred to as Polyester 905, to differentiate it from any other polyester fabric.

Polyester fiber is a synthetic fiber made primarily from polyethylene terephthalate, shown in Figure 1.3. Polyester is reported to be very hydrophobic, adsorbing around 1% of its mass in moisture at high humidities.[16]

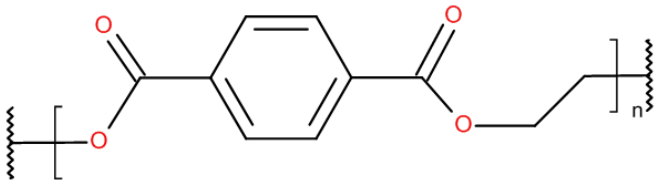

Figure 1.3. The polyethylene terephthalate monomer. The carbonyl oxygens are available as potential bonding sites during adsorption of water vapor.

In this manuscript, the cotton fabric will be referred to as Cotton 899, to differentiate it from any other cotton fabric.

Natural fibers such as cotton have been extensively studied, including studies of how cotton interacts with water.[16, 18] Cotton is composed of fibers built from cellulose (94% by weight), and hemicellulose (6% by weight).[18] It is very hydrophilic, adsorbing around

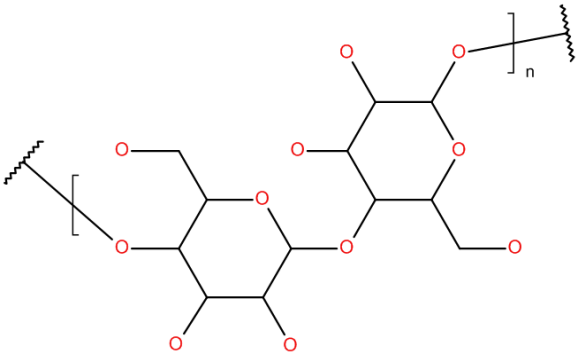

Figure 1.4. The cellulose monomer. The six hydroxyl groups are potential sites for strong hydrogen bonding during water vapor adsorption.

15% moisture content by mass near saturation.[16] Cellulose (shown in Figure 1.4) has the ability to undergo extensive hydrogen bonding, and this results in a very strong fiber.

In this manuscript, the nylon fabric will be referred to as Nylon 911, to differentiate it from any other nylon fabric.

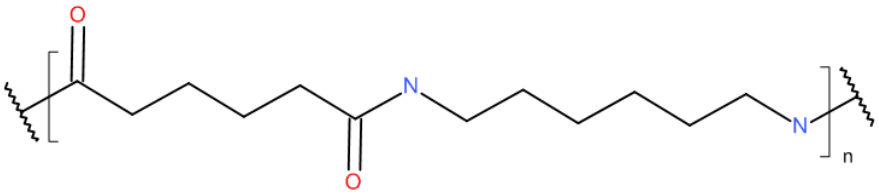

Figure 1.5. The nylon 6,6 monomer. Both amide groups provide potential sites for the adsorption of water vapor.

Nylon fibers are a polyamide. This particular fabric is nylon 6,6, and the monomer is shown in Figure 1.5. The amide groups provide sorption sites for moisture. Nylon shows a high degree of hydrophilicity for a synthetic fabric, and it is capable of adsorbing around half of the amount of moisture that cotton adsorbs at a given humidity.[16]

1.4 Overview of Steam Thermography

Steam thermography is a thermal imaging method in which chemical contrast between different surfaces during imaging is enhanced by taking advantage of the difference in the hydrophilicity of those different surfaces being imaged. While the surface is being imaged, it is exposed to steam or humid air. Surfaces exposed to water vapor respond with different thermal signatures, and the surfaces can then be differentiated more efficiently during imaging.

Steam thermography was first reported on by O'Brien et al. in a demonstration of the method in which thermal contrast was enhanced during thermographic imaging by the exposure of steam to an acrylic 917 fabric sample with dried blood stains made from dilute rat's blood.[5] In Reference 5, the enhancement of thermal contrast during thermographic imaging of dilute blood stains on a black polyester fabric with a metallic skull-and-crossbones print was also reported when the sample was exposed to steam. An application of steam thermography was published a second time in Belliveau, et al. (work which is described in detail in Chapter 6), when the method was applied to enhancing thermal contrast during thermographic imaging of simulated transfer fingerprints made with rat's blood on the acrylic (917), polyester (905), and cotton (899) fabrics described above.[6]

Six possible mechanisms for the response observed in a steam thermography measurement were previously identified.[5] One possible mechanism is that water vapor condenses into liquid water on the sample surface. The process of condensation is accompanied by a release of heat (2.45 kJ per gram of water), and the transfer of the heat of condensation to the sample surface could result in a differential heating between

sample surfaces with different heat capacities.[16] A second possible mechanism is the condensation of water vapor in the air before contacting with the sample surface, and then subsequently wetting the sample surface once in contact. The process of liquid water wetting a surface is also associated with a release of heat. This has been reported for fabrics such as cotton, in which the heat of wetting at 25 °C is 45.2 Joules per gram of dry cotton material.[19] Surfaces which have been wetted during imaging would likely show differential thermal responses due to the differences in the heats of wetting and heat capacities of the different materials. Additionally, the droplets formed in the air in transit to the sample may be of a different temperature than the sample surface after the processes of condensation and evaporative cooling, resulting in different amounts of heat transferred across the sample surface. Once wet, the diffuse component of a surface's reflectance is generally decreased. This would be detected during thermal imaging as an increase in signal intensity if the surface is a higher temperature than the ambient background (or vice versa for a lower temperature surface). A third possible mechanism is a radiant transfer of heat from the relatively hot source of steam to the sample surface, which would result in thermal responses of surfaces that would differ by a factor related to the optical properties (specifically reflectance) of the materials in the thermal infrared.[13, 15] A fourth possible mechanism is a convective transfer of heat as the relatively hot steam comes in contact with the sample surface. Similarly to the process of condensation described above, surfaces with differing heat capacities would show a differential thermal response under otherwise identical heat transfer scenarios.

A fifth possible mechanism is the transfer of heat to a surface as adsorption of water vapor occurs during imaging. The thermal response of a surface in this case is based on

the heat of adsorption, heat capacity, rate of vapor adsorption, and surface area of the surface material being imaged. This process is especially energetic among the so-far described possible mechanisms. For a dry sample that adsorbs liquid water until saturation, the transfer of energy is equal to the heat of wetting for a dry material, which may be on the order of tens of Joules per gram of dry fabric. For a dry sample that adsorbs water vapor until saturation, the transfer of energy is increased for every gram of water by the latent heat of vaporization (2.45 kJ per gram of adsorbed water from vapor). As an example, a hydrophilic fabric such as cotton can adsorb up to 15% to 20% of its dry mass in water. This equates to upwards of 0.2 grams of water per gram of cotton material, which in turn results in upwards of 490 Joules released per gram of dry cotton in addition to the heat of wetting for cotton. This yields a process which is around an order of magnitude more energetic than the wetting process, all else equal.[16]

A sixth possible mechanism is that adsorbed water alters the thermal emissivity of a surface. This process is a result of both the surface's emissivity changing such that the apparent emissivity is more like that of liquid water, and also that the light scattering of the surface is decreased as the adsorbed water acts to create a surface that has a lowered surface roughness.[20] The effect of adsorbed water changing the emissivity of a surface has been reported in literature for soils.[21,22] Surfaces for which the apparent emissivity is altered by the adsorption of water vapor would exhibit a differential thermal contrast related to the amount of water adsorbed, the difference in apparent emissivity of water and that surface, and the degree to which a surface's light scattering properties are reduced by the coating of adsorbed water.

1.5 Dissertation Outline

Chapter 2 describes measurements made to test several possible mechanisms of the chemical contrast enhancement observed during a steam thermography measurement. These measurements provide evidence further of water vapor adsorption as the primary mechanism, and also establish several necessary experimental conditions to test the enhanced chemical contrast of a steam thermography measurement.

The third chapter continues the work of Chapter 2 by demonstrating enhanced chemical contrast of dried blood on fabric surfaces *in vacuo* during both the adsorption and desorption of water vapor. Also described in this chapter are the results of a study into the chemical contrast enhancement observed as a result of the adsorption and desorption of vapors of eight solvents besides water, with varying degrees of polarity. The results of an experiment attempting to increase the chemical contrast of dried blood on cotton by silanizing the sample are given.

The work in Chapter 4 describes a study into the sensitivity the thermal emissivity of sample fabrics to adsorbed moisture. The calculation of thermal emissivity using a thermographic camera is derived. Interpretation of the moisture isotherm data using the Guggenheim, Anderson, de Boer (GAB) sorption model is discussed. Fabric emissivity as a function of moisture content is given, along with a proposed mechanism for the result. A novel use of household polyethylene film as an infrared window, and optical properties of the window used in this study are reported.

Chapter 5 details measurements of the emissivity of dried blood on fabric as a function of humidity, and the relationship of the emissivity of these surfaces to the

chemical contrast observed during a steam thermography measurement. This study shows that a differential change in emissivity does occur as water adsorbs to acrylic fabric, and that the differential change in emissivity acts to decrease the contrast between the surfaces.

Chapter 6 reports the application of steam thermography to the imaging of ridge patterns of blood-transferred simulated fingerprints. Microthermographic measurements of dried blood on acrylic, polyester, and cotton fabrics show greater detail than available during conventional thermographic measurements.

REFERENCES

1. R. Madding. Spectrally transmissive IR windows: how they affect your thermography results. In: *Proc. SPIE 5782, Thermosense XXVII* (eds R. Peacock, D. Burleigh, J. Miles), Orlando, FL, USA, 28 March 2005.

2. P. W. Nugent, J. A. Shaw, N. J. Pust, et al. Correcting calibrated infrared sky imagery for the effect of an infrared window. *J. Atmos. Oceanic Technol.* 2009; 26: 2403-2412.

3. R. Usamentiaga, P. Venegas, J. Guerediaga, et al. Infrared thermography for temperature measurements and non-destructive testing. *Sensors* 2014; 14: 12305-12347.

4. R. G. Belliveau, S. A. DeJong, B. M Cassidy, et al. Ridge patterns of Blood-Transferred Simulated Fingerprints Observed on Fabrics via Steam Thermography. *Forensic Chem*. 2016; 1: 74-77. https://doi.org/10.1016/j.forc.2016.07.005

5. W. L. O'Brien, N. D. Boltin, Z. Lu, et. al. Chemical contrast observed in thermal images of blood-stained fabrics exposed to steam. *Analyst* 2015; 140: 6222-6225. https://doi.org/10.1039/C5AN01413A

6. S. A. DeJong, Z. Lu, B. M. Cassidy, et. al. Detection limits for blood on four fabric types using infrared diffuse reflection spectroscopy in mid- and near-infrared spectral windows. *Anal. Chem*. 2015; 87: 8740-8747.

7. S. A. DeJong, B. M. Cassidy, Z. Lu, et al. Effect of azimuthal angle on infrared diffuse reflection spectra of fabrics. *Spectroscopy* 2015; 30(12): 23-25.

8. M. R. Baranowski, H. Brooke, J. N. McCutcheon, et al. Coating effects on mid-infrared spectra of fabrics. *Appl. Spectrosc.* 2011; 65(8): 876-884.

9. S. A. DeJong, W. L. O'Brien, Z. Lu, et al. Optimization of gap derivatives for measuring blood concentration of fabric using vibrational spectroscopy. *Appl. Spectrosc.* 2015; 69(6): 733-748.

10. Z. Lu, S. A. DeJong, B. M. Cassidy, et al. Detection limits for blood on fabrics using attenuated total reflection Fourier transform infrared (ATR FT-IR) spectroscopy and derivative processing. *Appl. Spectrosc.* 2017; 71(5): 839-846.

11. Z. Lu, B. M. Cassidy, S. A. DeJong, et al. Attenuated total reflection (ATR) sampling in infrared spectroscopy of heterogeneous materials requires reproducible pressure control. *Appl. Spectrosc.* 2017; 71(1): 97-104.

12. S. A. DeJong, Z. Lu, B. M. Cassidy, et al. Reversible gap derivatives and their integration. *Appl. Spectrosc.* 2016; 70(6): 1044-1054.

13. H. Brooke, M. R. Baranowski, J. N. McCutcheon, et al. Multimode imaging in the thermal infrared for chemical contrast enhancement. Part 1: Methodology. *Anal. Chem.* 2010; 82: 8412-8420.

14. H. Brooke, M. R. Baranowski, J. N. McCutcheon, et al. Multimode imaging in the thermal infrared for chemical contrast enhancement. Part 2: Simulation driven design. *Anal. Chem.* 2010; 82: 8421-8426.

15. H. Brooke, M. R. Baranowski, J. N. McCutcheon, et al. Multimode imaging in the thermal infrared for chemical contrast enhancement. Part 3: Visualizing blood on fabrics. *Anal. Chem.* 2010; 82: 8427-8431.

16. W. Morton, J. Hearle. Physical properties of textile fibers. Philadelphia: Woodhead Publishing, 2012, p. 178-228.

17. K. Sada, K. Kokado, Y. Furukawa. Polyacrylonitrile (PAN). In: *Encyclopedia of Polymeric Nanomaterials.* (eds. S. Kobayashi, K. Müllen), Berlin/Heidelberg, Germany: Springer-Verlag, 2014, p. 1-7.

18. C. A. S. Hill, A. Norton, G. Newman. The water vapor sorption behavior of natural fibers. *J. Appl. Polym. Sci.* 2009; 112: 1524-1537. https://doi.org/10.1002/app.29725

19. M. Wahba, S. Nashed. Change with temperature of the heat of wetting of dry cellulose in water, and its bearing on the specific heat of the adsorbed water and of the swollen cellulose. *Nature* 1950; 166: 998.

20. M. L. Myrick, M. N. Simcock, M. Baranowski, et al. The Kubelka-Munk diffuse reflectance formula revisited. *Appl. Spectrosc. Rev.* 2011; 46(2): 140-165.

21. J. Chen, B. Yang, R. Zhang. Soil thermal emissivity as affected by its water content and surface treatment. *Soil Sci.* 1989; 148(6): 433-435.

22. M. Mira, E. Valor, R. Boluda, et. al. Influence of soil water content on the thermal infrared emissivity of bare soils: Implication for land surface temperature determination. *J. Geophys. Res.* 2007; 112: 1-11.

CHAPTER 2: STEAM THERMOGRAPHY IN CONTROLLED CONDITIONS

2.1 INTRODUCTION

Following the work by O'Brien, which was described in section 1.5 (Overview of Steam Thermography) of Chapter 1, the exact conditions and mechanisms which drove the chemical contrast enhancement during the steam thermography measurement reported in that work were undetermined.[1] It was hypothesized that of the six potential mechanisms, water vapor adsorption was the primary source of the enhanced chemical contrast, and that four of the other potential mechanisms described at the end of Chapter 1 are at least somewhat a result of using a handheld steamer as the source of water vapor for a steam thermography measurement. The steamer itself is hot in relation to the sample (allowing for the radiative transfer of heat), the gas generated by the steamer is also hot in relation to the sample (allowing for the convective transfer of heat), the steam can condense into droplets in the air (allowing for wetting effects), and can condense into liquid water on the sample (allowing for a transfer of heat equal in magnitude to the latent heat of vaporization). The relative contribution of a differential change in emissivity was unknown based on measurements made with the steamer.

An additional problematic aspect of using a handheld steamer as the source of water vapor in a steam thermography measurement is the heterogeneous application of the

water vapor to the sample. The stream of steam coming from the steamer is about three inches in diameter. Moving the steamer during application of water vapor results in areas of the sample that were previously subject to vapor exposure becoming suddenly subject to the relatively dry, relative cool ambient conditions. This prevents any area of the sample larger than the steamer stream from being consistently exposed to steam. Additionally, the reverse process of water vapor adsorption, water desorption, begins to occur immediately after the sample surface is no longer subject to an increased concentration of moisture in the air, relative to the ambient conditions. The result of this is that during a typical 60-80 second steam thermography measurement of a sample the size of a handprint, various areas of the sample are adsorbing water vapor, desorbing water vapor, or not in contact with conditioned air at all. Figure 2.1 shows two frames from a recording of a previous steam thermography measurement of five blood stains on an acrylic 917 fabric, described below.[1] The left frame shows an intial exposure of

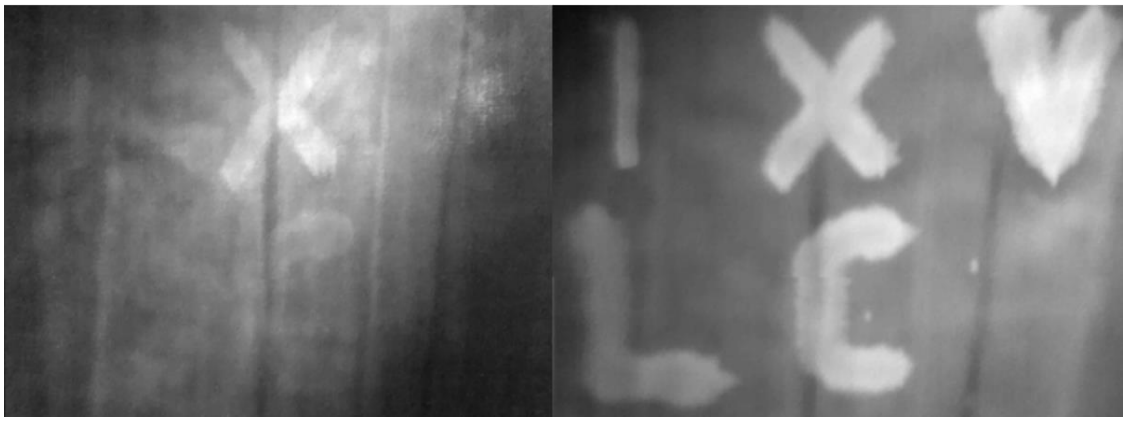

Figure 2.1. Two frames of the exposure of steam to an acrylic 917 fabric sample with 5 bloodstains on its surface, using a handheld steamer. The frames are approximately 15 seconds apart. The right frame shows the heterogeneous application of the steam. The left frame shows increase contrast for each stain after steam has been applied to each stain.

steam to the fabric. Contrast is enhanced for the 'X' stain, and some parts of the surrounding stains. The right frame shown in Figure 2.1 shows enhanced contrast for all five stains about 15 seconds later in the same recording, after the steam has been applied to each stain.

In several steam thermography video recordings of dried blood stains on acrylic (fabric ID 917) using a handheld steamer, it was observed that seconds prior to the steam coming in contact with the sample, the contrast between the blood stain and substrate fabric was increased. Figure 2.2 shows three frames from a steam thermography recording of dried blood on acrylic. In the left frame, there is no observed contrast. In the middle frame, the sample is not yet exposed to water vapor; however the steamer was placed in close proximity to the sample in preparation to expose the sample to steam. Contrast is observed between the blood-stained areas (which appear darker) and the blank

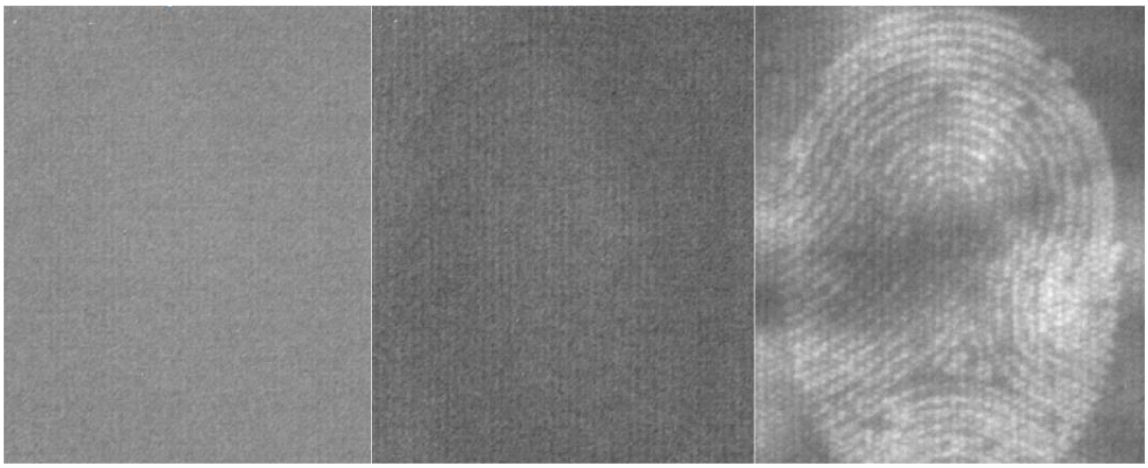

Figure 2.2. Three frames from a steam thermography recording of dried rat's blood on the acrylic 917 fabric. Left: Thermal imaging of the fabric prior to both exposure to water vapor or bringing the steamer in close proximity to the sample. Center: The hand-held steamer is positioned close to the sample in preparation to expose the sample to steam. Right: The sample during exposure to steam. This sample is described in detail in Chapter 6.

fabric areas in this frame. In the right frame, the sample is shown during exposure to steam, which results in an enhancement of contrast between the stain and fabric.

The contrast observed in the middle frame of Figure 2.2 is likely due to the difference in the reflectivity of thermal radiation between the stain and fabric.[2, 3] The bloodstain, during this time period of 1 to 2 seconds, reflects less of the thermal radiation emitted from the steamer to the camera than the fabric itself. The fabric is reflecting more of the radiation of the nearby steamer to the camera. The fabric is therefore observed to the brighter (a higher apparent temperature) than the blood. As the recording continues, it is not possible to differentiate the reflected thermal radiation from the thermal response of the surfaces as the exposure to steam occurs.

These situations, in addition to the need to prevent the source of water vapor used in the method from being near saturation conditions, highlight the need of an apparatus designed specifically to conduct a steam thermography measurement. Four goals for such an apparatus are:

- Create a controlled exposure of both increased and decreased water vapor concentrations.
- Maintain isothermal conditions to prevent convective and radiative heat transfer.
- Prevent conditions in which water may condense during a measurement.
- Allow for a sample to be thermographically imaged while being subject to the conditioned air while simultaneously protecting the camera from those conditions.

The work in this chapter describes the construction of this apparatus, and steam thermography measurements performed with the apparatus to validate the completion of the listed goals.

2.2 Experimental

2.2.1 Sample Conditioning

A diagram of the in-house built apparatus used to condition the fabrics prior to each measurement is shown in Figure 2.3. The apparatus is composed of three chambers constructed of plywood, connected by two 2" PVC ball valves. In Figure 2.3, the air in the left chamber is dehumidified using a commercially available Kenmore dehumidifier (Sears, Chicago, IL, Model 580) set to the highest fan setting and the driest humidity setting. During operation, the air in this chamber was conditioned to 5% relative humidity (RH) and 65 °C, heated only by the dehumidifier. In the right chamber shown in Figure 2.3, the air is humidified by a household humidifier, and heated using a 750 watt heater fan (Geneva Industrial Group, Northbrook, IL, Soleil brand, model LH-879G). The air in this chamber was conditioned to 95% RH and 35 °C. In the middle chamber shown in Figure 2.3, the sample fabric rests on a plastic mesh 12 inches from the bottom of the chamber. The sample is centered to allow an equivalent amount of airflow around each side of the sample. This is done to prevent a path of airflow with lower resistance to flow in other areas of the chamber such that a greater amount of moisture travels through the chamber in the direction of the lower resistance to flow. Airflow into the middle chamber shown in Figure 2.3 is controlled by two 2" PVC ball valves, one each of which is positioned between the middle chamber and the two side chambers. Airflow out of the sample chamber is controlled by two rack-mounted fans in the bottom of the chamber.

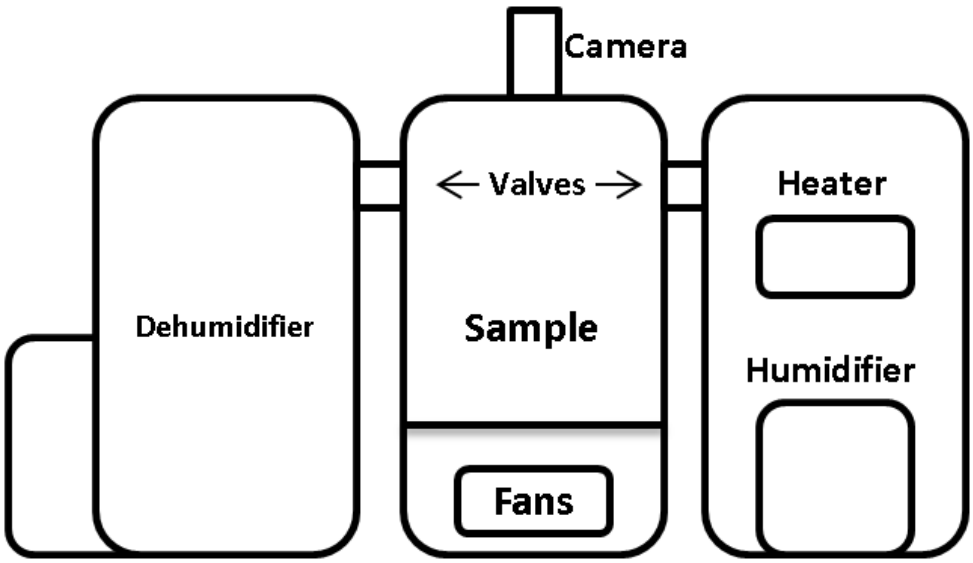

Figure 2.3. Diagram of the apparatus used to supply humidified or dehumidified air to a sample fabric during a steam thermography measurement. Dehumidified air is supplied to the sample (middle) chamber by opening the valve to the dehumidified air chamber (left) and closing the valve to the humidified air chamber (right). The conditions of the sample chamber are 35 °C and 30% RH while air to this chamber is supplied by the dehumidified air (left) chamber. The air in the humidified air chamber (right) was conditioned to 35 °C and 95% RH during this time. A steam thermography measurement was performed by initializing the camera recording, closing the valve to the dehumidified air chamber (left), opening the valve to the humidified air chamber (right), and engaging the exhaust fans under the sample fabric.

Prior to a measurement, the sample chamber is conditioned to 30% RH and 35 °C by opening the valve to the dehumidified air chamber and closing the valve to the humidified air chamber. Because the sample chamber reaches no less than 30% RH when conditioned by the dehumidified air chamber, this is humidity of the dehumidified air at the temperature of the sample chamber. In this study, when referring to an exposure of dehumidified air, that refers to the air which equilibrates at 30% RH and 35 °C in the sample chamber. The temperature in each chamber is measured by a thermocouple probe in inserted into the top of the interior of each chamber. The probe for the middle chamber is seen in Figure 2.4. Humidity is measured in each chamber using an RH probe (Omega

Engineering Inc., Norwalk, CT, model HX71-MA) with a measurement range of 5-95% RH and an accuracy of 4% RH. Measurements made by both temperature and humidity probes are converted to digital reading by a DAQPro Data Logger (Omega Engineering Inc., Norwalk, CT, model OM-DAQPRO-5300).

Figure 2.4. A photograph of the camera, which collects thermographic measurements through a sodium chloride window, and the temperature probe used to measure the temperature of the sample chamber.

2.2.2 THERMOGRAPHY

Thermal images are recorded through a sodium chloride salt window by a FLIR Systems A315 microbolometer-based camera (16 bit digitization, 240 x 320 pixel resolution, 30 Hz frame rate) operating in signal linear mode using an interface developed in-house in the LabVIEW 2013 programming environment (National Instruments, Austin, TX). The camera is mounted to the top of the sample chamber, shown in Figure 2.4. The camera focus is set by measuring the distance from the camera lens to the sample surface, and using the empirically-derived Equation 2.1 to determine the 'absolute position' (A) that the camera must be set to:

$$A = 3106.5 - \left(1885.4e^{(-0.03105x)}\right) \quad (2.1)$$

Where x is the distance in inches. This equation was determined by Nick Boltin in 2013, and was based on a curve fitting of focus-determination measurements from 6 to 37 inches. More details about the way camera measurements are made and processed can be found in Chapter 1.

A steam thermography recording using this apparatus is made by first conditioning the sample chamber of the apparatus to 35 °C and 30% RH by opening the sample chamber to airflow from the dehumidified air chamber. The humidified air chamber is conditioned to 35 °C and 95% RH. Then, an 80 second (2400 frame) thermal camera recording is initialized. The valve between the dehumidified air chamber and the sample chamber is closed, the valve between the humidified air chamber and sample chamber is opened, and then the exhaust fans underneath the sample fabric are turned on. This draws air from the humidified air chamber through the sample chamber. The corresponding rise in humidity is recorded, and the temperature is monitored to ensure the air in both chambers does not change.

After the sample exposure to humidified air is recorded, the exhaust fans are stopped and a second recording of 80 seconds is initialized. The valve between the humidified air chamber and the sample chamber is closed, the valve between the sample chamber and dehumidified air chamber is opened, and the exhaust fans under the sample are powered again, drawing dehumidified air into the sample chamber.

The two recordings of 2400 frames each are then processed using MATLAB R2012b (The MathWorks, Inc., Natick, MA).

2.2.3 Sample Fabric

This study reports the results of controlled steam thermography measurements of blood stains on the acrylic 917 fabric referenced in Chapter 1. This sample will be referred to throughout this manuscript as Fabric 1. It was prepared in 2010 and is described in more detail in Brooke et al. and O'Brien et al.[1, 2] Rat's blood was applied to the surface of the fabric by dripping the blood or blood dilution from a glass pipette. Five figures were made on the surface of the fabric in the shape of Roman numerals. I for whole blood, X for 10x dilute blood, V for 25x dilute blood, L for 50x dilute blood, and C for 100x dilute blood.

2.3 Results & Discussion

An individual frame from a steam thermography recording of Fabric 1 is shown in Figure 2.5. All five Roman numerals can be seen in the image, although the 25x dilute blood stain (V, top right), the 50X dilute stain (L, bottom left), and the 100X dilute stain (C, bottom center) are only faintly visible. Dilute stains appear to have less definition than the whole blood stain, which is likely due to the blood dilution wicking into the fabric when the stains were first created.[4]

After exposure of Fabric 1 to humid air for 30 seconds, the air supplied to the sample is switched from humid air to dehumidified air. An individual frame from a steam thermography recording measured 15 seconds after the apparatus is switched to expose

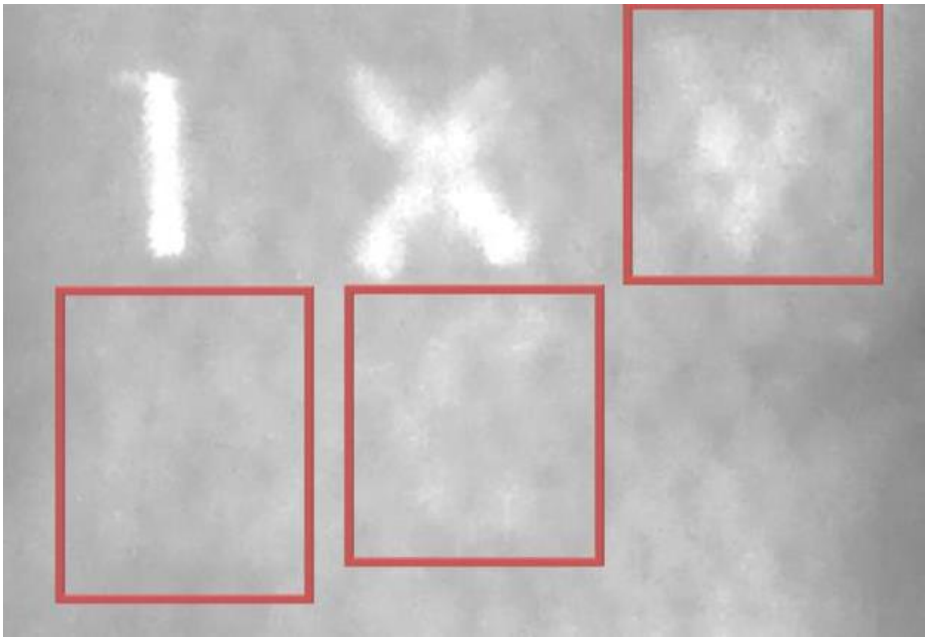

Figure 2.5. A frame from a steam thermography recording of Fabric 1 during exposure to humid air. All five blood stains have an increased contrast compared to the surrounding fabric. The red outlines show the locations of the 25X dilute stain (V) in the top right, the 50X dilute stain (L) on the bottom left, and the 100X dilute stain (C) at the bottom center.

the sample to dehumidified air is shown in Figure 2.6. All five Roman numerals can be seen, but the stains appear darker (a lower apparent temperature) than the surrounding fabric. More dilute stains appear to have less definition than the whole blood stain, similarly to the stains during exposure to humid air (Figure 2.5). However, the contrast between the fabric and stains is stronger in this case when measuring a humidified sample being exposure to dried air, than a dried sample during exposure to humid air.

The enhanced contrast observed in Figures 2.5 and 2.6 demonstrate several qualities of a steam thermography measurement. The humidified air exposure measurements reported here are at isothermal conditions, such that the enhanced contrast cannot be a

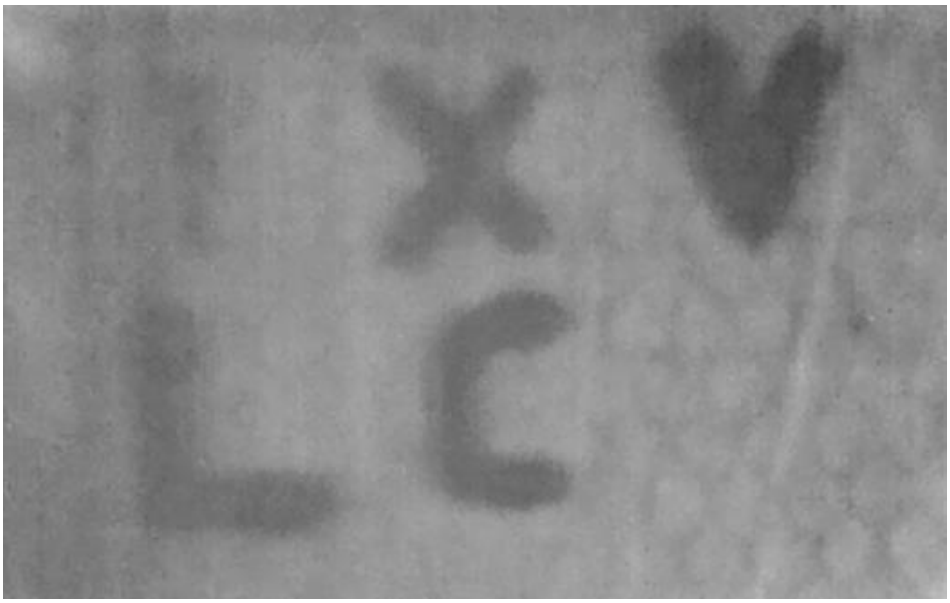

Figure 2.6. A frame from a steam thermography recording of Fabric 1 after exposure to humid air. Within 30 seconds of the end of exposure to humid air (~95% RH), the sample is exposed to dehumidified air (~30% RH). This frame is within five seconds of the exposure to dehumidified air. All five blood stains have an increased contrast compared to the surrounding fabric.

result of a convective or radiative heat transfer. While the air in the humidified air chamber is near saturation conditions, the air that reaches the sample during exposure is mixed with dried air in transit, and as a result is not near saturation conditions. This is not conclusive, but is additional evidence that water vapor is not condensing on the sample surface, possibly contributing to the enhanced contrast. This also is evidence that water was not condensed in the air before reaching the sample, as water vapor in the humidified air chamber was not subject to conditions in transit to the sample that would result in droplet condensation.

While the contrast observed during the humidifying phase of the experiment does not provide evidence of the processes of a differential emissivity change between the fabric and stain, the contrast observed during the drying phase of the experiment is inconsistent

with the type of thermal response that a differential change in emissivity would exhibit. Additionally, any thermal response due to a change in either fabric or bloodstain emissivity would be retained while the moisture content of the material is constant. These results therefore provide insight for a potential method of understanding the change in surface emissivity as a function of moisture content. The emissivity considerations of a steam thermography measurement are addressed further in Chapters 4 and 5.

2.4 Conclusions

This work illustrates that the chemical contrast observed in a steam thermography measurement of blood on fabrics is not a result of radiative or convective differential heat transfer, and that the method does not require a sample to be exposed to steam, only to humidified air. Chemical contrast can be observed between blood and fabrics in isothermal measurement conditions in at least some cases. These results also suggest that the primary mechanism by which the chemical contrast during a steam thermography measurement is enhanced is by water vapor adsorption, based on observations that the samples have a positive thermal response (heating) on exposure to air containing increased water vapor concentrations, and a negative thermal response (cooling) on exposure to air containing lower water vapor concentrations.

REFERENCES

1. W. L. O'Brien, N. D. Boltin, Z. Lu, et. al. Chemical contrast observed in thermal images of blood-stained fabrics exposed to steam. *Analyst* 2015; 140: 6222-6225.

2. H. Brooke, M. R. Baranowski, J. N. McCutcheon, et al. Multimode imaging in the thermal infrared for chemical contrast enhancement. Part 1: Methodology. *Anal. Chem.* 2010; 82: 8412-8420.

3. H. Brooke, M. R. Baranowski, J. N. McCutcheon, et al. Multimode imaging in the thermal infrared for chemical contrast enhancement. Part 3: Visualizing blood on fabrics. *Anal. Chem.* 2010; 82: 8427-8431.

4. R. G. Belliveau, S. A. DeJong, B. M Cassidy, et al. Ridge patterns of Blood-Transferred Simulated Fingerprints Observed on Fabrics via Steam Thermography. *Forensic Chem.* 2016; 1: 74-77. https://doi.org/10.1016/j.forc.2016.07.005

CHAPTER 3: THERMOGRAPHY OF THE ADSORPTION AND DESORPTION OF VAPORS IN VACUO

3.1 INTRODUCTION

The preliminary work done to establish basic controls of a steam thermography measurement described in Chapter 2 demonstrates that the enhanced contrast observed in a steam thermography measurement does not require any radiative or convective heat transfer to the sample, provides evidence that the contrast enhancement is independent of any sample wetting by condensed water, and also evidence that the contrast is independent of liquid water condensation on a sample surface. Furthermore, the work described in Chapter 2 demonstrates evidence that the adsorption of water vapor to a surface results in an increase in the temperature of that surface, even under isothermal conditions (i.e. the surface and water vapor are the same temperature). It also demonstrates that once the supply of increased water vapor concentration to the surface is stopped, the surface begins to cool, which is likely evaporative cooling caused by the reverse of the adsorption process. Of the six identified possible mechanisms to explain the chemical contrast enhancement observed during a steam thermography measurement (differential radiant heating, differential water vapor adsorption, differential condensation of water vapor, a differential change in emissivity, the deposition of liquid water droplets, differential convective heating), isothermal measurement conditions exclude radiant and convective heating as possible mechanisms. The possible mechanisms of enhanced

chemical contrast which remain in question after examination of the results shown in Chapter 2 are that the fabric and bloodstains are differentially heating due to the adsorption of water vapor, that the fabric and bloodstains are undergoing a differential change in their thermal emissivities due to the introduction of water vapor to the sample, and/or that water vapor is condensing on the sample surface. It was also not conclusive that water droplets were not reaching the sample surface and contributing to the contrast enhancement that was observed.

During the disequilibrium of a sample exposure to a change in humidity, it would not be possible to de-couple the thermal response of a sample during the adsorption of water vapor (which creates differential heating of the surfaces) with the thermal response of a differential change in thermal emissivity also due to the adsorption of water vapor. However, it would be possible to exclude other possible factors, such as the possibility of water vapor condensation on a surface contributing to a thermal response observed by the thermal camera during a measurement. The work presented in this chapter aims to definitively demonstrate that the exposure of water vapor to a sample surface results in a thermal response which is independent of both vapor condensation into a liquid and wetting by liquid droplets of airborne water by reporting the results of a series of thermography measurements made on bloodstained fabrics exposed to water vapor while under vacuum at ambient temperatures. To prevent any water vapor condensation, the vapor pressure of water vapor introduced *in vacuo* must never rise close to saturation conditions (~24 Torr at 25 °C). This chapter describes three studies of thermography measurements of various fabric and bloodstained fabric samples exposed to vapor pressures of no greater than 10 Torr at 25 °C. First, the results of a bloodstained acrylic

sample exposed to water vapor are presented. This study is analogous to a steam thermography measurement, with the difference being that the sample is maintained under vacuum prior to the measurement, and then a fixed amount of water vapor is introduced to the sample.

The work described in the latter two studies in this chapter are motivated by the theory that water vapor adsorption is the primary mechanism of the contrast enhancement in a steam thermography measurement. If water vapor adsorption is the primary cause of the thermal response observed on a given surface by a thermal imager, then factors affecting that response are the heat of adsorption for a given vapor adsorbing on the surface, the heat capacity of the surface, the rate of vapor adsorption onto/into the surface material, and available surface area of the material. This indicates that different vapors would result in different thermal responses. The heat of adsorption is a result the adsorbent-adsorbate complex creating a system of reduced free energy compared to the free vapor and surface. The degree to which the free energy is reduced is a factor of, among other properties, the polarities of the adsorbent and adsorbate.[1, 2] The implication of this is that the exposure of different solvent vapors of varying polarity will correlate with the thermal response of a surface during thermographic imaging. To study this, results from thermographic measurements of bloodstains on fabrics and blank fabrics during exposure to vapors of varying degrees of polarity are presented and discussed.

The results of the solvent study provide further motivation for the third study presented in this chapter. Cotton fabric is highly hydrophilic, having both a high capacity for water adsorption, and a high enthalpy of adsorption.[3, 4] The thermal response of a cotton fabric exposed to water vapor during a thermographic recording is predictably

large in magnitude compared to the acrylic fabric which has been so far reported. However, bloodstains on cotton are also highly hydrophilic, having also both a high capacity for moisture adsorption, and a high enthalpy of adsorption.[5, 6] The result of these factors, which is further highlighted in the solvent study, is that the differential response of dried blood on cotton fabric and blank cotton fabric is relatively small.

As described in Chapter 1, the available adsorption sites on a cellulose monomer are hydroxyl groups. Due to the complicated composition of blood, the available adsorption sites for dried blood vary considerably.[6, 7] However, blood contains a large number of amide groups, which can act as potential sites for vapor adsorption.[8] A reduction in the overall number of hydroxyl sites available for adsorption on a bloodstained cotton surface could increase the differential thermal response of a bloodstain on cotton, provided that the number of amide adsorption sites of the dried blood is left unchanged.

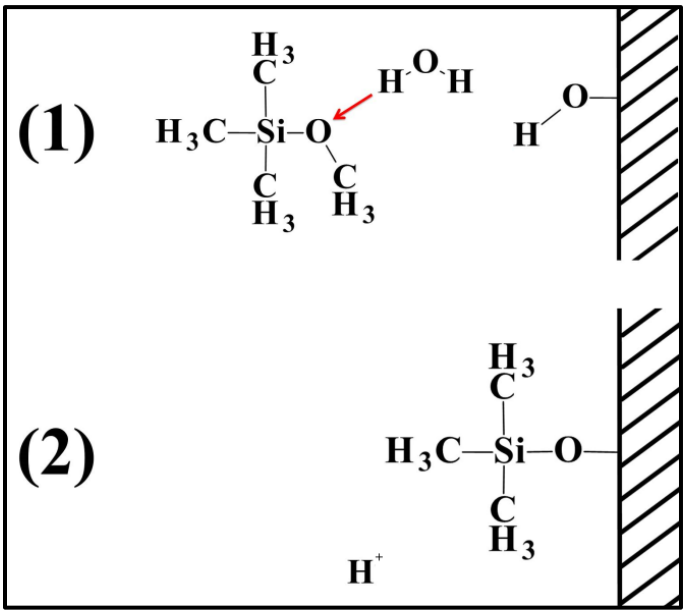

Figure 3.1. Trimethylmethoxysilane during the silanization process. 1) Water hydrolyzes the methoxyl group of the silane. 2) The silicon atom then covalently bonds to the surface hydroxyl's oxygen.[10]

One method of altering the hydroxyl groups of the cotton material without negatively impacting the quality of a dried bloodstain on the fabric is silanization by vapor deposition.[9] A silanization procedure involves introducing a silane with one or more hydroxyl or alkoxy groups to hydroxyl bonding sites on a substrate in the presence of a hydrolyzing catalyst. The silicon atom of the silane then covalently bonds to the oxygen of the substrate's hydroxyl group. The catalyst for the hydrolyzation step is typically acidic, and commonly water is employed in this step.[10, 11] A diagram of the mechanism for trimethymethoxylsilane is shown in Figure 3.1.

Silane-fiber bonds act to prevent water molecules from interacting with the cellulose substrate, increasing the hydrophobicity of the surface.[9] In order to perform the silanization of a surface by chemical vapor deposition, a silane, many of which are liquids, must be vaporized without breakage of the alkyl groups bonded to the silicon. Many silanes have low boiling points, making this process as simple as heating the liquid silane in humid conditions while in the presence of the substrate surface.

3.2 Materials and Methods

3.2.1 Samples

Figure 3.2 shows an aged, 7 cm by 7 cm square sample of acrylic 917 fabric with dried bloodstains applied by splattering rat's blood across the fabric surface, produced in September 2009 for developmental laboratory imaging studies. This sample will be referred to as the bloodstained acrylic sample throughout this chapter.

Finished samples used in the solvent study are shown in Figure 3.3. Samples for this study are made using a variation of a procedure found in Cassidy, et al.[12] Specifically,

1”x1” (2.5x2.5 cm) squares of the acrylic 917, cotton 899, nylon 911, and polyester 805 fabrics are imprinted with a hydrophobic polymer ring made from LocTite vinyl, fabric,

Figure 3.2. An aged, bloodstained acrylic fabric sample, produced in September 2009.

and plastic adhesive (Henkel Co., Rocky Hill, Ct. Item# 1360694). The adhesive was applied by coating the surfaces of two 1” O.D./ ½” I.D. (2.5 cm O.D./ 1.3 cm I.D.) steel washers, pressing the washers together with the fabric sandwiched between them, and clamping the washer-fabric-washer assembly together for 24 hours to cure. After the 24 hour curing period the samples are unclamped and the washers removed. For the blank fabric samples, 100 µL of deionized water was applied to the fabric surface inside of the polymer ring by pipette, and allowed to dry for 24 hours. For the neat (whole blood) samples, 100 µL of whole rat blood was applied to the fabric surface inside of the polymer ring by pipette, and allowed to dry for 24 hours. For the 10X dilute samples, 1 mL of rat’s blood was diluted to a 10 mL solution using deionized water, and 100 µL of the dilution was applied to the fabric samples by pipette, and allowed to dry for 24 hours. The rat blood dries partially on the surface of the fabric, and partially is adsorbed into the

fabric. Visible within some of the bloodstains shown in Figure 3.3 is a "coffee ring" pattern on the sample, implying some heterogeneity in the deposition process.[13, 14] The face of the fabric on which the blood was applied and dried is the face of the fabric observed during a measurement.

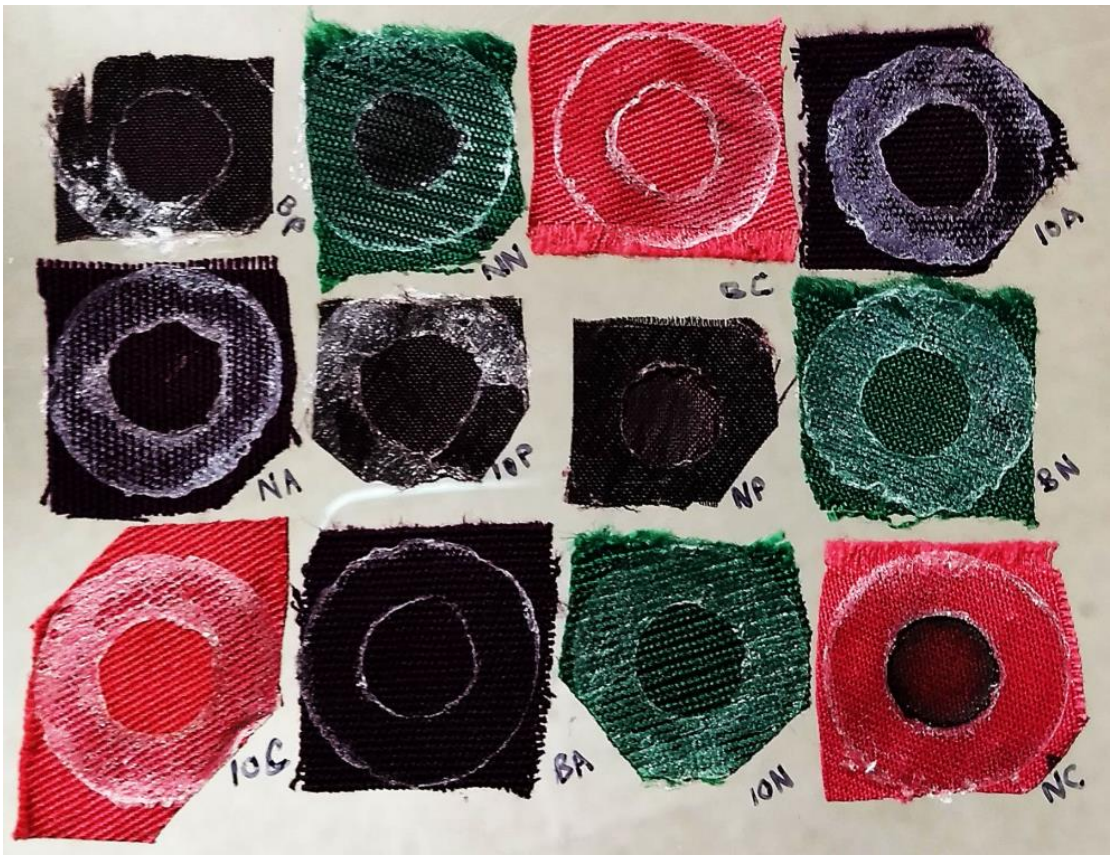

Figure 3.3. The arrangement of fabric samples used in the solvent study. The samples are labeled to their lower right. Each label is composed of two indicators. A label of 'B' is for a blank, 'N' is for a neat (whole blood) bloodstain, and '10' is for a stain of 10X diluted blood. Then, they are lettered 'A' for acrylic, 'N' for nylon, 'P' for polyester, and 'C' for cotton. For example, the top right-most sample is labeled '10A', which corresponds to an acrylic fabric sample stained with 10X diluted blood.

The sample for the third study described in this chapter is a 7" x 3" cut of the cotton 899 fabric. This fabric, which is shown in Figure 3.4, is sectioned into three bloodstained areas. The first bloodstained area on this fabric sample is a transfer stain made with 10X

dilute rat's blood and is faintly visible on the left side of the fabric shown in Figure 3.4. The second bloodstained area is another transfer stain made with undiluted (whole) rat's blood and is visible in Figure 3.4 as the stain in the center of the fabric. The third bloodstained area is made with whole rat's blood also, but is a spatter stain. The spatter pattern was produced by first covering the 2/3 of the sample area containing the transfer prints with aluminum foil, placing the 2/3 covered sample on an adsorbent pad, then placing the sample in an enclosed acrylic plastic chamber lined with aluminum foil. 1 mL of whole rat's blood in a 1 mL syringe was sprayed onto the chamber wall forcefully. A

Figure 3.4. The bloodstained cotton sample used in the silanization study. Three areas of this fabric are bloodstained as follows: 1) a transfer stain made with 10X dilute rat's blood which is faintly visible on the left side of the fabric. 2) A second transfer stain made with undiluted (whole) rat's blood and is visible as the stain in the center of the fabric. 3) A spatter pattern made with whole rat's blood, partly visible on the right side of the fabric. The description of how each stain was applied to the fabric surface is given in the text.

second quantity of 1 mL of whole rat's blood in a 1 mL syringe was again sprayed onto the chamber wall forcefully. A photograph of the chamber after the two syringes of blood had been sprayed onto the chamber wall is shown in Figure 3.5. The spatter pattern

created by this method is visible in the image on the white adsorbent pad lining the bottom of the enclosure.

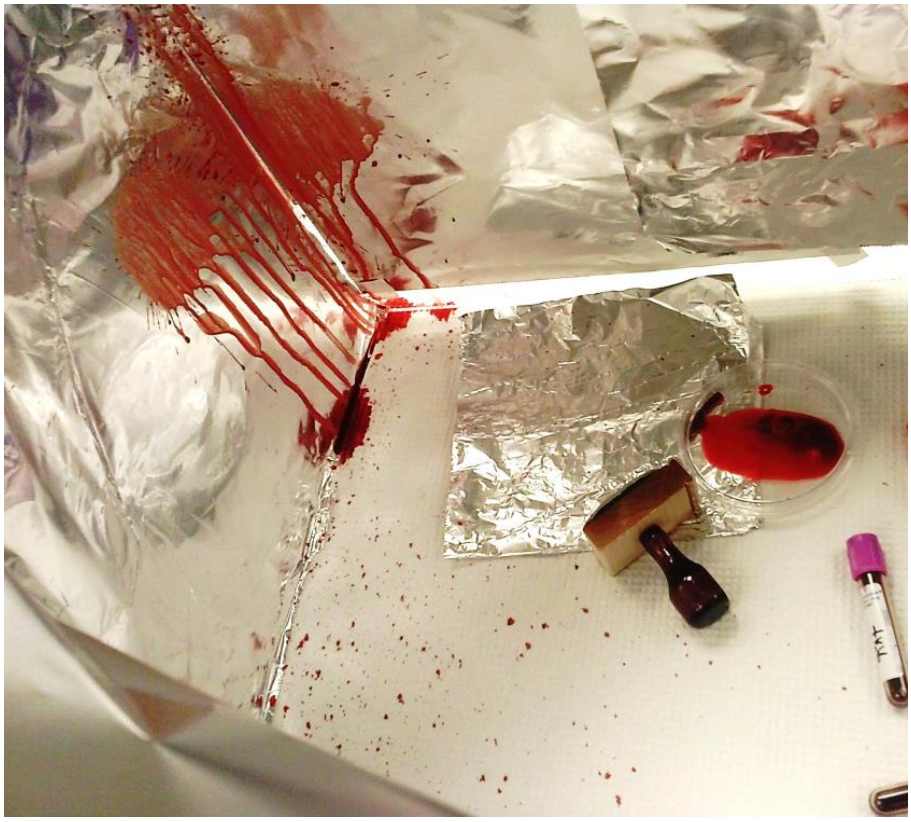

Figure 3.5. A photograph of the chamber used to create the spatter pattern on the cotton fabric used in the silanization study. The blood was sprayed onto the wall by syringe, and as a result, droplets of blood deposited onto the uncovered sample face (sample not shown in this image).

The transfer prints were made using a custom rubber stamp (Smith Rubber Stamps & Seals, Columbia, SC) which was photographed after use in the bottom of the enclosure in Figure 3.5. The stamp was designed by adapting artificial fingerprint artwork (Figure 3.6) that was purchased from shutterstock.com (Image ID: 180872426). The final stamp is 51 x 33 mm in size, which is approximately 50% larger than a natural fingerprint; the size was chosen as the minimum that allowed the rubber stamp to be commercially fabricated with preserved ridge detail. To form the transfer prints on fabrics, the face of the stamp

was completely wetted with rat's blood by pressing the stamp into a dish containing a thin layer of fresh rat blood, and then pressed once onto the surface of the cotton 899 fabric sample. At the time of these experiments the bloodstains had dried and aged in air for 14 months. Thermographic measurements of the thermal response of this sample to the exposure of water vapor were made twice: once pre-silanization, and once post-silanization.

Figure 3.6. Left: Artificial fingerprint artwork. This pattern was used to create a rubber stamp as described as in the text. Right: The custom rubber stamp used to create the transfer prints.

The visible light images of the transfer prints (Figure 3.4) show that on the right edge of the whole blood transfer print, the blood did not maintain the ridge structure after it was stamped. The fused ridges were produced while transferring the blood to the fabric using the stamp, and are not a defect of the stamp itself, nor an artifact of steam thermography.

3.2.2 SOLVENTS

Nine solvents are used in the solvent exposure study, across a range of polarities, which are listed in Table 3.1. The relative polarities listed in Table 3.1 are extracted from Reference 15, and are values on the normalized E_T^N scale.[15] This scale is a measure of polarity based on spectroscopic absorbance peak shifts of a variety of probe dyes. It is given relative to tetramethylsilane (TMS) and water as the two extreme ends of solvent polarity. Cyclohexane is very near to the same polarity as TMS, having a relative polarity of 0.006, and represents the non-polar extreme in the scale of solvents used in this study. Water is used as the polar extreme (having a value of 1 on the scale). The nine solvents used are a representative sampling of polarities throughout the scale, meaning each sample fabric is exposed to the full range of the E_T^N scale without large interpolations within the scale. The solvents are exposed to the fabric sample array in the order in which they are listed in Table 3.1.

Table 3.1. Solvents used in the solvent exposure study. The solvents are exposed to the fabric sample array in the order in which they are listed. Relative polarity values were extracted from Reference 15.

Solvent	Relative Polarity
Water	1.000
Methanol	0.762
Toluene	0.099
Acetonitrile	0.46
Cyclohexane	0.006
Ethanol	0.654
Chloroform	0.259
Acetone	0.355
Dichloromethane	0.309

3.2.3 SILANIZATION

The cotton sample used in this study was subject to this procedure 2 days after the thermography measurements of the sample under vacuum during exposure to water vapor (referred to as the pre-silanization measurements). Trimethylmethoxysilane (TMMS) (99% purity, purchased from Sigma Aldrich, CAS no 1825-61-2, S. Louis, MO, USA) was used as purchased as the silanization agent in the cotton silanization study. The sample was positioned horizontally over an open dish of TMMS, with the bloodstained face towards the dish, as the TMMS was heated to a gentle boil (to prevent splashing of the TMMS) in an enclosed 65% RH environment. The boiling point of the TMMS is 58 °C, indicating that the temperature reached during the silanization process is not high enough to adversely affect the sample fabric or bloodstain. The sample was exposed to the TMMS in this way for 2 hours. The fabric sample was stored in air for one week prior to the post-silanization measurements under vacuum.

3.2.4 VAPOR EXPOSURE IN VACUO

Fabric samples are exposed to solvent vapors using a vacuum chamber apparatus, a diagram of which is shown in Figure 3.7. The apparatus consists of a rotary vane vacuum pump (Varian, Palo Alto, CA, model DS-402) connected to a pneumatically-actuated valve (Varian, Palo Alto, CA, model L9181613). These components are then connected to a manually-actuated 1” aluminum block valve (Varian, Palo Alto, CA, model L9180302) and thermocouple sensor vacuum gauge (Dunaway Stockroom, Corp., Fremont, CA, model DST-531), which measures the pressure inside the chamber during operation. The sample chamber is constructed from 2” walls of laminated acrylic.

The sample is imaged through a 1” wide, 0.118” (3 mm) thick zinc selenide window by a thermal camera described below in the Thermography section of this chapter. The

camera was positioned approximately 1 ft. from the sample and 1" from the window. A photograph of the chamber, the ZnSe window assembly attached to the chamber, and the infrared camera is shown in Figure 3.8.

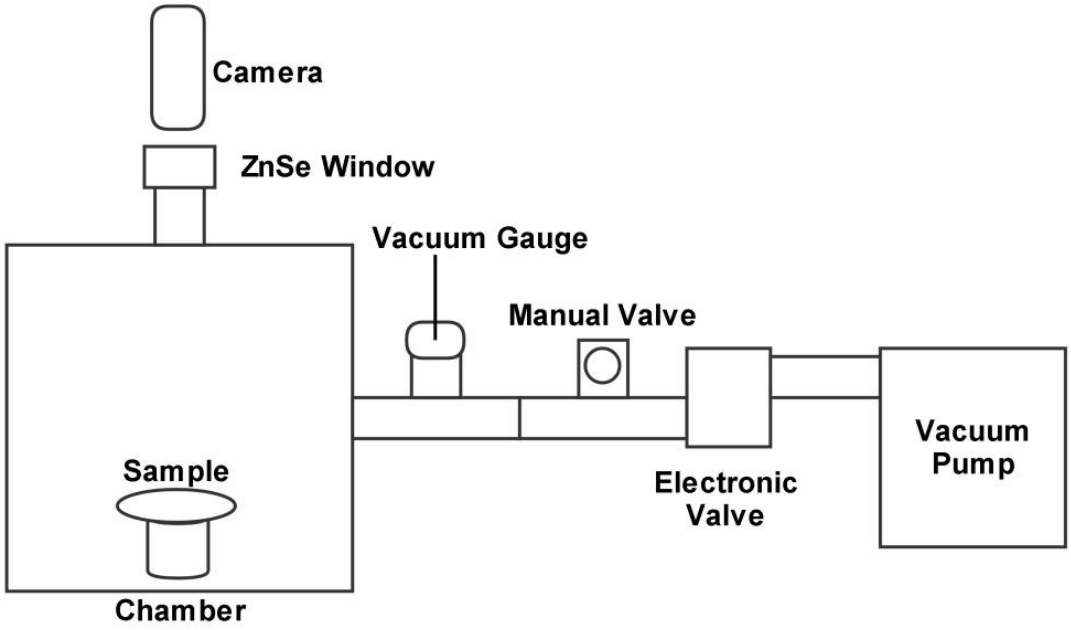

Figure 3.7. Diagram of the apparatus used to introduce vapor to fabric samples in the solvent exposure and cotton silanization studies. Briefly, a vapor is introduced to a sample via a sponge loaded with 3 mL of solvent placed into the void space of the manual valve. After the sample has equilibrated at vacuum conditions, the sample is exposed to the vapor by opening the manual valve for the duration of a thermographic recording.

Vapor exposure using the apparatus depicted in Figure 3.7 is performed as follows. After securing the sample inside of the chamber and then sealing the chamber, the vacuum pump is engaged to decrease the chamber pressure to 100 mTorr. A sponge loaded with 3 mL of deionized water (for the bloodstained acrylic and silanized cotton samples) or one of the nine solvents listed in Table 3.1 (for the solvent exposure study) is placed into the void space inside of the manually-actuated valve, the valve is re-sealed, and opened to vacuum for approximately one second before again re-sealing the valve.

This was done to purge atmospheric gases from the valve void space, leaving only water or solvent vapor. The chamber is then returned to 100 mTorr.

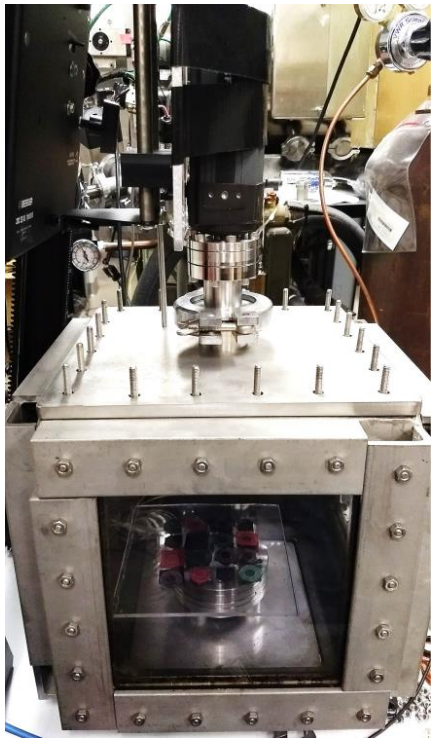

Figure 3.8. The acrylic-walled vacuum chamber apparatus used in the solvent exposure study and the cotton silanization study. A ZnSe window is pictured connected to the top of the chamber body, directly below a FLIR 315A thermal imaging camera.

While the pressure in the chamber is being reduced, and for a short while after the chamber reaches 100 mTorr the sample is not at thermal equilibrium, likely due to desorption of water and gasses trapped in the fabric. After the sample reaches thermal equilibrium with the chamber (approximately 30 minutes), the vacuum pump is disengaged, and the sample is exposed to vapor by opening the manually-actuated valve containing the sponge. After a measurement is completed, the vacuum pump is returned to normal operation, and the manually-actuated valve is closed. The pressure in the chamber at the end of each measurement is 10 Torr.

3.2.4 THERMOGRAPHY

Thermographic images were recorded with a FLIR Systems A315 microbolometer-based camera (16 bit digitization, 240 x 320 pixel resolution, 30 Hz frame rate) operating in signal linear mode using an interface developed in-house in the LabVIEW 2013 programming environment (National Instruments, Austin, TX). Once the sample was allowed to equilibrate as described above, an 80 second long recording (2400 image frames) of the sample was acquired. For the solvent exposure study, after a recording is completed and the operation of the vacuum pump is resumed, another 80 second recording is initialized to record the thermal response of the sample fabrics as the solvent is removed from the chamber. Therefore, there are two recordings of each sample fabric per solvent: one during exposure (adsorption of the solvent) and one during the solvent removal from the chamber (desorption of the solvent).

3.2.6 IMAGE PROCESSING

Thermographic recordings are processed using MATLAB R2012b (The MathWorks, Inc., Natick, MA). For each recording, the mean signal intensity of the first 200 frames of the recording per pixel (the average image of the first 200 frames) is subtracted from each frame. This removes features from recording that are static in signal intensity with respect to time, such as the chamber, the flange of the lens attachment on the chamber, sample holder, and also the reflection of the camera body.

The sample area within each polymer ring of the fabric sample array used in the solvent exposure study are each averaged in each recording, such that a single mean signal intensity value represents the measurement of single sample in a single frame. The mean signal intensity for frames 1000 to 1500 (33 to 50 seconds into the recording) are also averaged such that for each of the twelve fabric samples, a single mean signal

intensity value represents the measured thermal response of the adsorption/desorption of a given solvent on a sample fabric in these conditions for an entire recording. The difference in the signal intensity values for a whole blood stain and a blank fabric for each fabric are then calculated as a representation of the chemical contrast enhancement of a bloodstain on a fabric provided by each solvent for that fabric. The MATLAB code used in this processing is provided in Appendix A.

Recordings of the cotton 899 fabric sample used in the silanization study are processed in the same way as the solvent exposure study recordings. The thermal responses of the fabric and bloodstain of the whole blood print, and the chemical contrast calculations for these areas of the sample in the pre-silanization measurement are compared to the thermal responses of the fabric and bloodstain of the whole blood print, and the chemical contrast calculations for these areas of the sample in the post-silanization measurement. The MATLAB code used in this processing is also provided in Appendix A.

3.3 Results and Discussion

3.3.1 Bloodstained Acrylic Fabric

The right panel of Figure 3.9 shows an image (post-processing) from the thermographic recording of the bloodstained acrylic 917 sample during the exposure to water vapor while *in vacuo*. This image shows strong chemical contrast between the stain and fabric as a direct result of the exposure of water vapor in isothermal conditions.

Figure 3.10 shows the signal intensity increase of dried blood on acrylic fabric (red) and unstained acrylic fabric (purple) after the exposure of the bloodstained acrylic sample to water vapor *in vacuo*. The first ~200 frames were averaged and the average image of

those frames was subtracted from the values of every frame in the recording, resulting in values close to zero for the frames prior to the exposure of water vapor.

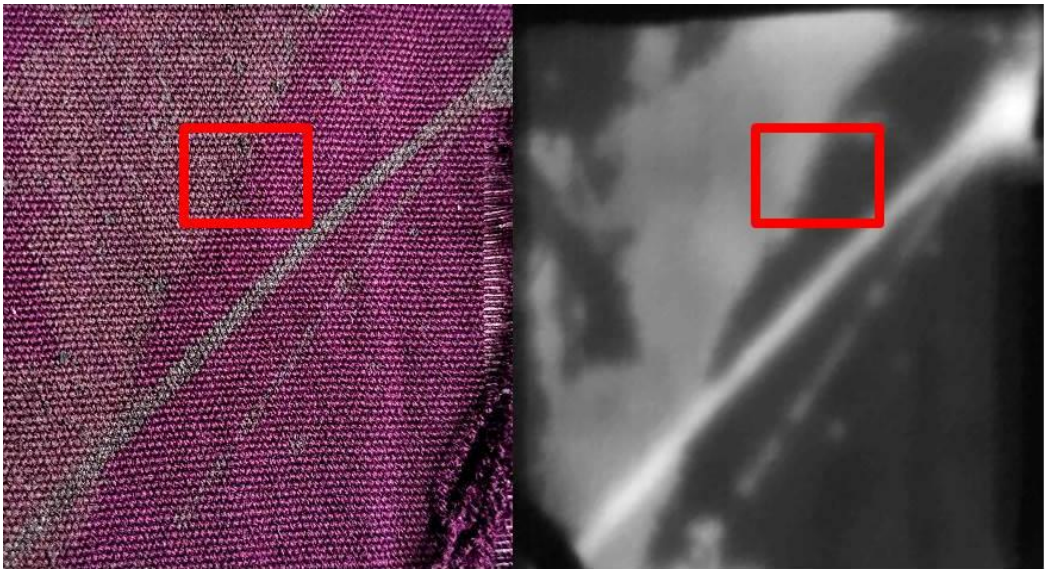

Figure 3.9. Left: a visible light photograph of the bloodstained acrylic sample. Right: a post-processed image from a thermographic recording of the bloodstained acrylic during the exposure of the sample to water vapor while *in vacuo*. Signal intensity values for this measurement are extracted from the bloodstained and unstained fabric areas within the red outline.

The signal intensity increase of acrylic fabric during this exposure is close to 400 counts, which corresponds to an approximate apparent temperature increase of 1.7 °C. The signal intensity increase of the bloodstained area during this exposure is close to 900 counts, which corresponds to an approximate apparent temperature increase of 3.9 °C. The difference in the two curves shown in Figure 3.10 is shown in Figure 3.11, and represents the increase in contrast between the two surfaces.

The differential signal intensity increase between the bloodstained areas and the unstained acrylic fabric reaches a peak of 613.2 counts at 511 frames into the recording, which is nine seconds after the exposure of the sample to the water vapor begins to result

in a thermal response (nine seconds from the cut-on of the contrast increase to the peak contrast). A difference of 613 counts corresponds to an approximate apparent temperature

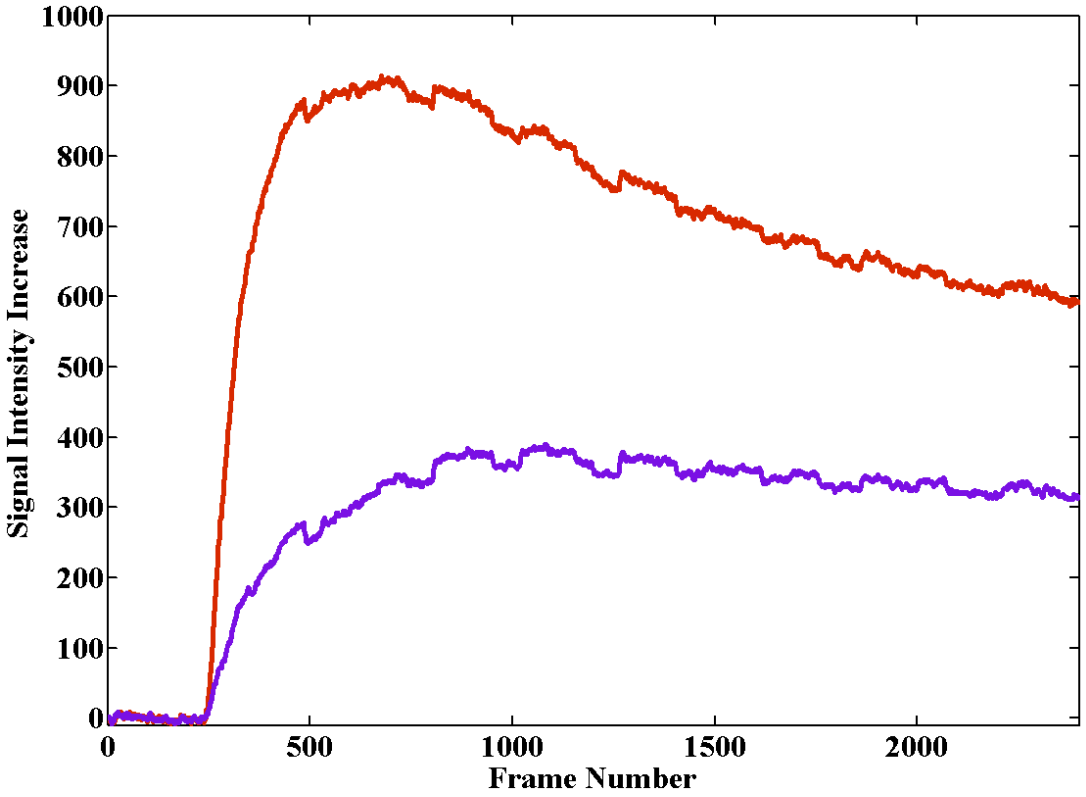

Figure 3.10. The signal intensity increase of dried blood on acrylic fabric (red) and acrylic fabric (purple) after exposure of the bloodstained acrylic sample to water vapor *in vacuo*.

difference of 2.7 °C. This is greater than the difference between the maximum signal intensity increases of each of the bloodstained area of the sample and the unstained area of the fabric. This is because the acrylic fabric reaches the peak of its thermal response much later than the bloodstained area of the sample. The maximum signal intensity increase of the acrylic fabric takes place nearly 30 seconds after the sample initially measures a thermal response, while the bloodstained area reaches its peak signal intensity about 15 seconds after exposure.

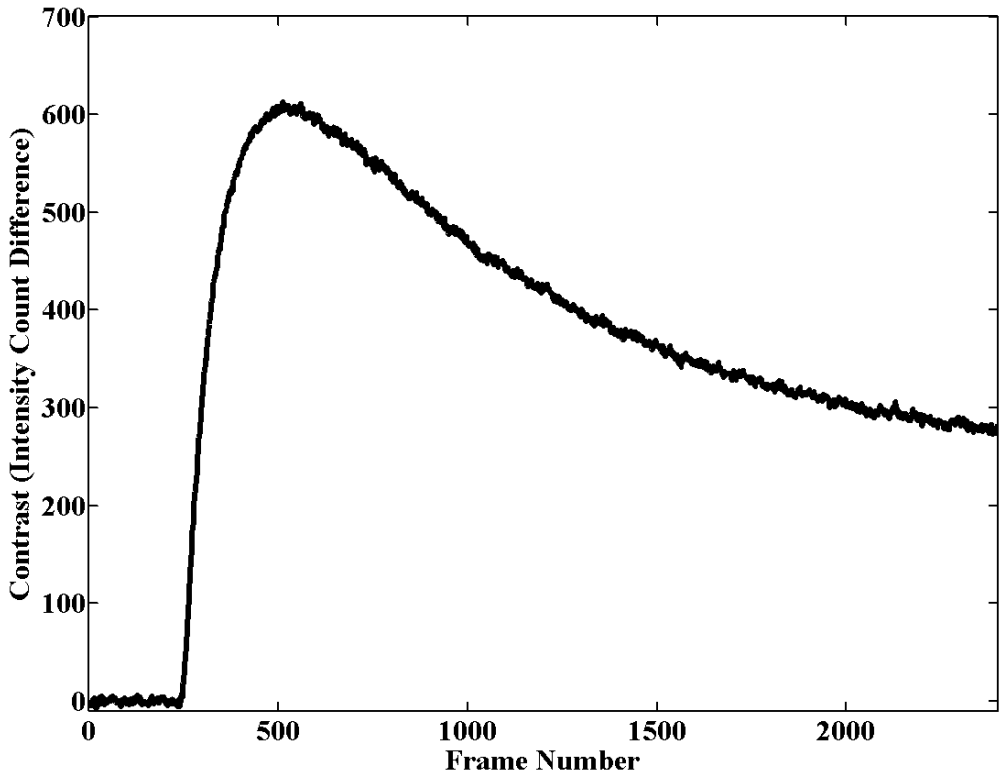

Figure 3.11. The differential signal intensity increase of dried blood on acrylic fabric and acrylic fabric after exposure of the bloodstained acrylic sample to water vapor *in vacuo*. This differential intensity is a measure of the contrast between the two surfaces during exposure to water vapor.

The chemical contrast enhancement in this measurement cannot be fully or partially a result of condensation, as the pressure of water vapor in the chamber only rises to 10 Torr over the course of the recording, while saturation conditions require 24 Torr of vapor pressure for water vapor to condense at 25 °C. Additionally, this means that no water vapor can condense into droplets in transit to the sample. In this measurement, there are no nearby sources of heat to radiantly transfer heat to the sample, and the water vapor is never warmed, which excludes any warming of the sample through convective means.

The two remaining proposed mechanisms that may contribute to the chemical contrast enhancement observed in this measurement are water vapor adsorption, and a

differential change in thermal emissivity. While there may not be a way to measure the thermal response of a surface during adsorption and also prevent a change in the surface's emissivity (provided that the emissivity is indeed changing), it is possible to measure the surface's altered thermal emissivity without also measuring the thermal response of adsorption on a surface. The thermal response that is observed requires a greater amount of adsorption to a surface than desorption (or vice versa), such that the two processes are at disequilibrium. However, if the two processes are at equilibrium, the net heat exchange is zero, there is no observed thermal response, and the surface is in thermal equilibrium with its surroundings (all else equal). This is the typical case during conventional thermographic imaging of a surface, and is the case for samples in this chapter prior to vapor exposure. The implication of this is that the change in thermal emissivity caused by a change in amount of adsorbed moisture can be measured at equilibrium conditions. By varying the amounts of moisture adsorbed on a fabric sample and/or bloodstained fabric sample, the change in emissivity as a function of adsorbed moisture can be measured, and the contribution of the emissivity change to the chemical contrast enhancement can be determined. Chapters 4 and 5 discuss this in further detail.

3.3.2 Solvent Exposure Study

Results of the exposure of acrylic, nylon, cotton, and polyester fabrics stained with whole blood, 10X dilute blood, and no blood to nine solvents are expressed as the signal intensity change relative to the signal intensity of the sample at thermal equilibrium prior to exposure. Table 3.2 shows the signal intensity change of the samples during the adsorption of each solvent, and Table 3.3 shows the signal intensity change of the samples during the desorption of each solvent.

Table 3.2. The signal intensity change of each sample during adsorption of each vapor.

	Polyester			Acrylic			Nylon			Cotton		
Solvent	Whole	10X	Blank	Whole	10X	Blank	Whole	10X	Blank	Whole	10X	Blank
Water	1327	217	108	1504	426	347	2025	646	701	1843	1637	1591
Methanol	112	42	28	196	46	41	239	80	85	224	107	82
Toluene	38	20	19	46	35	33	51	25	29	80	85	57
Acetonitrile	93	23	9	132	28	23	135	33	34	156	92	74
Cyclohexane	1	-6	-12	7	-4	-3	13	-6	-2	16	4	1
Ethanol	85	44	39	130	54	49	151	60	66	146	109	91
Chloroform	22	-3	-7	37	0	0	49	10	7	41	26	24
Acetone	44	13	12	68	22	20	77	27	29	78	57	50
Dichloromethane	16	1	1	24	5	3	23	8	5	31	18	16

The thermal response (the signal intensity change) of the samples to the exposure of water vapor is much greater (an order of magnitude in many cases) than the thermal response of the sample to any other solvent tested. The thermal responses of the whole blood samples are greater than the thermal responses of the corresponding blank fabric samples in every instance. The thermal responses of most 10X dilute samples are not significantly different than the thermal responses of blank fabric samples. This is based on an estimation of a 'significant difference' as a change in the signal greater than the signal required to observe a change greater than the NETD of the camera. The NETD of the camera is 0.05 °C, and a change in signal intensity of ~230 intensity units is approximately equivalent to observing a change in temperature of 1 degree Celsius. This means that the NETD of 0.05 °C is equivalent to a change in signal intensity of 11.5. Therefore, any reported signal intensity changes, or differences in signal intensity of less than 11.5 will be regarded as not significant.

The approximate apparent temperature changes of the whole blood samples exposed to water vapor range from 5.8 to 8.8 °C. This blank acrylic, polyester, and nylon fabrics each show a markedly smaller thermal response during water vapor adsorption. However, the thermal response of the blank cotton sample exposed to water vapor is of a similar

magnitude to that of the bloodstained cotton samples. While this is much larger of a response than the other three blank fabrics demonstrate, it is in good agreement with the trend in the equilibrium moisture content of the fabrics at 65% RH.[3] The coefficient of determination for a simple linear regression of the thermal response of each blank fabric exposed to water vapor (values from Table 3.2) and the equilibrium moisture content of the fabrics at 65% RH (extracted from page 188 of Reference 3) is 0.993.

Table 3.3. The signal intensity change of each sample during desorption of each vapor.

	Polyester			Acrylic			Nylon			Cotton		
Solvent	Whole	10X	Blank	Whole	10X	Blank	Whole	10X	Blank	Whole	10X	Blank
Water	-3168	-339	-170	-2681	-758	-610	-3115	-1146	-1088	-3154	-2911	-2784
Methanol	-204	-59	-42	-348	-83	-60	-412	-154	-167	-377	-206	-154
Toluene	-34	-22	-18	-49	-30	-38	-55	-18	-22	-73	-78	-52
Acetonitrile	-100	-37	-32	-160	-53	-44	-164	-53	-56	-175	-122	-94
Cyclohexane	3	17	22	-5	12	12	-12	10	12	-12	-4	2
Ethanol	-93	-37	-31	-151	-55	-46	-155	-59	-65	-162	-119	-99
Chloroform	-39	-14	-15	-60	-22	-16	-61	-26	-27	-61	-44	-41
Acetone	-40	-12	-9	-69	-23	-19	-76	-24	-28	-78	-56	-46
Dichloromethane	-40	-25	-26	-51	-31	-29	-51	-29	-28	-56	-47	-42

The results of the desorption of each solvent from each sample are similar to the adsorption results in terms of relative trends between samples and solvents. However, most thermal responses in the desorption measurement are larger in magnitude. This may not be a result of the difference between the two processes, as the changes in pressure when a sample is exposed to a solvent compared to when a solvent is pumped from the chamber is not the same. In order to directly compare thermal responses of samples during the adsorption and desorption processes, it would be necessary to conduct the measurements while undergoing the same rate of change in pressure over time across both measurements, except that the rate would be reversed from one process to the next. This factor was not controlled in these experiments, and so the comparison between the

overall magnitude of thermal responses of the adsorption and desorption measurements can only be observational.

Table 3.4. The difference in the signal intensities of the blood-stained fabric samples and the blank fabric sample during the adsorption of each solvent.

	Polyester		Acrylic		Nylon		Cotton	
Solvent	Whole	10X	Whole	10X	Whole	10X	Whole	10X
Water	1219	109	1157	79	1324	-55	251	45
Methanol	84	14	155	5	154	-6	142	26
Toluene	19	1	14	3	22	-3	22	28
Acetonitrile	84	14	109	5	101	0	82	18
Cyclohexane	13	6	11	-1	15	-4	15	3
Ethanol	45	4	81	5	85	-6	55	18
Chloroform	28	4	37	0	43	3	17	2
Acetone	31	1	48	2	49	-2	28	7
Dichloromethane	15	0	21	2	19	3	15	2

As a measure of contrast, the differences between the signal intensity change values reported in Table 3.2 for adsorption of solvents on the whole blood and blank fabric samples and also between the 10X dilute bloodstains and blank fabric samples for each fabric type and each solvent are shown in Table 3.4. Additionally, the differences between the signal intensity change values reported in Table 3.3 for desorption of solvents on the whole blood and blank fabric samples and also between the 10X dilute bloodstains and blank fabric samples for each fabric type and each solvent are shown in Table 3.5. In both cases, the contrast between 10X dilute bloodstains and their respective blank fabrics is less than 11.5 intensity units, indicating that the contrast for these samples is not high enough to be considered significant. In the case of the adsorption measurements, besides during water vapor adsorption, the 10X dilute bloodstain samples showed insignificant contrast in all of the acrylic and nylon measurements, and in all of

the polyester measurements except for methanol and acetonitrile (in which the contrast is small enough that it is still arguably insignificant). Small degrees of contrast are observed for the 10X dilute stain on cotton for water, methanol, toluene, acetonitrile, and ethanol. Of those solvents, toluene is surprising as it is very non-polar, yet created a similar amount of contrast as methanol, which is very polar. In the case of the desorption measurements, the 10X dilute bloodstain samples for polyester, acrylic, and nylon all showed insignificant amounts of contrast for every solvent except water and methanol.

Table 3.5. The difference in the signal intensities of the blood-stained fabric samples and the blank fabric sample during the desorption of each solvent.

	Polyester		Acrylic		Nylon		Cotton	
Solvent	**Whole**	**10X**	**Whole**	**10X**	**Whole**	**10X**	**Whole**	**10X**
Water	-2998	-169	-2071	-148	-2026	-58	-370	-126
Methanol	-162	-17	-289	-23	-246	13	-223	-51
Toluene	-16	-4	-11	7	-32	4	-22	-26
Acetonitrile	-68	-4	-116	-9	-108	3	-81	-28
Cyclohexane	-18	-5	-18	0	-24	-2	-14	-6
Ethanol	-62	-6	-105	-9	-90	6	-63	-19
Chloroform	-24	1	-43	-6	-34	1	-20	-3
Acetone	-32	-3	-50	-4	-48	3	-32	-10
Dichloromethane	-13	2	-22	-3	-23	-1	-15	-6

The whole blood stained samples for each fabric showed significant contrast (greater than 11.5 intensity units) for every solvent except in the case of cyclohexane adsorption on acrylic and toluene desorption on acrylic. A plot of the contrast between whole blood stained samples and blank samples for each fabric against the relative polarity of each solvent except water is shown in Figure 3.12. The trend of increasing contrast with increasing relative polarity is in good agreement except for a relatively high contrast observed during the exposure of acetonitrile to the samples. Water is not shown in Figure

3.12 due to the scale of the contrast observed with the exposure of water vapor to the samples.

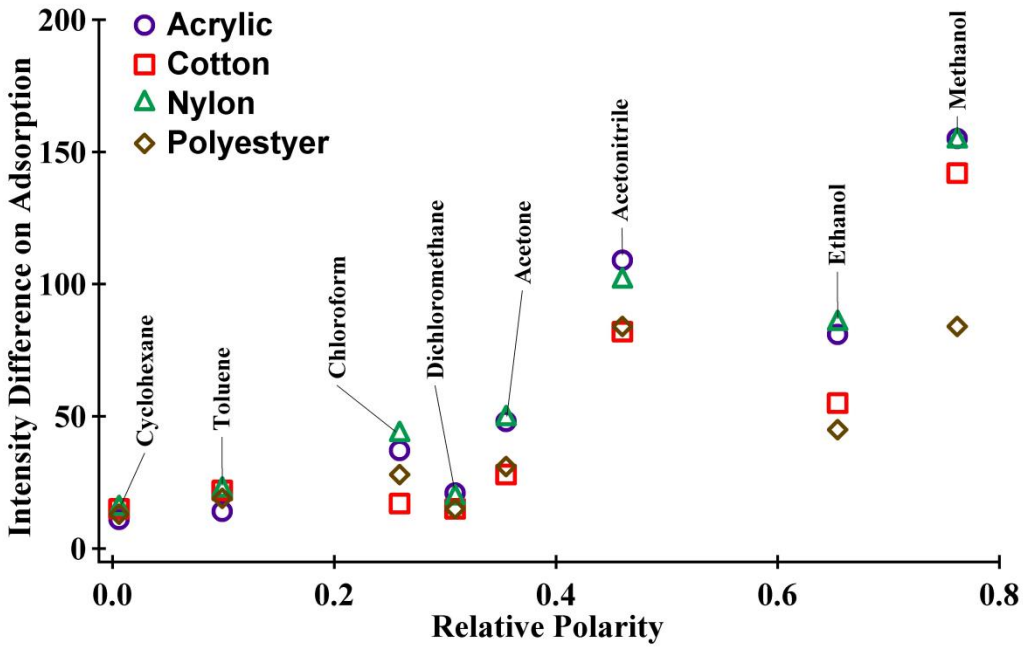

Figure 3.12. A plot of the contrast between the whole-blood stained sample and blank sample for each fabric during vapor adsorption (represented as the signal intensity difference in the two samples) vs the relative polarity of each solvent (based on the E_T^N scale). Results of the exposure of the samples to water vapor are not included in this plot, but are given in Table 3.4.

Figure 3.12 shows that for a given solvent, there is generally less contrast for whole blood stains on polyester and/or cotton than for whole blood stains on other fabrics. This is true for all the solvents shown in Figure 3.12 except the two least-polar solvents (cyclohexane and toluene), which show little difference in contrast values from fabric to fabric. Of the four fabrics, the cotton and polyester have the greatest and smallest specific surface areas, respectively, so the trend of contrast magnitude for a given solvent in Figure 3.12 does not appear to be based on surface area.[8] However, the common factor between polyester and cotton are the oxygen-based adsorption sites (hydroxyl for cotton,

carbonyl for polyester), whereas the adsorption sites for acrylic and nylon are nitrogen-based (nitrile for acrylic, and amide for nylon).

3.3.3 Cotton Silanization Study

Thermographic recordings of the whole blood stained transfer print on the cotton 899 fabric show contrast in both the silanized and un-silanized samples. However, the 10X dilute blood transfer print and the whole blood spatter stains are not visible in the recordings, and intensity values for those bloodstains are not reported. The results of the solvent study indicate that contrast between the 10X dilute transfer print and the blank cotton fabric is not significant. Figure 3.13 shows the whole blood transfer print on the silanized cotton 899 sample (left) along with a processed thermographic image of the transfer print.

Spatter stains of whole blood on the cotton fabric are not visible, although the transfer print of whole blood is visible. A possible reason why this is the case is that the small droplets of blood that contacted the cotton surface while the blood was first applied and wet did not dry on top of the fabric surface, but were instead wicked into the fabric structure, in effect diluting the blood. The lack of contrast for the spatter stains is consistent with regions of the whole blood transfer stains with are not visible in the photograph or thermographic images as amounts of blood that were small enough amounts to be wicked into the fabric structure. This implies that the stains visible in the photograph and thermographic images are areas of the stains in which the amount of blood was large enough to wet the cotton material without wicking all of the blood in that

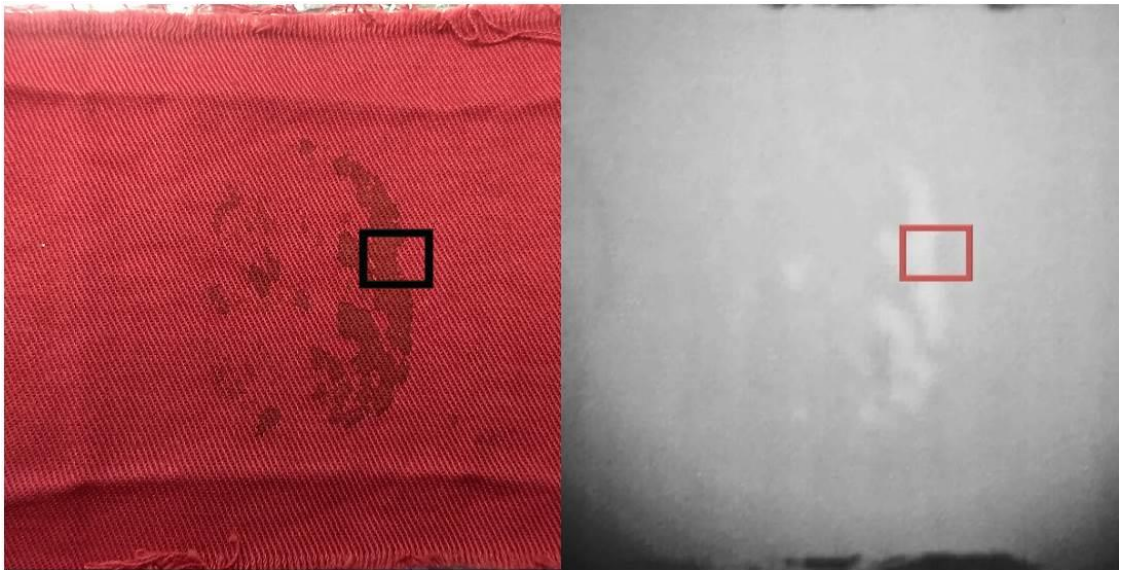

Figure 3.13. Left: a visible light photograph of the bloodstained cotton 899 sample. Silanization produced no visible changes to the sample. Right: a post-processed image from a thermographic recording of the silanized bloodstained cotton fabric sample during the exposure of the sample to water vapor while *in vacuo*. Signal intensity values for this measurement are extracted from the bloodstained and unstained fabric areas within the outlined area.

area, which left some amounts of blood on the fabric surface to dry. These dried surface stains appear to be the only stains visible to the eye and achieving significant contrast during thermal imaging. It is likely then, that the detection of dried blood on cotton fabrics is not dependent on the concentration of the blood before contacting the fabric, but on the concentration of the blood left on the surface after it has wetted the fabric. It is possible then that there is an amount of blood needed to wet a given fabric area that acts as a required threshold volume. Volumes of liquid whole blood greater than the threshold volume for a given area of fabric will then become detectable during steam thermography. The dried whole blood stains visible in Figure 3.13 appear to meet this criterion.

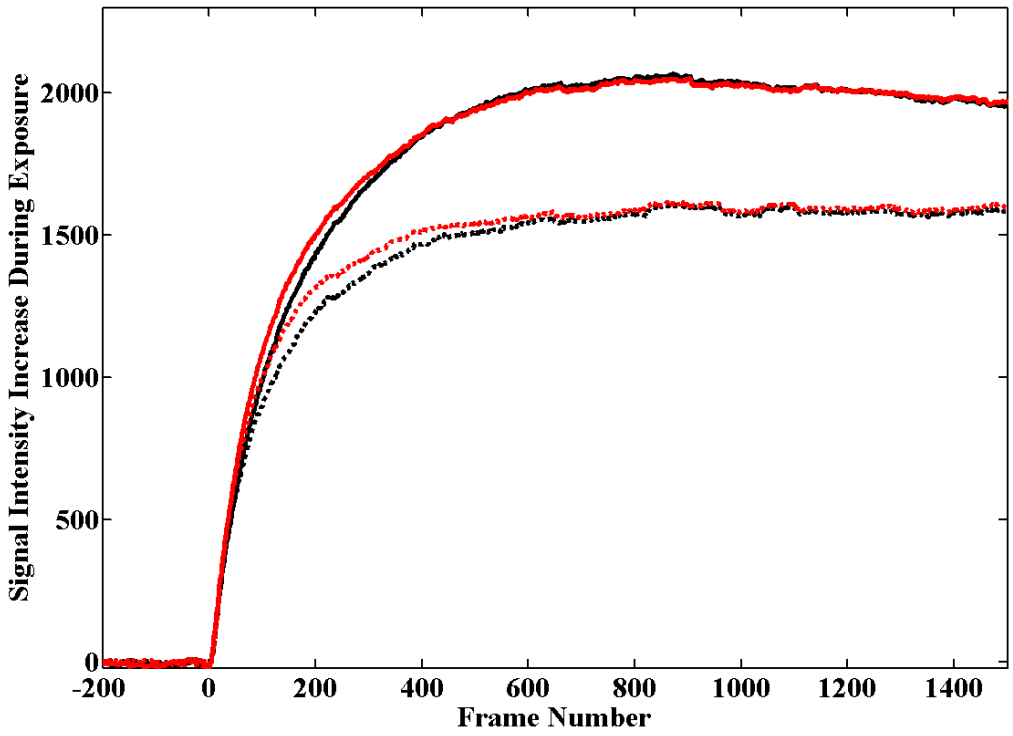

Figure 3.14. The signal intensity increase of the whole blood transfer print area (red) and blank cotton 899 fabric area (black) for the cotton sample before silanization (solid lines) and after silanization (dotted lines). The signal intensity curves are shown relative to the 'cut-on' of thermal response as the zeroth frame, and the average signal intensity of the first 200 frames of each recording is subtracted from the entire curve to establish the origin point of each signal intensity curve as ~0 intensity, 0 frames.

The signal intensity increase of the whole blood transfer print area and blank fabric area is shown in Figure 3.14 for the cotton sample before silanization (solid lines) and after silanization (dotted lines). The signal intensity curves are shown relative to the 'cut-on' of thermal response for each curve as the zeroth frame. The overall intensity of the thermal responses of the post-silanization measurements is lower than the overall intensity of the thermal responses of the pre-silanization. This is consistent with a lower amount of water vapor adsorption due to the silanization.

There is a slight divergence between the whole blood transfer print response and blank fabric response during both the pre-silanization measurement and post-silanization measurement. The difference in the thermal responses of the whole blood transfer print and the blank cotton fabric are shown in Figure 3.15 for both the silanized (gray) and un-silanized measurements (black).

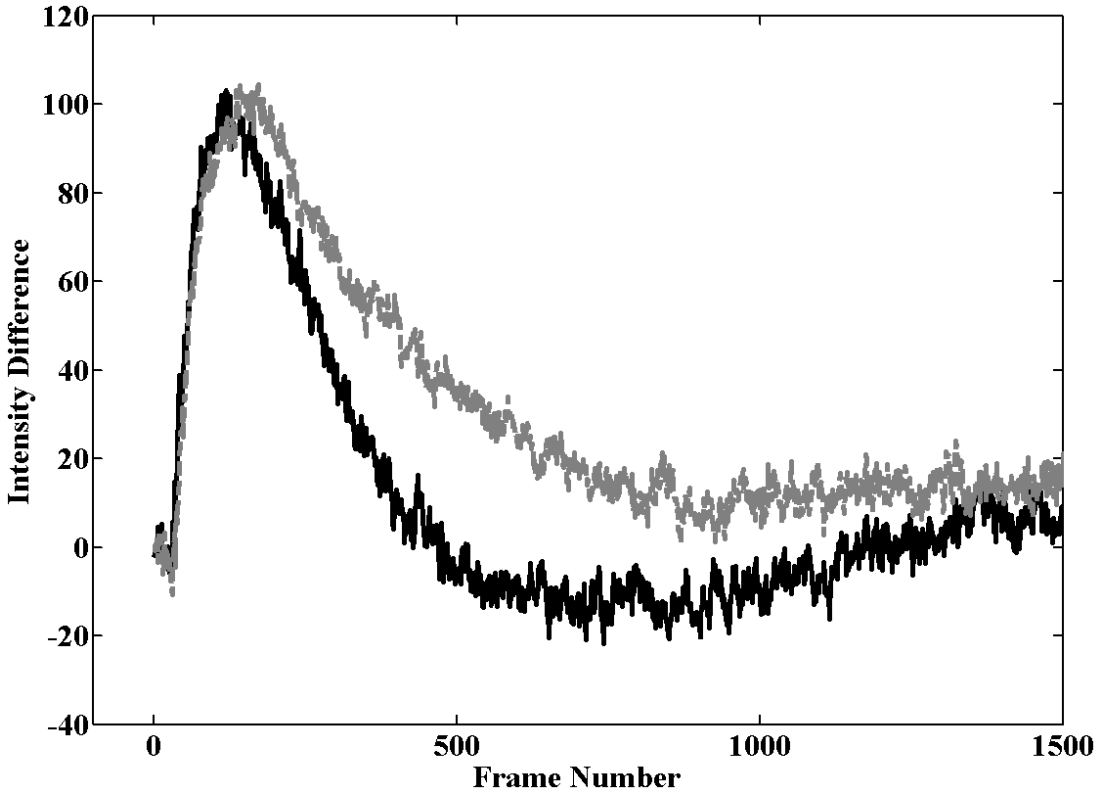

Figure 3.15. The signal intensity difference (contrast) between the whole blood transfer print on cotton and the blank cotton fabric, before silanization (black) and after (gray). Pre- and Post-silanization measurements show similar amounts of overall contrast, however, post-silanization measurements show an enhanced contrast for more than twice the amount of time compared to pre-silanization measurements.

The magnitude of contrast between the two measurements is almost the same, and reaches a maximum very close in time to each other (a 1-2 second difference to peak contrast). However, the contrast enhancement of the sample post-silanization is greater

than the NETD (as estimated above as a difference in signal intensity of 11.5 counts) for 760 frames (25.3 seconds), compared to 353 frames (11.8 seconds) for the pre-silanization measurement. This indicates that the silanization of the bloodstained cotton sample had the effect of slowing the adsorption process. Based on the lower overall magnitude of the thermal response of the sample to the exposure of water vapor, the slowing of the process is in addition to decreasing the overall amount of vapor being adsorbed.

3.4 Conclusions

This work is motivated by an interest in a better understanding of the mechanism of chemical contrast enhancement in a steam thermography measurement. Thermography measurements of samples of dried blood on fabrics *in vacuo* during an exposure to water vapor are presented, along with measurements of the exposure of eight other solvent vapors to the fabrics and bloodstained fabric samples. This work provides evidence that the chemical contrast observed during a steam thermography measurement is a direct result of the adsorption of water vapor. While the results reported in this study do not address the effect of a differential change in thermal emissivity possibly enhancing chemical contrast, a method of measuring the impact of a differential change in a thermal emissivity is proposed.

REFERENCES

1. M. Suzuki. Adsorption Engineering. New York: Elsevier, 1990.

2. F. L. Slejko. Adsorption Technology: A Step-by-Step Approach to Process Evaluation and Application. Boca Raton, FL, USA: CRC Press, 1985.

3. W. Morton, J. Hearle. Physical properties of textile fibers. Philadelphia: Woodhead Publishing, 2012, p. 178-228.

4. C. A. S. Hill, A. Norton, G. Newman. The water vapor sorption behavior of natural fibers. *J. Appl. Polym. Sci.* 2009; 112: 1524-1537. https://doi.org/10.1002/app.29725

5. J. Stencl, J. Gotlhardova, P. Homola. Equilibrium moisture content of dried blood flour in the temperature range of 20 – 50 °C, *Drying Technol*. 1998; 16: 1729-1739.

6. R. A. M. Delaney. Protein concentrates from slaughter animal blood. II. Composition and properties of spray dried red blood cell concentrates. *Int. J. Food Sci. Technol.* 1977; 12: 355-368.

7. N. Laan, F. Smith, C. Nicloux, et al. Morphology of drying blood pools. *Forensic Sci. Int.* 2016; 267: 104-109. https://doi.org/10.1016/j.forsciint.2016.08.005

8. S. A. DeJong, Z. Lu, B. M. Cassidy, et. al. Detection limits for blood on four fabric types using infrared diffuse reflection spectroscopy in mid- and near-infrared spectral windows. *Anal. Chem*. 2015; 87: 8740-8747.

9. L. K. Lazzari, V. B. Zampieri, M. Zanini, et al. Sorption capacity of hydrophobic cellulose cryogels silanized by two different methods. *Cellulose* 2017; 24: 3421-3431. http://dx.doi.org/10.1007/s10570-017-1349-z

10. Y. Wang, M. Lieberman. Growth of ultrasmooth octadecyltrichlorosilane self-assembled monolaters on SiO2. *Langmuir* 2003; 19: 1159-1167.

11. M. Beaumont, M. Bacher, M. Opietnik, et al. A general aqueous silanization protocol to introduce vinyl, mercapto, or azido functionalities onto cellulose fibers and nanocelluloses. *Molecules* 2018; 23(6): 1-15.

12. B. M. Cassidy, Z. Lu, J. P. Martin, S. K. Tazik, K. W. Kellogg, S. A. DeJong, E. O. Belliveau, K. E. Kilgore, S. M. Ervin, M. Meece-Rayle, A. M. Abraham, M. L. Myrick, S. L. Morgan, A quantitative method for determining a representative detection limit of the forensic luminol test for latent bloodstains, *Forensic Sci. Int.* 2017; 278: 396-403.

13. F. Ramsthaler, J. Schlote, C. Wagner, J. Fiscina, M. Kettner, The ring phenomenon of diluted blood droplets, *Int. J. Legal Med*. 2016; 130: 731-736.

14. T. C. DeCastro, Forensic interpretation of bloodstains on fabrics, in *Forensic Textile Science* (ed. D. Carr): Woodhead Publishing, Cambridge, MA, 2017, p 127-167.

15. C. Reichardt. Solvatochromic dyes as solvent polarity indicators. *Chem. Rev.* 1994; 94: 2319-2358. https://doi.org/10.1021/cr00032a005

CHAPTER 4: MID-INFRARED EMISSIVITY OF NYLON, COTTON, ACRYLIC AND POLYESTER FABRICS AS A FUNCTION OF MOISTURE CONTENT[a]

4.1 INTRODUCTION

Numerous textile applications of infrared thermography can be found in the literature, including measuring energy dissipation during stretching, fabric radiant thermal conductivity, spreading of pyrolysis during combustion, and smoldering ignition in upholstery fabrics.[1-4] All of these thermographic measurement methods are dependent on the apparent emissivity of the measurement targets. Emissivities for a number of materials are given in literature, and those of some fabrics have been reported by Zhang et al. and Brown et al.[5-6]

This laboratory recently reported steam thermography for imaging stains on fabrics through contrast in the apparent fabric temperature immediately on exposure to water vapor.[7-8] In our report we identified possible mechanisms for the apparent temperature contrast, one of which was differential infrared emissivity of the fabric on exposure to moisture. Moisture uptake is known to affect other textile properties such as swelling, heat transport, electrical conductivity, and the perceived comfort of clothing.[9-15]

[a] Reproduced and modified from R. G. Belliveau, S. A. DeJong, N. D. Boltin, et al. Mid-infrared emissivity of nylon, cotton, acrylic and polyester fabrics as a function of moisture content. Text. Res. J. accepted for publication, 2019. Reproduced with permission from Sage Publishing.

Studies of soil provide precedent for a dependence of infrared emissivity on moisture content as several reports show that the emissivity of sand and soil increases with moisture content.[16-19] No such study has been reported to date for fabrics, however. Furthermore, different fabrics may show markedly different behaviors because they vary in ability to adsorb water depending on their chemical composition. Hydrophobic fabrics (e.g., polyester), for instance, adsorb no more than a percent of water by mass from air in moist conditions.[20] In comparison, hydrophilic textiles such as cotton may adsorb more than 14% water by mass from air in high humidity conditions.[21]

We report the emissivity of cotton, nylon, polyester, and acrylic fabrics used in our studies across a range of measured moisture concentrations from nearly zero to 90% relative humidity at a nominal temperature of 40 °C. We find that nylon and cotton, both of which adsorb significant amounts of moisture, show little change in emissivity with moisture content. Polyester adsorbs little moisture and also shows little change in emissivity. Acrylic fabrics, on the other hand, show ~10% increase in emissivity even though its adsorption of water is similar in magnitude to polyester. We also observed that the moisture content of all the fabrics as a function of humidity shows hysteresis, indicating slow kinetics for the loss of water on drying. The emissivity of acrylic fabric shows a direct relationship to its moisture content rather than the ambient humidity.

4.2 Experimental

4.2.1 Sample fabrics

The purple acrylic, brown polyester, green nylon, and red cotton fabrics used in this study have been the subject of several publications by this laboratory, and information about the properties of the fabrics and the fibers they are composed of, including the dyes

used for each fabric are provided in Table 1.1.[7-8, 22-31] Each fabric was commercially obtained undyed, and subsequently triple-dyed at North Carolina State University's Wilson College of Textiles in 2004. These four fabrics have previously been the subject of a number of spectroscopic measurements by this research group, and references to these measurements are given for each fabric sample separately in Table 1.1.

Because the cotton and nylon fabrics are twills, they have two distinct faces. One of the faces has warp threads that are the most prominent, while the other is dominated by weft threads. In both cases, however, the two types of threads contribute to the exposed surface. The warp-dominant side of the fabric was the face used in these measurements for both fabrics.

Each fabric sample is a 7.5 cm by 7.5 cm square, and two sheets of fabric are layered on top of one another in the sample assembly to ensure the fabric was optically dense. The dry mass of each fabric is 3.498 g for the acrylic, 2.935 g for the polyester, 3.971 g for the nylon, and 3.015 g for the cotton.

4.2.2 SAMPLE CONDITIONING

An apparatus built in-house was used to condition the fabrics prior to each measurement, shown in Figure 4.1. Air is supplied from the top right in the figure by an air compressor (Northern Tool + Equipment, Bursville, MN, model Northstar XQ1508VP), which passes through a moisture separator (W. W. Grainger, Lake Forest, IL, model Speedaire 4 GNL3) to remove oil and water droplets in the compressed air. The compressed air is then split into three streams.

In the figure, the rightmost filtered compressor stream is used as a source of 0% humidity air, and is passed into a drying column (Drierite Co., Xenia, OH, Drying Column model 26800) packed with 3Å molecular sieves (Sigma-Aldrich Corp., St. Louis, MO), then into a region heated to 40 °C where it meets a brass and bronze 3-way ball valve (Conbraco Industries Inc., Matthews, NC, model Apollo 70-603).

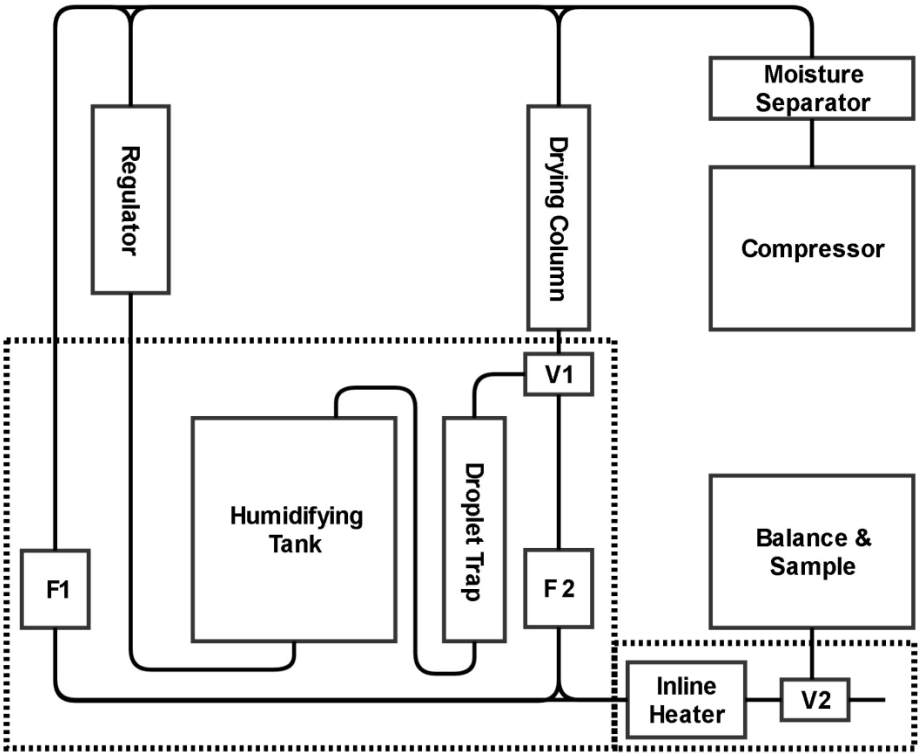

Figure 4.1. Diagram of the apparatus used to condition the samples at a set temperature and humidity. Compressed air is produced by the compressor (top right), then split into three streams. From left to right these are: a stream of room temperature air, a stream of heated air that is saturated with moisture, and a stream of heated air that has been dried to ~0% RH. These three streams are supplied to the sample chamber in controlled ratios to give a fixed humidity for a nominal temperature of 40 °C. The dashed-line box in the figure shows areas of the apparatus that are heated. More details are found in the text.

The center stream in the figure is used as a source of air saturated with moisture. The filtered compressor air stream is passed through a regulator (Fisher Scientific

International, Hampton, NH, model F5-50) into the heated (40 °C) region of the system, and then aspirated through a porous plastic frit into a sealed, heated tank of water. The air passes through the water, out the top of the tank, and then through an impingement-style droplet trap. The air is then passed to the same 3-way valve as the dry air.

Only one stream of these two streams of air coming to the 3-way valve, either dry or wet depending on the final humidity requirement, is passed to a flowmeter (King Instrument Co., Garden Grove, CA, model 75301112C17).

The leftmost stream of filtered air from the compressor with an intermediate level of moisture passes into the heated region of the system and through an identical flowmeter and combines with the air which was conditioned either dry or wet to produce a mixed sample with a controlled moisture content. This combined air stream beginning at 40 °C is then heated above 40 °C by the inline heater (Tutco-Farnam Custom Products, Arden, NC, model HT050) so that after cooling on the way to the sample compartment the temperature will be nominally 40 °C in the sample compartment. The moist gas at the elevated temperature leaves the inline heater, passes through another 3-way valve (identical to the other 3-way valve), and then to the sample chamber. The sample is maintained at constant humidity and temperature for 24 hours prior to a recording to give time for equilibration under a given condition. The 3-way valve directly before the sample chamber is then used to divert the air stream from the sample chamber during the 80 second measurement. Temperature, relative humidity (RH), and mass are recorded in the sample chamber.

Figure 4.2 shows the sample chamber, which includes a thin-film capacitance humidity sensor (Measurement Specialties Inc., Hampton, VA, model HTS2030SMD) that has a 1% relative humidity accuracy across a range of 0% to 100% humidity. Temperature inside the chamber is determined by thermal emission from a polytetrafluoroethylene (PTFE) reference inside the sample chamber. Instead of trying to keep a fixed temperature inside the chamber, the system was operated to maintain a fixed

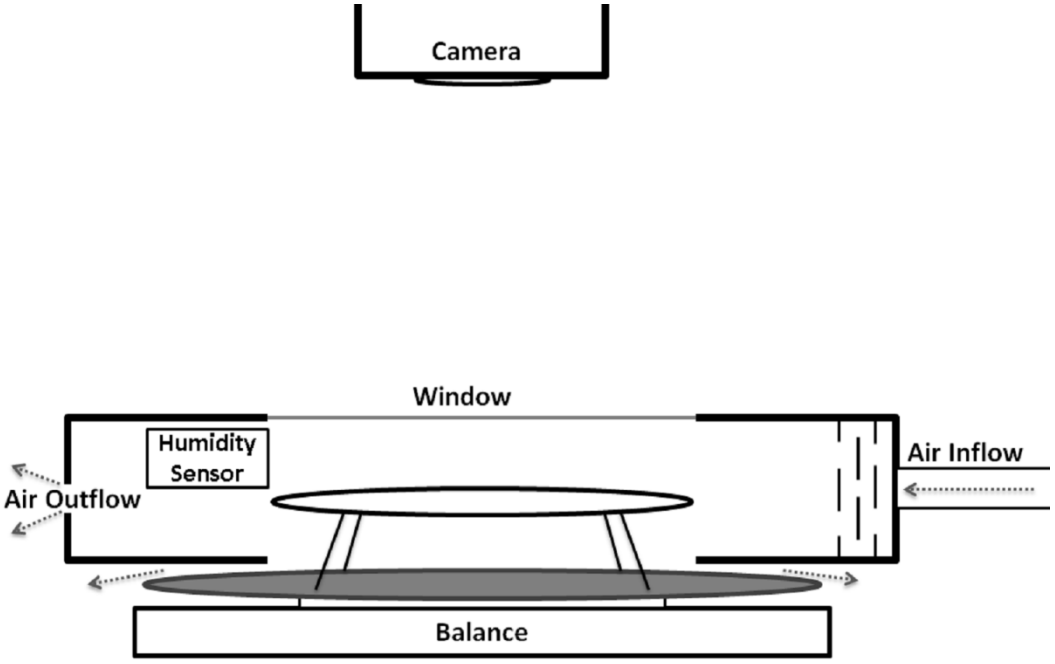

Figure 4.2. A representation of the balance and sample chamber, not to scale. The sample is held in a metal wire frame horizontally and flat. The camera views the sample from 25 cm above, through a window of polyethylene film. Air flows into the chamber conditioned to the humidity and temperature of the measurement, and escapes through small gaps near the humidity sensor and between the chamber and balance (shown by dashed-arrows). Airflow is maintained at a set temperature and humidity for 24 hours, is turned off during a measurement, and turned back on immediately after.

signal intensity from the PTFE reference that corresponds to a nominal temperature of 40 °C. This was done to avoid a temperature differential between a thermocouple or other temperature measurement device and the samples being studied.

The chamber also includes an electronic balance (Denver Instrument, Bohemia, NY, model APX-100), and the camera (see below). The sample is fixed by a metal holder (shown in Figure 4.2) that keeps the fabric taut and horizontal, as well as allowing for

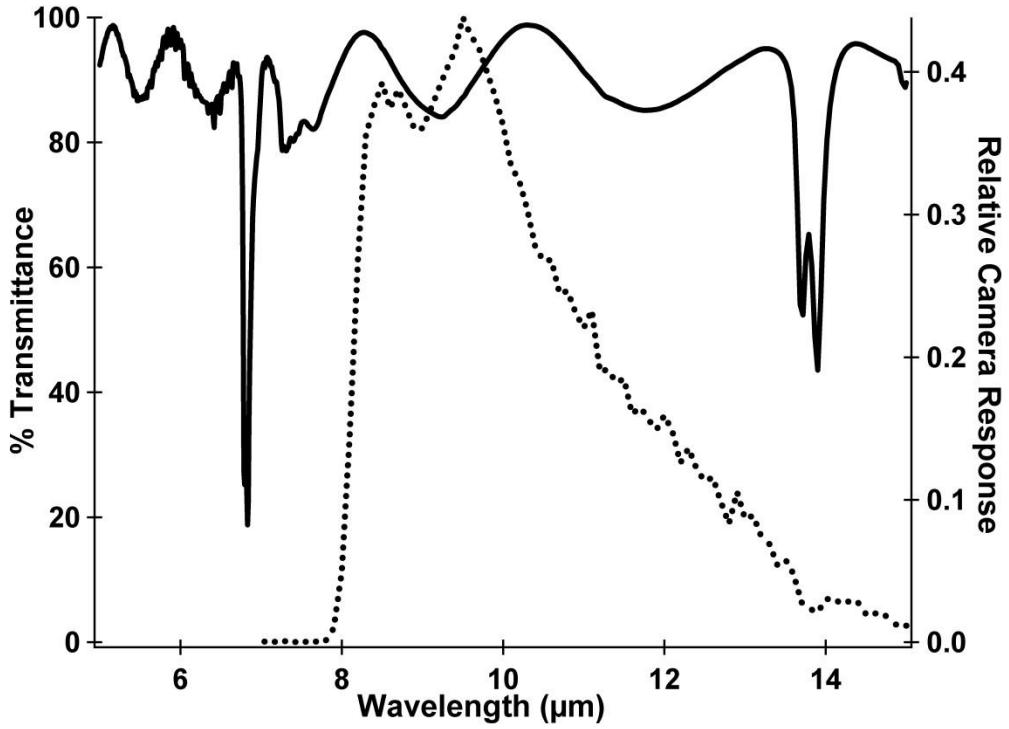

Figure 4.3. The solid black line is the transmission spectrum of the 13.5 μm thick polyethylene film used as a window. The overlaid dotted black line shows the camera response curve.

airflow under the sample. Air enters from the right of the chamber as seen in Figure 4.2, passes through a series of baffles spaced 1 cm apart to distribute the air through the chamber, and then exits on the left of the chamber, opposite where it entered. The chamber itself is 3D printed polylactic acid (PLA). The interior of the chamber where the

sample is housed is 12 x 12 x 4.5 cm. The window was made from an infrared-transparent polyethylene film (Kroger, Cincinnati, OH, Home Sense Plastic Film); the film has high transparency in the 7.5 - 13 μm spectral region detected by the camera as shown in the transmission spectrum of a representative sample of the film in Figure 4.3.

4.2.3 THERMOGRAPHY

Thermographic images were recorded with a FLIR Systems A315 microbolometer-based camera (16 bit digitization, 240 x 320 pixel resolution, 30 Hz frame rate) operating in signal linear mode using an interface developed in-house in the LabVIEW 2013 programming environment (National Instruments, Austin, TX). Once the sample was allowed to equilibrate as described above, an 80 second long recording (2400 image frames) of the sample was acquired.

The measurements are taken in series, starting at 0% humidity, and increasing in humidity in 10% RH steps every 24 hours. After reaching 90% RH, measurements continue by decreasing the humidity in 10% RH steps every 24 hours until 0% humidity is reached again. At each humidity point, a set of three measurements are taken as follows. The air flow is shut off, the camera records for 80 seconds, and then the air flow is returned. After 10 minutes, this is repeated. A third recording is obtained the same way, and then the sample chamber conditions are set to the next humidity point to be measured by adjusting the ratio of wet and dry air. A full series of measurements for a single fabric requires measurements at 19 humidity conditions over the course of approximately 3 weeks if there are no breaks or repeats required. If any significant breaks occurred during a set of measurements, for example due to the need to repair or replace a compressor, the set of data was discarded and begun again so that the

equilibration time between points could be kept constant and the hysteresis would be consistent through the measurement series. The first measurement in each case – the initial 0% humidity point – was sustained at the 0% RH condition as long as necessary so that the mass of the fabric would plateau. This never took less than 3 days for any of the fabrics, with nylon requiring the longest initial equilibration of approximately 7 days.

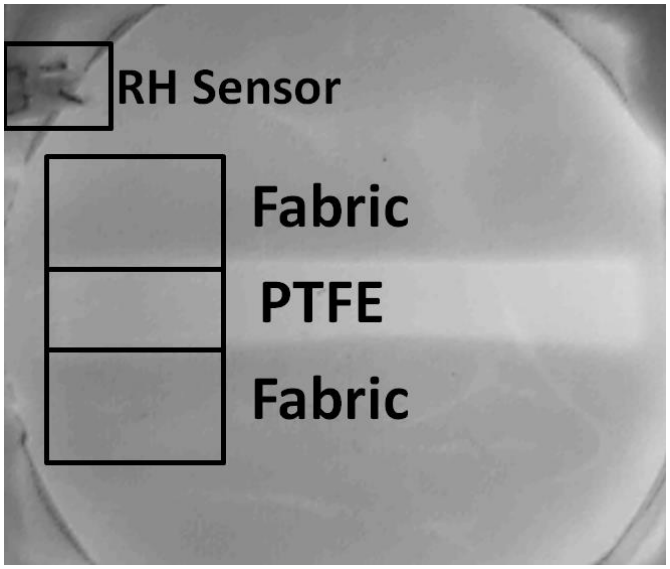

Figure 4.4. An individual frame from a recording of acrylic fabric. The airflow to the sample is cut off during this recording, but prior to the recording, it flows from right to left. The RH sensor is located in the top left of the image, and is positioned just over the sample. The white strip across the middle of the fabric is a 1.67 mm thick PTFE strip, which is used as a reference material. The black boxes show the areas of the image used: the middle box encompasses an area of the PTFE strip only, while the top and bottom box encompass areas of the fabric only. These areas of the image are used because they show the smallest temperature gradient of all the areas of the fabric.

Figure 4.4 shows a frame from a recording of the acrylic fabric at 0% humidity and nominally 40 °C. The sample is kept flat and raised to allow airflow underneath it. A 1-cm-wide, 1.67 mm thick glossy strip of PTFE rests on the fabric to serve as an emissivity reference in each image. PTFE adsorbs very little moisture from air and is resistant to degradation under the measurement conditions.[32]

Recordings were processed with MATLAB R2012b (The MathWorks, Inc., Natick, MA). The values for the fabric sample signal intensity and the PTFE reference signal intensity are calculated from the recording by first averaging the video frames together in time to form a single average image. Regions of interest for the two materials as outlined in Figure 4.4 are then averaged to give a single average signal intensity value for each material.

4.2.4 Data Analysis

The radiation measured by the camera from a fabric or PTFE sample located inside the sample chamber is modeled as coming from four distinct sources, shown in Figure 1.1. Based on Equation 1.9 in Chapter 1, which describes the radiation measured by the camera, the derivation of the thermal emissivity of a sample surface is as follows.

Three measurements are required to determine the emissivity of the reference PTFE for comparison to literature. These are $I^{ref}_{T_{ref},w}$, $I^{BB}_{T_{ref},w}$, and $I^{a}_{T_a,w}$. These are the measured total signal intensities for the imaged reference at an elevated temperature, an imaged blackbody aperture at the same elevated temperature, and a surface in equilibrium with the ambient room temperature, respectively. These three signals are described by:

$$I^{ref}_{T_{ref},w} = \frac{\varepsilon_{ref}\tau_w}{1-r_w r_{ref}} \int_{\lambda_0}^{\lambda_\infty} L^{BB}_{T_{ref},\lambda} R_\lambda \, d\lambda + \left[1 - \frac{\varepsilon_{ref}\tau_w}{1-r_w r_{ref}}\right] \int_{\lambda_0}^{\lambda_\infty} L^{BB}_{T_a,\lambda} R_\lambda \, d\lambda + C \qquad (4.1)$$

$$I^{BB}_{T_{ref},w} = \tau_w \int_{\lambda_0}^{\lambda_\infty} L^{BB}_{T_{ref},\lambda} R_\lambda \, d\lambda + [1-\tau_w] \int_{\lambda_0}^{\lambda_\infty} L^{BB}_{T_a,\lambda} R_\lambda \, d\lambda + C \qquad (4.2)$$

$$I^{a}_{T_a,w} = \int_{\lambda_0}^{\lambda_\infty} L^{BB}_{T_a,\lambda} R_\lambda \, d\lambda + C$$
$$\left(= I^{BB}_{T_a} = I^{ref}_{T_a} = I^{fab}_{T_a} = I^{BB}_{T_{a,w}} = I^{ref}_{T_{a,w}} = I^{fab}_{T_{a,w}} \right) \tag{4.3}$$

In these equations the subscript ref indicates a property of the reference PTFE material (e.g., its emissivity, reflectivity or temperature) while the superscript ref refers to a measured quantity from observation of the reference. Equation 4.3's second line indicates that a blackbody, the reference material, and the fabric material all give the same measured intensity whether they have a window in front of them or not, as long as they (and the window, if included) are in thermal equilibrium with the ambient room environment and protected from any sources of disequilibrium.[33]

Taking the difference of Equations 4.1 and 4.3 and dividing by the difference in Equations 4.2 and 4.3, yields on simplification:

$$\frac{I^{ref}_{T_{ref},w} - I^{a}_{T_a,w}}{I^{BB}_{T_{ref},w} - I^{a}_{T_a,w}} = \frac{\varepsilon_{ref}}{1 - r_w r_{ref}} \equiv \mathbf{M} \tag{4.4}$$

where ε_{ref} is the graybody approximation of the PTFE reference surface emissivity, and r_{ref} is the graybody approximation of the PTFE reference surface reflectivity. ε_{ref} and r_{ref} are related by $\varepsilon_{ref} + r_{ref} = 1$ since the sample is opaque. The PTFE reference emissivity is then given by:

$$\varepsilon_{ref} = \frac{\mathbf{M} - r_w \mathbf{M}}{1 - r_w \mathbf{M}} \tag{4.5}$$

Determining the value of **M** requires that we measure the reference material and a blackbody at an elevated temperature in thermal equilibrium with one another. The

simplest way to accomplish this task is to image a block of the reference material with a hole drilled into it to serve as an effective blackbody radiator.[34-36] The ambient measurement can be made of the reference material before heating. The value of **M** is determined from our experiments to be 0.903. The calculated value of the weighted window reflectance, r_w, is (*vide infra*) 0.083. These two values allow the emissivity of the reference to be calculated as $\varepsilon_{ref} = 0.895$.

Three measurements are also required to determine the emissivity of a fabric sample: $I^{fab}_{T_{fab},w}$, $I^{ref}_{T_{fab},w}$, and $I^{a}_{T_a,w}$ These are the measured total signal intensities for the imaged fabric sample at an elevated temperature, the imaged reference material at the same elevated temperature as the fabric sample, and a surface in equilibrium with the ambient room temperature, respectively. The third of these signals is described in Equation 4.3 above. The first two are described by:

$$I^{fab}_{T_{fab},w} = \frac{\varepsilon_{fab}\tau_w}{1 - r_w r_{fab}} \int_{\lambda_0}^{\lambda_\infty} L^{BB}_{T_{fab},\lambda} R_\lambda \, d\lambda + \left[1 - \frac{\varepsilon_{fab}\tau_w}{1 - r_w r_{fab}}\right] \int_{\lambda_0}^{\lambda_\infty} L^{BB}_{T_a,\lambda} R_\lambda \, d\lambda + C \qquad (4.6)$$

$$I^{ref}_{T_{fab},w} = \frac{\varepsilon_{ref}\tau_w}{1 - r_w r_{ref}} \int_{\lambda_0}^{\lambda_\infty} L^{BB}_{T_{fab},\lambda} R_\lambda \, d\lambda + \left[1 - \frac{\varepsilon_{ref}\tau_w}{1 - r_w r_{ref}}\right] \int_{\lambda_0}^{\lambda_\infty} L^{BB}_{T_a,\lambda} R_\lambda \, d\lambda + C \qquad (4.7)$$

Taking the difference of Equations 4.6 and 4.3 and dividing by the difference between Equations 4.7 and 4.3 gives:

$$\frac{I^{fab}_{T_{fab},w} - I^{a}_{T_a,w}}{I^{ref}_{T_{fab},w} - I^{a}_{T_a,w}} = \frac{\varepsilon_{fab}(1 - r_w r_{ref})}{\varepsilon_{ref}(1 - r_w r_{fab})} \equiv \mathbf{N} \qquad (4.8)$$

Determining the value of **N** requires that we measure the fabric and reference materials at an elevated temperature in thermal equilibrium with one another. This was done in our sample compartment by placing a strip of the thin reference material over the fabric and averaging fabric measurements from each side of the reference material. The ambient measurement can again be done before the fabric/reference are heated. The emissivity of the reference material is given by Equation 4.5 above. Again recognizing the relationship between emissivity and reflectivity for opaque materials, the fabric sample emissivity can be written as:

$$\varepsilon_{fab} = \frac{\mathbf{NM} - r_w\mathbf{NM}}{1 - r_w\mathbf{NM}} \tag{4.9}$$

Equation 4.9 is used in this manuscript to generate fabric emissivity values at differing humidity values, assuming the emissivity of the reference PTFE is independent of humidity.

It is notable that provided the reference and blackbody are at the same temperature, and that the fabric and reference are at the same temperature, neither temperatures T_{ref} or T_{fab} nor the transmission of the window (τ_w), appear in Equation 4.9, provided that all measurements are taken with the window in place. If the temperatures are insufficiently different from ambient, or if the window transmission is low, both **N** and **M** approach indeterminate values and become susceptible to large errors for that reason. Fundamentally, this is because we assume the window is at ambient temperature. If either the sample is at ambient temperature, or the window is opaque so that the sample cannot be viewed, then the scene viewed by the camera will always appear to be at ambient temperature.

4.3 Results and Discussion

4.3.1 Adsorption isotherms

Adsorption isotherms of the four fabric samples at a nominal temperature of 40 °C are shown in Figure 4.5, where the moisture content of the fabric in weight percent is plotted against the relative humidity. Fabrics are defined as "dry" in these experiments using an operational definition of having reached a plateau of mass with respect to further drying over the course of 24 hours. "Dry" does not mean there is no moisture in the fabrics; the first monolayer of water on all the surfaces of the fabrics is a small mass percentage and is very difficult to eliminate without baking *in vacuo* at an elevated temperature, which would induce undesirable side reactions and processes in the fabrics such as permanent loss of oils and waxes or decomposition as well.[37]

From the dry state as defined above, acrylic and polyester show a low capacity for adsorption, 2 weight percent or less, up to 90% RH. Nylon and cotton both adsorb much more water under these conditions. This is in good agreement with literature reports of moisture isotherms for these fabrics.[20-21, 37-40] Additionally, we observe that the relationship between the fabrics' capacity for moisture at a high humidity (e.g., 70% RH) is approximately linear with respect to the specific surface area of these four fabrics, consistent with reports in the literature relating specific surface area and moisture sorption capacity.[22, 41-43] Polyester deviates most from this linear relationship, possibly indicating an error in the BET isotherm measurement of the specific surface area (0.057 m^2/g) reported earlier for this fabric.[22] In support of this conclusion, polyester had the highest reported error among the four fabrics in Reference 22, and a geometric area calculation based on an SEM-estimated fiber diameter, assuming a cylindrical fiber

shape, gave an estimated specific surface area near 0.14 m^2/g for this fabric. This geometrically-estimated specific surface area is still the smallest of the four fabrics, but is consistent with the moisture measurement of the other three using their BET-determined areas.

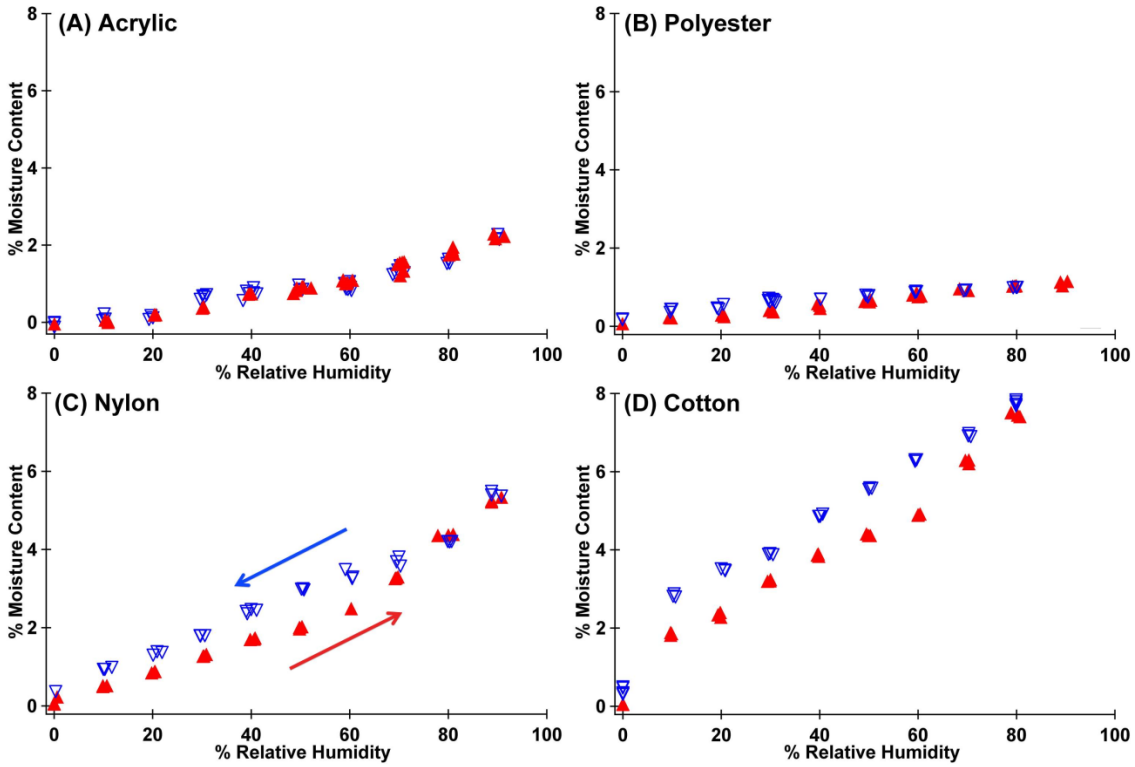

Figure 4.5. Adsorption isotherm plots of (A) acrylic, (B) polyester, (C) nylon, and (D) cotton. Triangles (▲) indicate measurements taken in a series of increasing humidity steps, while inverted triangles (▽) indicate measurements taken in a series of decreasing humidity steps. The scale bar represents an increase of 1% moisture content by mass. (C) includes a right-pointing arrow indicating the data points taken in order of increasing humidity, and a left-pointing arrow indicating data taken in order of decreasing humidity.

Fabrics and the fiber materials they are composed of are the subject of a large number of moisture sorption studies because the propensity of a fabric to adsorb moisture can affect the microbial safety of the material, the physiochemical properties of the fabric, and therefore the industrial applications it may be suitable for. [20-21, 37-40, 44-50] In such

studies, moisture isotherms of fabrics generally follow the sigmoidal shape of the IUPAC type-II isotherm, although more hydrophobic materials may show a more linear appearance.[20] The theoretical sigmoidal shape is defined on the low moisture end by a region of rapid uptake of moisture on strongly-adsorbing active sites (such as the hydroxyl and nitrile groups of the cellulose and nylon monomers respectively) that ends with full monolayer formation. At intermediate humidities, approximately linear moisture uptake with increasing humidity results as multilayers of water are formed on top of the initial monolayer. Then at the highest humidities, a final rapid increase in moisture content occurs as capillary condensation, i.e., water condensing in pores and between fibers in the weave, takes place. Capillary condensation occurs in both natural and synthetic fabrics, and is related to the fabric physical properties rather than chemical properties of the fiber material.[51] This last stage of adsorption is the point at which a fabric would begin to appear "wet" in a macroscopic sense.

Assuming the first monolayer of water is never completely removed from the fabric fibers during our measurements, the low-humidity region of monolayer formation in the isotherm described above is likely absent from our measurements. In Figure 4.5, only cotton shows a region of rapid uptake at low humidity, suggesting that only in this fabric have at least some of the stronger adsorption sites been exposed by drying, possibly because this is the only natural fiber-based fabric in the set and contains the greatest number and heterogeneity of adsorption sites. The other isotherms observed in Figure 4.5, and the cotton isotherm above 10% RH, are ~linear with increasing humidity consistent with the development of additional layers of water over the initial monolayer. The isotherms in Figure 4.5 intentionally end as capillary condensation begins to

dominate. Capillary condensation was observed to coincide with extensive condensation on all surfaces of the apparatus, so we avoided exploring the most extreme humidity conditions to prevent it. For the synthetic fabrics the curves all end at 90% RH, while for cotton the curve ends at 80% RH.

Each of the fabrics exhibits some degree of hysteresis in its water adsorption isotherm shown in Figure 4.5. In terms of absolute moisture content, the acrylic shows the least (approaching zero) and cotton shows the most (around 1% moisture content). Fabrics made from natural fibers typically exhibit hysteresis, while hydrophobic synthetic fabrics typically show little.[20-21, 44-48] For example, while acrylic and polyester are reported to exhibit very little hysteresis, hysteresis in cotton has been described by Hill et. al.[21, 37] Nylon is a hydrophilic synthetic fiber for which Forward and Smith have reported hysteresis in the moisture isotherm.[48] Hysteresis indicates a kinetic limitation for moisture exchange, which can be minimized by allowing fabrics to equilibrate longer.[45] The hysteresis in the fabric isotherms shown in Figure 4.5 likely results from 24 hours at each humidity point being insufficient to reach full equilibrium.

Hysteresis in the moisture uptake isotherm, and the uptake of moisture by fabrics under low humidity conditions, is also related to the degree of hydrophilicity of the fabric.[20] Literature studies of the surfaces of the fabric fibers report the water contact angle and surface free energy (SFE) of the fiber materials.[52-55] These measurements show that water contact angles increase in the order of cotton < nylon < acrylic < polyester. Lower contact angles indicate a more thermodynamically favorable interaction between water and the fiber material. This indicates that the order of hydrophilicity among the materials follows the trend in the contact angles. Additionally, the SFE of the materials

increases in order of acrylic<polyester~nylon<cotton.[52-55] Higher SFE indicates a greater degree of work needed to re-create a dry fiber surface. Acrylic, having the smallest energetic barrier to re-creating the dry fiber surface, exhibits no hysteresis. On the other hand, cotton, having the highest SFE of the materials, shows the greatest degree of hysteresis due to the relatively large energetic barrier to removing the adsorbed water from its surface and recreating the dry, high energy state. We observe that the overall magnitude of water adsorption in the fabric isotherms in Figure 4.5 follows the same trend in hydrophilicity observed in water contact angles, and that the degree of hysteresis in the fabric isotherms follows the trend in fiber SFE.

The data for each adsorption and desorption isotherm were fit by the Guggenheim, Anderson, de Boer (GAB) sorption model, which is given in Equation 4.10.[56-58]

$$M = \frac{M_o C K a_w}{(1 - K a_w)(1 - K a_w + C K a_w)} \qquad (4.10)$$

Where M is the moisture content at a water activity a_w $\left(\frac{RH}{100}\right)$, M_o is the monolayer moisture content (in weight percent), C is the Guggenhiem constant for the material, and K is a multilayer formation factor. Modeling is performed by fitting a custom-input equation of the GAB model to the plot of moisture content versus water activity using IGOR Pro 6.04 (Wavemetrics, Inc., Lake Oswego, OR) such that the coefficients M_o, C, and K are modeled directly instead of linearizing the model as is commonly found in literature. Several reports in literature have found improved goodness-of-fit measurements using a direct fitting of the coefficients.[59-62] The model coefficients, along

with standard deviations of the coefficients, the coefficient of determination (R^2), and root-mean-square-error (RMSE) are given in Table 4.1.

Table 4.1. GAB model parameters (M_o, C, and K) for adsorption and desorption moisture isotherms of each fabric. Reported uncertainties are one standard deviation. The coefficient of determination (R^2) and root-mean-square-error (RMSE) for each fit are provided.

		M_o (wt %)	C	K	R^2	RMSE
Cotton	Adsorption	2.911±0.103	14.689±1.83	0.779±0.017	0.995	0.145
	Desorption	4.176±0.165	22.286±2.89	0.618±0.024	0.994	0.240
Acrylic	Adsorption	1.341±0.619	1.740±0.769	0.664±0.116	0.986	0.083
	Desorption	0.695±0.092	5.230±1.88	0.787±0.038	0.958	0.121
Nylon	Adsorption	2.222±0.279	2.484±0.446	0.730±0.031	0.995	0.115
	Desorption	2.404±0.024	7.876±1.67	0.653±0.039	0.984	0.197
Polyester	Adsorption	0.830±0.233	3.433±0.021	0.498±0.438	0.982	0.047
	Desorption	0.724±0.096	31.761±9.10	0.443±0.103	0.947	0.080

4.3.2 Fabric Emissivity

While hysteresis is seen in the fabric isotherms, all four fabrics showed virtually no difference between measurements of the emissivity during the adsorption cycle versus the desorption cycle, as long as the emissivity was reported as a function of moisture weight percent. Additionally, the overall effect of humidity on the measured emissivity was small or negligible for each fabric except acrylic.

Emissivities for cotton, nylon, and polyester are high and occur in a narrow range of ~0.02 emissivity units regardless of moisture content, while the emissivity for acrylic increases monotonically with moisture weight percentage from 0.81 to 0.88.

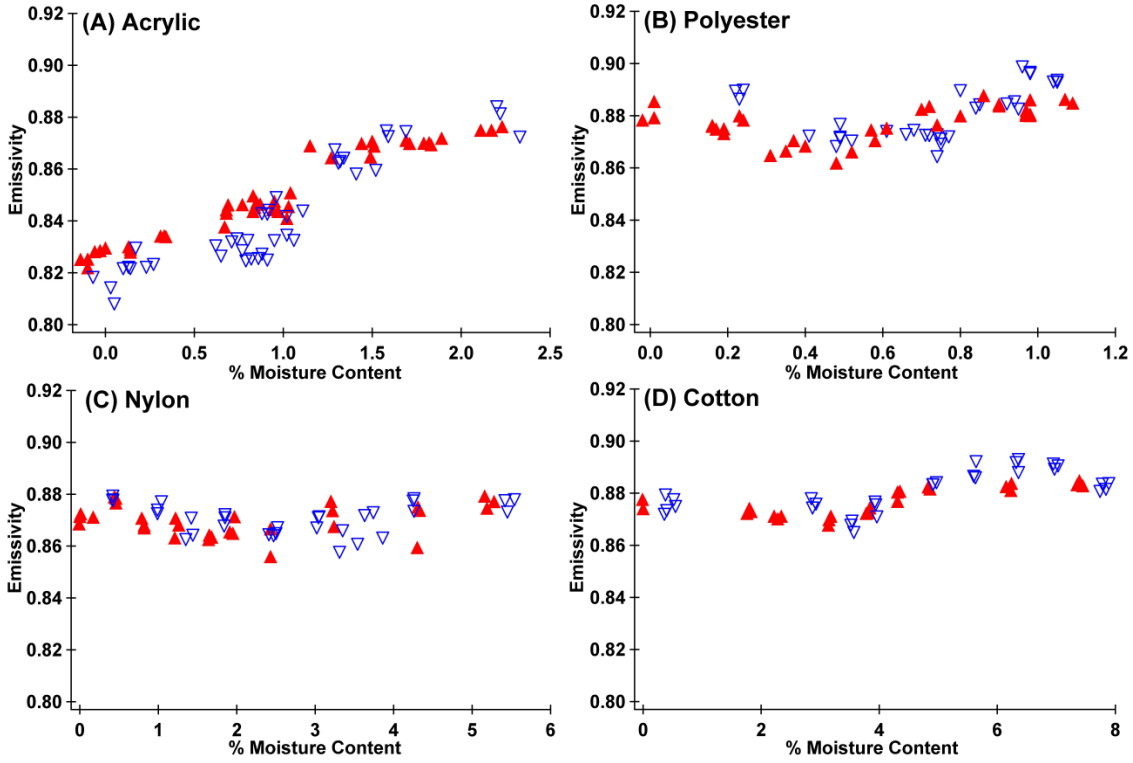

Figure 4.6. Emissivity vs % moisture content plots of (A) acrylic, (B) polyester, (C) nylon, and (D) cotton, set to a common scale. Triangles (▲) indicate measurements taken in a series of increasing humidity steps, while inverted triangles (▽) indicate measurements taken in a series of decreasing humidity steps. Of the four fabrics, acrylic shows a strong change in emissivity with moisture content, while cotton shows a weaker trend at high moisture content. At high moisture content, all four fabrics show similar emissivities.

Chen et al. offers the capillary condensation explanation for the emissivity increase in soils at high moisture content: that the pore space between soil particles becomes filled with water.[16] When capillary condensation occurs, light scattering at particle interfaces will decrease; this increases the attenuation of light in scattering media, regardless of whether the condensing fluid absorbs light or not.[63] The same phenomenon can occur in the inter-fiber space of fabrics. However, since we have chosen conditions to minimize capillary condensation, the emissivity behavior in Figure 4.6 is explained differently. Water exhibits relatively strong and broad absorption of infrared light. The lack of an

observed emissivity-moisture content relationship in nylon and polyester, along with the weaker trend in cotton can be explained by closer examination of the infrared absorption properties of these fabrics. These three fabrics absorb most incident 8 – 12 micrometer light even in the absence of adsorbed water, and therefore they have relatively high emissivities even when dry.[22] Until capillary condensation occurs, the change in the absorption of light in the thermal infrared wavelength range due to the adsorbed water in the fabric is therefore relatively small. Acrylic shows the lowest average absorption of light among the four fabrics, and thus its thermal emissivity is relatively low compared to the other fabrics when dry. However, as more water adsorbs on the acrylic fibers, the measured emissivity increases to the same levels observed in the other fabrics at high moisture levels.

4.3.3 Polyethylene "Cling Wrap" as a Thermographic Infrared Window

In the work presented here, we used an unusual infrared window material made from a commercial polyethylene kitchen wrap. Equation 1.9 allows us to determine the optical properties (transmissivity, reflectivity, and emissivity) of this thin polymer film in the thermal infrared window. While the final equations do not require a knowledge of the emissivity or transmittivity of the window thanks to an assumption that the window is at room temperature, window emissivity would appear if the window were at elevated temperature. Further, emissivity is numerically equal to absorptivity, so a good measurement of window emissivity is relevant to the quality of a window material for infrared studies.

We are interested in both the weighted transmittivity of the window and the weighted window emissivity. Figure 4.3 shows a measured transmission spectrum of the window

with interference effects superimposed on absorption features, together with the measured camera response function. In principal, emissivity can be estimated from these data, but with errors consistent with the uncertainty of a transmission measurement. Better estimates of both the weighted window transmittivity and the weighted window emissivity come from thermographic measurements than from attempting to numerically weight the transmission measurements directly.

Three measurements are required to determine the weighted window transmittivity. Two of these are measurements of a blackbody source at an elevated temperature with and without the window present: $I^{BB}_{T_s,w}$ and $I^{BB}_{T_s}$, respectively. The third is again the ambient temperature measurement of an equilibrated surface. Under the same assumptions used previously, the transmittivity of the window is given by:

$$\tau_w = \frac{I^{BB}_{T_{BB},w} - I^{a}_{T_a,w}}{I^{BB}_{T_{BB}} - I^{a}_{T_a}} \tag{4.11}$$

where $I^{BB}_{T_{BB}}$ is the signal intensity of a perfect blackbody at temperature T_{BB} viewed by the camera without the window. τ_w is calculated to be 0.905 using this method.

The window reflectivity, r_w, is a function of wavelength due to interference effects. Assuming the material is effectively a transparent thin dielectric film in air, Equation 4.12 gives the reflectivity as a function of wavelength and film thickness at near-normal incidence.

$$r_w = \frac{\cos\left(\frac{2\pi nd}{\lambda}\right)^2 - 1}{\cos\left(\frac{2\pi nd}{\lambda}\right)^2 - \frac{(n^2+1)^2}{(n^2-1)^2}} \tag{4.12}$$

where n is the refractive index of the window material, and d is the thickness of the window. Using this equation to fit the window thickness based on the wavelengths of maxima and minima in the transmittivity shown in Figure 4.3, and using a refractive index of polyethylene film at 10μm wavelength of n~1.53, gives a film thickness (d) of 13.5μm.[64] The weighted reflectivity, r_w, as a function of wavelength can then be calculated from the camera response as 0.083. The relative error in this reflectivity is probably no better than the relative error in a direct numerical calculation of τ_w, but since the value of r_w is an order of magnitude smaller than τ_w, the absolute error is thought to be similarly small. Then, since reflectivity, transmittivity and absorptivity of a window add to unity, the absorptivity of the window – and therefore its emissivity – is found to be 0.012. With an emissivity value this low, the effect of an error in our earlier assumption that the window is at room temperature is minimized. Although we have not yet attempted to do so, it is possible that the window absorptivity could be further reduced by stretching the film to reduce its thickness.

4.4 Conclusions

Our interest in better understanding the mechanisms of steam thermography motivates this work. Moisture adsorption isotherms for acrylic, cotton, polyester, and nylon fabrics are presented, along with measurement results for the effect of fabric moisture content on apparent thermal emissivity. This work provides evidence that of the fabrics in this study, moisture content has a significant impact on the apparent emissivity

of acrylic, but not for nylon, cotton, or polyester. An estimate of the contribution of emissivity on steam thermography observations requires knowledge of both the emissivity of the fabrics as shown here as well as the emissivity of blood-coated fabrics. A separate report on the apparent emissivity of blood on these four fabrics is presented in Chapter 5.

REFERENCES

1. K. B. Gautier, C. W. Kocher, J. Y. Drean. Anisotropic mechanical behavior of nonwoven geotextiles stressed by uniaxial tension. *Text. Res. J.* 2007; 77(1): 20-28.

2. A. K. Puszkarz, I. Krucinska. The study of knitted fabric thermal insulation using thermography and finite volume method. *Text. Res. J.* 2017; 87(6): 643-656.

3. Y. Gao, G. Zhu, H. Zhu, et al. Experimental study of moisture content effects on horizontal flame spread over thin cotton fabric. *Text. Res. J.* 2018; 0(00): 1-12.

4. S. Gandhi, S. Spivak, B. Pourdeyhimi. A study of smoldering conditions in upholstery fabrics using thermal imaging. *Text. Res. J.* 1998; 68(9): 687-696.

5. H. Zhang, T. L. Hu, J. C. Zhang. Surface emissivity of fabric in the 8–14 μm waveband. *J. Text. Inst.* 2009; 100(1): 90-94.

6. R. Brown, B. Young. Spectral emission signatures of ambient temperature objects. *Appl. Optics* 1975; 14(12): 2927-2934.

7. R. G. Belliveau, S. A. DeJong, B. M. Cassidy, et al. Ridge patterns of Blood-Transferred Simulated Fingerprints Observed on Fabrics via Steam Thermography. *Forensic Chem*. 2016; 1: 74-77.

8. W. L. O'Brien, N. D. Boltin, Z. Lu, et al. Chemical contrast observed in thermal images of blood-stained fabrics exposed to steam. *Analyst* 2015; 140: 6222-6225.

9. A. Assaf, R. Hass, C. Purves. A new interpretation of the cellulose-water adsorption isotherm and data concerning the effect of swelling and drying on the colloidal surface of cellulose. *J. Am. Chem. Soc.* 1944; 66(1): 66-73.

10. A. Walker. Moisture in textiles. *J. Appl. Phys.* 1937; 8: 261-268.

11. T. Dias, G. Delkumburewatte. The influence of moisture content on the thermal conductivity of a knitted structure. *Meas. Sci. Technol.* 2007; 18: 1304-1314.

12. P. Chitrphiromsri, A. Kuznetsov. Modeling heat and moisture transport in firefighter protective clothing during flash fire exposure. *Heat Mass Transf.* 2005; 41: 206-215.

13. Y. Li. Perceptions of temperature, moisture and comfort in clothing during environmental transients. *Ergonomics* 2005; 48(3): 234-248.

14. X. F. Lin, Y. Li, J. Y. Zhou, et al. Effects of fabrics with dynamic moisture transfer properties on skin temperature in females during exercise and recovery. *Text. Res. J.* 2015; 85(19): 2030-2039.

15. Y. P. Guo, Y. Li, H. Tokura, et al. Impact of fabric moisture transport properties on physiological responses when wearing protective clothing. *Text. Res. J.* 2008; 78(12): 1057-1069.

16. J. Chen, B. Yang, R. Zhang. Soil thermal emissivity as affected by its water content and surface treatment. *Soil Sci.* 1989; 148(6): 433-435.

17. M. Mira, E. Valor, R. Boluda, et al. Influence of soil water content on the thermal infrared emissivity of bare soils: Implication for land surface temperature determination. *J. Geophys. Res.* 2007; 112: 1-11.

18. J. W. Salisbury, D. M. D'Aria. Infrared (8 – 14 μm) remote sensing of soil particle size. *Remote Sens. Environ.* 1992; 42: 157-165.

19. J. W. Salisbury, L. S. Walter, N. Vergo. Mid-Infrared (2.1-25 μm) spectra of minerals: First Edition. Report for Department of the Interior U.S. Geological Survey. Report no. 87-263, 1991.

20. J. Fuzek. Absorption and desorption of water by some common fibers. *Ind. Eng. Chem. Prod. Res. Dev.* 1985; 24: 140-144.

21. C. A. S. Hill, A. Norton, G. Newman. The water vapor sorption behavior of natural fibers. *J. Appl. Polym. Sci.* 2009; 112: 1524-1537.

22. S. A. DeJong, Z. Lu, B. M. Cassidy, et al. Detection limits for blood on four fabric types using infrared diffuse reflection spectroscopy in mid- and near-infrared spectral windows. *Anal. Chem.* 2015; 87: 8740-8747.

23. S. A. DeJong, B. M. Cassidy, Z. Lu, et al. Effect of azimuthal angle on infrared diffuse reflection spectra of fabrics. *Spectroscopy* 2015; 30(12): 23-25.

24. M. R. Baranowski, H. Brooke, J. N. McCutcheon, et al. Coating effects on mid-infrared spectra of fabrics. *Appl. Spectrosc.* 2011; 65(8): 876-884.

25. S. A. DeJong, W. L. O'Brien, Z. Lu, et al. Optimization of gap derivatives for measuring blood concentration of fabric using vibrational spectroscopy. *Appl. Spectrosc.* 2015; 69(6): 733-748.

26. Z. Lu, S. A. DeJong, B. M. Cassidy, et al. Detection limits for blood on fabrics using attenuated total reflection Fourier transform infrared (ATR FT-IR) spectroscopy and derivative processing. *Appl. Spectrosc.* 2017; 71(5): 839-846.

27. Z. Lu, B. M. Cassidy, S. A. DeJong, et al. Attenuated total reflection (ATR) sampling in infrared spectroscopy of heterogeneous materials requires reproducible pressure control. *Appl. Spectrosc.* 2017; 71(1): 97-104.

28. S. A. DeJong, Z. Lu, B. M. Cassidy, et al. Reversible gap derivatives and their integration. *Appl. Spectrosc.* 2016; 70(6): 1044-1054.

29. H. Brooke, M. R. Baranowski, J. N. McCutcheon, et al. Multimode imaging in the thermal infrared for chemical contrast enhancement. Part 1: Methodology. *Anal. Chem.* 2010; 82: 8412-8420.

30. H. Brooke, M. R. Baranowski, J. N. McCutcheon, et al. Multimode imaging in the thermal infrared for chemical contrast enhancement. Part 2: Simulation driven design. *Anal. Chem.* 2010; 82: 8421-8426.

31. H. Brooke, M. R. Baranowski, J. N. McCutcheon, et al. Multimode imaging in the thermal infrared for chemical contrast enhancement. Part 3: Visualizing blood on fabrics. *Anal. Chem.* 2010; 82: 8427-8431.

32. Y. Awakuni, J. H. Calderwood. Water vapour adsorption and surface conductivity in solids. *J. Phys. D: Appl. Phys.* 1972; 5: 1038-1045.

33. B. G. Vainer. Focal plane array based infrared thermography in fine physical experiment. *J. Phys. D: Appl. Phys.* 2008; 41: 1-12.

34. B. Chu, G. Machin. A low-temperature blackbody reference source to -40 °C. *Meas. Sci. Technol.* 1999; 10: 1-6.

35. B. Chu, H. McEvoy, J. Andrews. The NPL reference sources of blackbody radiation. *Meas. Sci. Technol.* 1994; 5: 12-19.

36. G. Mei, J. Zhang, S. Zhao, et al. Simple method for calculating the local effective emissivity of the blackbody cavity as a temperature sensor. *Infrared Phys. Technol.* 2017; 85: 372-377.

37. W. Morton, J. Hearle. Physical properties of textile fibers. Philadelphia: Woodhead Publishing, 2012, p. 178-228.

38. M. Fukuda. Moisture sorption and diffusion in polyacylonitrile fiber: interaction between nitrile groups and sorbed water. *J. Soc. Fiber Sci. & Tech. Japan (Sen-i Gakkaishi)* 1997; 53(8): 313-320.

39. A. R. Urquhart, N. Eckersall. The moisture relations of cotton. vii – A study of hysteresis. *J. Text. Inst. Trans.* 1930; 21(10): T499-T510.

40. A. R. Urquhart, A. M. Williams. The absorption and desorption of water by soda-boiled cotton at 25 °C. *J. Text. Inst. Trans.* 1930; 15(9): T433-T442.

41. H. A. Ruiz, G. O. Sarli, C. E. G. R. Schaefer, et al. Specific surface of oxisols and its relationship with water retention. *Revista de la Facultad de Ciencias* 2016; 48(2): 95-105.

42. A. M. Amer. Moisture adsorption capacity and surface area as deduced from vapour pressure isotherms in relation to hygroscopic water of soils. *Biologia* 2009; 64(3): 516-521.

43. C. B. Hedley, S. Saggar, B. K. G. Theng, et al. Surface area of soils of contrasting mineralogies using para-nitrophenol adsorption and its relation to air-dry moisture content of soils. *Australian J. Soil Res*. 2000; 38(1): 155-168.

44. C. A. S. Hill, A. Norton, G. Newman. The water vapor sorption behavior of flax fibers - analysis using the parallel exponential kinetics model and determination of the activation energies of sorption. *J. Appl. Polym. Sci.* 2010; 116: 2166-2173.

45. P. G. Cookson, I. J. Slota. Hysteresis effects associated with the adsorption and desorption of water by woven wool fabrics. *Text. Res. J.* 1993; 63(9): 495-503.

46. O. Ceylan, K. De Clerck. Moisture sorption in naturally coloured cotton fibres. *IOP Conf. Ser.: Mater. Sci. Eng.* 2017; 254: 142006.

47. I. Auerbach, M. L. Carnicom. Sorption of water by nylon 66 and kevlar 29. Equilibria and Kinetics. *J. Appl. Polym. Sci.* 1991; 9: 2417-2427.

48. M. V. Forward, S. T. Smith. Letters to the editor. *J. Text. Inst. Trans.* 1955; 46: T158-T160.

49. E. Ayranci, O. Duman. Moisture sorption isotherms of cowpea (*Vigna unguiculata* L. Walp) and its protein isolate at 10, 20 and 30 °C. *J. Food Eng.* 2005; 70: 83-91.

50. S. Tunc, O. Duman. Thermodynamic properties and moisture adsorption isotherms of cottonseed protein isolate and different forms of cottonseed samples. *J. Food Eng.* 2007; 81: 133-143.

51. S. J. Gregg, K. S. W. Sing. Adsorption, surface area, and porosity. 2nd ed. New York: Academic Press Inc., 1982, p. 112.

52. H. S. Whang, B. S. Gupta. Surface wetting characteristics of cellulosic fibers. *Text. Res. J.* 2000; 70(4): 351-358.

53. D. G. Waugh, J. Lawrence, D. J. Morgan, et al. Interaction of CO2 laser-modified nylon with osteoblast cells in relation to wettability. *Mater. Sci. Eng., C* 2009; 29(8): 2514-2524.

54. Y. C. Lui, D. N. Lu. Surface energy and wettability of plasma-treated polyacrylonitrile fibers. *Plasma Chem. Plasma Process* 2006; 26: 119-126.

55. A. A. El-Saftawy, A. Elfalaky, M. S. Ragheb, et al. Electron beam induced surface modifications of PET film. *Radiat. Phys. Chem.* 2014; 102: 96-102.

56. E. A. Guggenheim. Application of statistical mechanics. 1st ed. Oxford: Clarendon Press, 1966, p. 186-206.

57. R. B. Anderson. Modification of the Brunauer, Emmett and Teller equation. *J. Am. Chem. Soc.* 1946; 68: 686-691.

58. J. H. DeBoer. The dynamical character of adsorption. Oxford: Clarendon Press, 1953, p. 61-81.

59. C. M. Samaniego-Esguerra, I. F. Boag, G. L. Robertson. Comparison of regression methods for fitting the GAB model to the moisture isotherms of some dried fruit and vegetables. *J. Food Eng.* 1991; 13: 115-133.

60. Z. B. Maroulis, E. Tsami, D. Marinos-Kouris, et al. Application of the GAB model to the moisture sorption isotherms for dried fruits. *J. Food Eng.*1988; 7: 63-78.

61. T. Kablan, Y. Clement, K. A. Francoise, et al. Determination and modelling of moisture sorption isotherms of chitosan and chitin. *Acta Chim. Slov.* 2008; 55: 677-682.

62. W. Schar, M. Ruegg. The evaluation of GAB constants from water vapor sorption data. *Lebensm.-Wiss. Technol.* 1985; 18(4): 225-229.

63. M. L. Myrick, M. N. Simcock, M. Baranowski, et al. The Kubelka-Munk diffuse reflectance formula revisited. *Appl. Spectrosc. Rev*. 2011; 46(2): 140-165.

64. J. Horwitz. Infrared refractive index of polyethylene and a polyethylene-based material. *Opt. Eng.* 2011; 50(9): 1-4.

CHAPTER 5: A STUDY OF THE MID-INFRARED EMISSIVITY OF DRIED BLOOD ON FABRICS[b]

5.1 INTRODUCTION

Blood contains ~20% blood solids consisting mostly of proteins including hemoglobin, along with salts and lipids.[1, 2] When whole blood is deposited on a substrate, these blood solids remain in place after drying. The detection of dried blood on commonplace substrates such as fabrics is the subject of numerous reports in forensic science with the goal of increasing the ability of law enforcement to obtain evidence for criminal investigations.[3-8] For this purpose, the most common methods in use for the detection of dried blood deposited on a variety of substrates include luminol chemiluminescence, fluorescein fluorescence, colorimetric tests using tetramethylbenzidine (TMB, brand name Hemastix), phenolphthalein (Kastle-Meyer), and leucomalachite green, and alternative light sources (ALS).[4, 9-11]

This laboratory has reported an alternate thermographic method for detecting blood called steam thermography.[12, 13] Most of our prior work has focused on fabric samples as substrates. In steam thermography of a blood-stained fabric, the sample is exposed to warm, moist air while being observed with a thermographic infrared camera. In some cases, trace levels of dried blood can be detected as bright (warm) stains on a darker

[b] Reproduced and modified from R. G. Belliveau, S. A. DeJong, N. D. Boltin, et al. A study of the mid-infrared emissivity of dried blood on fabrics. Submitted to Forensic Chem. 2019. Reproduced with permission from Elsevier.

(cooler) fabric background. Effort has been directed in our laboratory to understand and deconvolute the factors that lead to visualizing dried blood stains on fabrics via this new method.

One of the factors that may play a role in steam thermography is differential changes in thermal emissivity between blood and the underlying fabric due to water adsorption. Chapter 4 examines the effect of moisture on the emissivity of clean fabrics. The thermal emissivity of acrylic fabrics was shown to be moderately dependent on moisture content, while a smaller emissivity dependence of cotton, nylon, and polyester fabrics on moisture content was also reported.[14] This chapter describes work to examine the emissivity of dried blood on the same fabrics, and to study the emissivity changes of blood on acrylic as a function of humidity.

5.2 Materials and Methods

5.2.1 Studies

Two types are studies are reported. In one, small fabric samples with polymer rings (referred to in this chapter as the Ring samples) are used to determine the emissivity of dried blood on the fabrics at a fixed humidity point (0% relative humidity). The samples are described in the work reported in Chapter 3, where they are the subject of a study detailing the thermal response of each sample to the exposure of nine solvents. In the second study in this chapter, an aged sample of dried blood on acrylic (referred to in this chapter as the Aged sample) is studied over a range of humidities in an effort to determine how the emissivity of blood on acrylic fabric depends on the ambient humidity level. This latter study was motivated by the fact that of the fabrics under study, acrylic forms the strongest contrast with blood.

5.2.2 SAMPLE FABRICS

A purple acrylic (fabric 917), brown polyester (fabric 905), green nylon (fabric 911) and red cotton (fabric 899) fabrics used in this study were described in detail in Table 1.1 of Chapter 1. Each fabric was commercially obtained unfinished, and then triple-dyed to their respective colors at the North Carolina State University Wilson College of Textiles in 2004. The cotton and nylon are 2/1 twills, while the acrylic and polyester are both plain weaves.

Examples of finished Ring samples used in the fixed humidity study are shown in Figure 5.1. Samples for this study are made using a variation of a procedure found in Cassidy et al.[15] Specifically, 1"x1" (2.5x2.5 cm) squares of the acrylic 917, cotton 899, polyester 905, and nylon 911 fabrics are imprinted with a hydrophobic polymer ring made from LocTite vinyl, fabric, and plastic adhesive (Henkel Co., Rocky Hill, Ct. Item# 1360694). The adhesive was applied by coating the surfaces of two 1" O.D./ ½" I.D. (2.5 cm O.D./ 1.3 cm I.D.) steel washers, pressing the washers together with the fabric sandwiched between them, and clamping the washer-fabric-washer assembly together for 24 hours to cure. After the 24 hour curing period the samples are unclamped and the washers removed. 100 μL of whole rat blood was applied to the fabric surface inside of the polymer ring by pipette, and allowed to dry for 24 hours again. The rat blood dries partially on the surface of the fabric, and partially is adsorbed into the fabric. In some of the photographs in Figure 5.1 a "coffee ring" pattern is produced on the sample, implying some heterogeneity in the deposition process.[16, 17] The face of the fabric on which the blood was applied and dried is the face of the fabric observed during a measurement.

Figure 3.2 shows the Aged sample, a small square of the same acrylic 917 fabric with whole rat blood spatter patterns produced in September 2009 for developmental

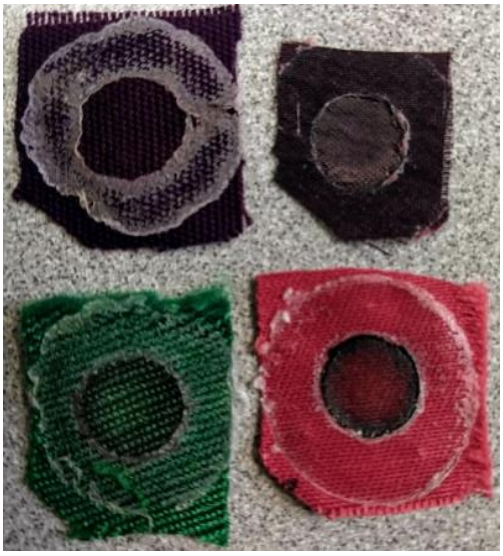

Figure 5.1. The four Ring samples, where 100 µL of blood is deposited on each acrylic (top left), polyester (top right), nylon (bottom left), and cotton (bottom right). The blood is contained within a 0.9 cm^2 area inside of the polymer ring.

laboratory imaging studies. This sample was used in the study of humidity effects on the emissivity of blood on fabric. Measurements were made in the spring of 2015.

5.2.3 Sample Conditioning

Samples for both studies were conditioned using an apparatus developed in-house which was described in detail in Belliveau et al.[14] In brief, compressed air is heated and moisture is added or removed from the compressed air to achieve a constant temperature (nominally 40 °C) and humidity (an experimental variable ranging from 0 - 90% relative humidity, RH) in the sample chamber.

The sample chamber is 3D printed polylactic acid (PLA), with interior dimensions of 12 x 12 x 4.5 cm. Samples are imaged by a thermographic camera (described below)

through a window made from infrared-transparent polyethylene film (Kroger, Cincinnati, OH, Home Sense Plastic Film). The optical characteristics of the IR window material are described in Chapter 4.

Inside the sample chamber, humidity is measured by a thin-film capacitance humidity sensor (Measurement Specialties Inc., Hampton, VA, model HTS2030SMD). The signal intensity of a polytetrafluoroethylene (PTFE) reference inside the chamber is kept constant such that the PTFE is at a nominal temperature of 40 °C.

5.2.4 THERMOGRAPHY

Thermographic videos were recorded with a FLIR Systems A315 microbolometer-based camera using an interface developed in-house in the LabVIEW 2013 programming environment (National Instruments, Austin, TX). Recordings for the Ring samples coated with 100 uL of blood are taken after each of these samples has conditioned at 40 °C and 0% RH for 24 hours. Recordings for the Aged sample are taken in series starting at 0% RH and increasing in humidity by 10% to 90% RH. The fabric is equilibrated for 2 hours at each humidity before a measurement is taken. For all samples, immediately prior to the start of a recording, the airflow to the chamber is cut off, the recording is taken, and then the airflow is returned to the chamber. After 10 minutes, this is repeated, and then a third measurement is taken in the same way after a further 10 minutes for a total of three recordings. For the Aged sample, after the third recording, the sample chamber conditions are set to the next humidity measurement point.

Each recording is 80 seconds long, recorded at 240 x 230 pixel resolution and a 30 Hz frame rate. This results in a 2400 frame long recording, each of which represents an array of individual measurements of the total signal intensity of the imaged surface. Processing

for each recording is done in MATLAB R2012b (The MathWorks, Inc., Natick, MA). The signal intensity of each pixel included in an area of interest (e.g. the area of blood on a fabric, or an area of uncoated fabric) is averaged, and used to calculate an emissivity value for each frame.

5.3 Calculations

5.3.1 Emissivity Calculation

A detailed description of how emissivity is determined experimentally is provided in Chapter 4. In short, beginning with a surface with known emissivity as a reference, three measurements are needed to determine the emissivity of an unknown surface. These measurements are of the total signal intensity for the sample surface (I_{sample}) at an elevated temperature (nominally 40 °C in these measurements), a measurement of the total signal intensity for the reference surface (I_{ref}) at the same elevated temperature, and a measurement of either surface in equilibrium with the ambient room temperature (I_{amb}). The calculation of emissivity based on these three measurements and including correction for the usage of an infrared window with a known reflectivity is performed using Equations 4.4, 4.8, and 4.9. The emissivity values which are calculated for a given area of interest for each frame in a recording are averaged to give an average emissivity for each recording.

The emissivity of each fabric at 0% RH reported in Chapter 4 (shown in Table 5.1) was used as a reference for calculating the emissivity of blood on that fabric. The reported uncertainties in Table 5.1 for the fabric and blood-stained fabric emissivities are the 95% confidence interval, calculated based on the calculated emissivity of three recordings for each fabric sample. The uncertainties for the reported emissivity

differences are calculated by first taking the difference in fabric and blood-stained area emissivities for each recording, then calculating the 95% confidence interval calculated based on the calculated emissivity differences of three recordings for each fabric sample.

5.3.2 Acrylic Emissivity-Humidity Model

The variable humidity study was performed on acrylic fabric because it forms the strongest contrast with blood. However, the emissivity of acrylic also shows moderate sensitivity to humidity that needed to be modeled before it could be used as a reference material.

Reference emissivity values for the acrylic 899 fabric used in this chapter are based on the adsorption isotherm measurements reported in Chapter 4. Modeling is performed by fitting a second-order polynomial (curve in Figure 5.2) to the plot of emissivity versus relative humidity (circles in Figure 5.2) using IGOR Pro 6.04 (Wavemetrics, Inc., Lake Oswego, OR). The emissivity values at 60% and 70% RH fall furthest outside of the model. In the 60-70% humidity range, capillary condensation begins to occur in the space between fibers.[18, 19] This causes both decreased scattering and increased absorption, both of which decrease the reflectance of the sample and thus increase the apparent emissivity of the surface.[20-22] The polynomial model used in this study does not capture this physical change in the sample, but results in absolute errors less than 0.01 emissivity for humidities in the 60-70% RH range. The fit equation and the fit coefficients are provided on Figure 5.2.

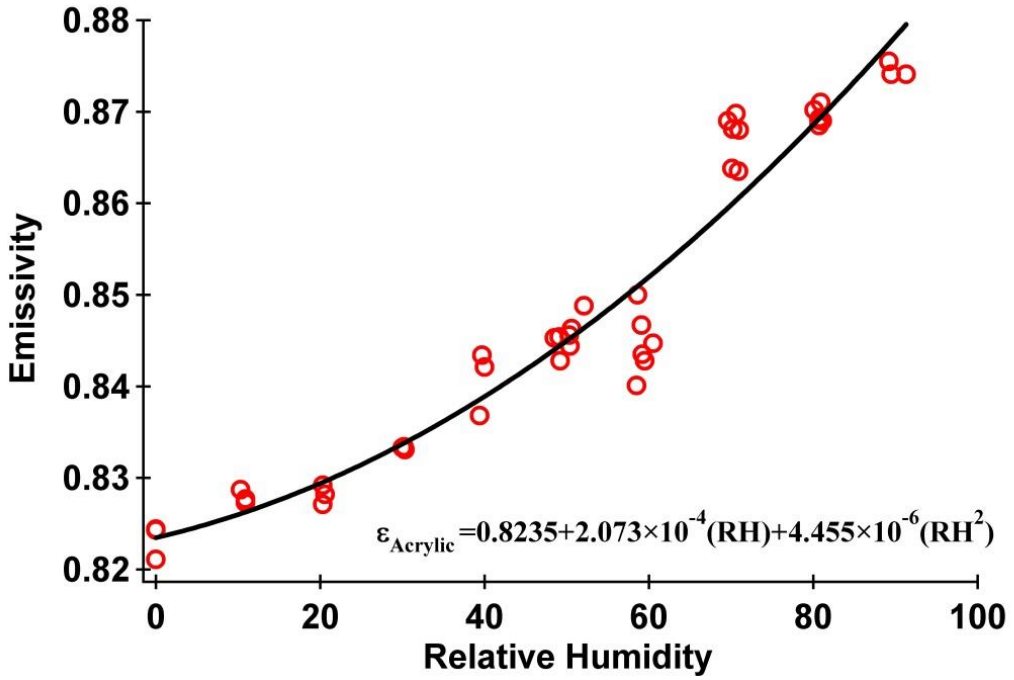

Figure 5.2. Fit of a second-order polynomial function to the acrylic emissivity vs relative humidity data, used to model the emissivity of the acrylic fabric areas on the BS fabric sample. The mean relative deviation modulus (P, Equation 5.1) was calculated to be 0.3562. The root-mean-square-error (RMSE, Equation 5.2) was calculated to be 0.0043.

The mean relative deviation modulus (P), a measure of the average relative deviation, is described by Equation 5.1 and provided as a measure of goodness-of-fit for this model, was calculated to be 0.3562. Values under 10 are considered to indicate an acceptable fit.[23]

$$P = \frac{100}{n}\sum_{i=1}^{n}\left(\frac{\left|\varepsilon_i^{exp} - \varepsilon_i^{pred}\right|}{\varepsilon_i^{exp}}\right) \quad (5.1)$$

Where n is the number of measurements, and ε_i^{exp} and ε_i^{pred} are the experimentally measured and predicted emissivity values. ε_i^{pred} is calculated based on the model given in Figure 5.2 for the same relative humidities at which each ε_i^{exp} value was measured. The

root-mean-square-error (RMSE, shown in Equation 5.2) of the model predicted emissivities compared to the experimentally measured data was calculated to be 0.0043.

$$\mathrm{RMSE} = \sqrt{\frac{\sum_{i=1}^{n}\left(\varepsilon_i^{exp} - \varepsilon_i^{pred}\right)^2}{n}} \tag{5.2}$$

5.4 Results and Discussion

5.4.1 Emissivity of Blood on Four Dry Fabrics

Emissivity values for the Ring sample fabric areas, the fabric areas coated in 100 μL of blood, and the difference in emissivity between the two surfaces at 0% RH are shown in Table 5.1.

Table 5.1. Emissivities of the four Ring sample fabrics, of blood on each fabric, and the difference in the average emissivity of each fabric and blood on that fabric. Each emissivity shown is an average of three measurements at 0% RH. The uncertainties given in the table are 95% confidence intervals. The emissivity difference between blood and cotton is negligible, however the emissivity differences between blood and the other three fabrics are significant, with acrylic having the largest emissivity difference from blood.

Fabric	Fabric ε	Blood ε	ε Difference
Acrylic	**0.8233±0.0047**	**0.8756±0.0032**	**0.0523±0.0068**
Polyester	**0.8802±0.0096**	**0.9102±0.0028**	**0.0300±0.0117**
Nylon	**0.8700±0.0050**	**0.8807±0.0051**	**0.0107±0.0064**
Cotton	**0.8753±0.0054**	**0.8811±0.0013**	**0.0058±0.0066**

Each emissivity value is the average of three measurements of 2400 frames, and the given uncertainty values are one standard deviation. Emissivity differences increase in the order of cotton<nylon<polyester<acrylic, with the emissivity difference on acrylic being ~9x the emissivity difference on cotton. The apparent difference in temperature at

40 °C between blood-coated acrylic and uncoated acrylic is about 0.76 °C, while the apparent temperature difference between blood-coated cotton and uncoated cotton (0.09 °C) is approaching the detection limit of our A315 camera (a noise equivalent temperature difference, NETD, of 0.050 °C).

5.4.2 Blood Emissivity on Acrylic as a Function of Humidity

Figure 5.3 shows the modeled thermal emissivity of a reference acrylic fabric sample versus measurements of blood coated regions of the Aged sample as a function of humidity. The emissivity of the Aged sample shows a negligible change at humidities less than 60%, but increases at humidities higher than 60% RH, increasing from 0.90 to nearly 0.94.

Capillary condensation of moisture within the dried blood begins to occur at these higher humidities, and similarly to the changes in the acrylic emissivity, will result in a decrease in light scattering.[24, 25] The increase in emissivity may not be as large in magnitude as the increase in acrylic emissivity with humidity because the apparent emissivity of blood is relatively high and is similar to that of water. As more water coats the surface, the emissivity of the water dominates the measured signal intensity. However, if the water and blood emissivities are similar, the apparent change in emissivity with increasing humidity is small.

Figure 5.4 shows the difference in the emissivity of the uncoated acrylic fabric and the blood-coated acrylic fabric as a function of humidity. The emissivity difference decreases from a difference of ~0.08 when the fabric is at a dry state, to ~0.05 at high

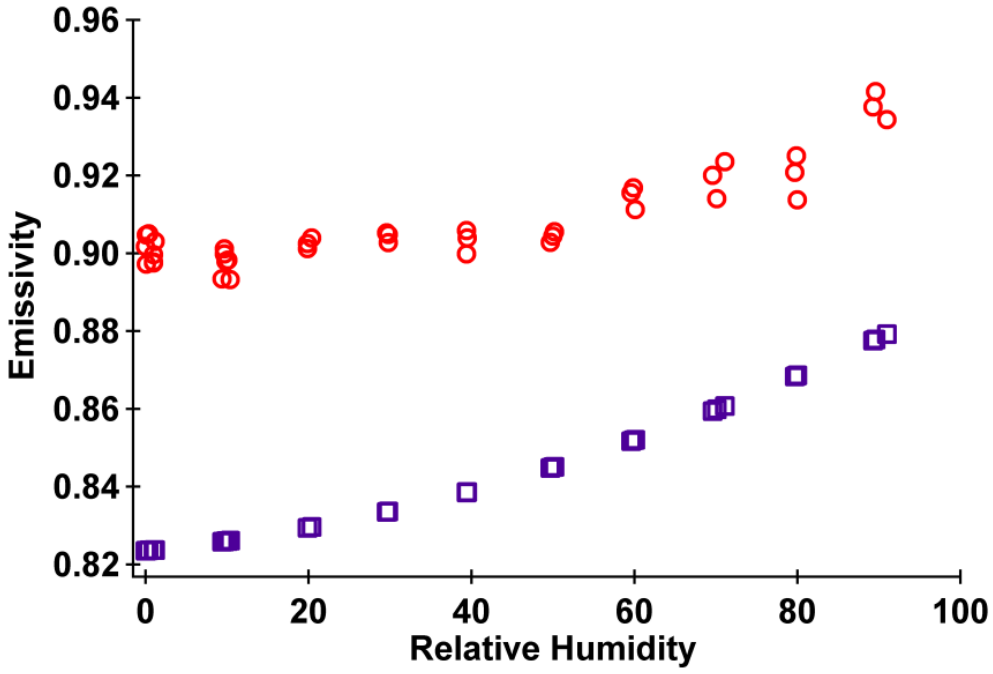

Figure 5.3. Modeled acrylic fabric emissivity vs relative humidity (squares), and calculated emissivity of the blood coated regions of the Aged acrylic fabric vs relative humidity (circles).

humidity. This decrease in the emissivity difference between the two surfaces manifests during thermal imaging as a decrease in the contrast in the apparent temperature of the two surfaces. The apparent temperature contrast in an image between the blood-coated surface and uncoated surface at 40 °C is greater at lower humidities (~1.5 °C) than at higher humidities (~0.95 °C).

At 0% RH, the difference in the emissivity of blood on the acrylic Ring sample (mean ε of 0.8756) and the acrylic Aged sample (mean ε of 0.9004) is likely because of the difference in the thickness of the coating of blood between the two samples. The increase in the emissivity of the acrylic fabric substrate between 60% and 70% RH is not reflected in the Aged sample emissivity, indicating that the thermal radiation measured by the

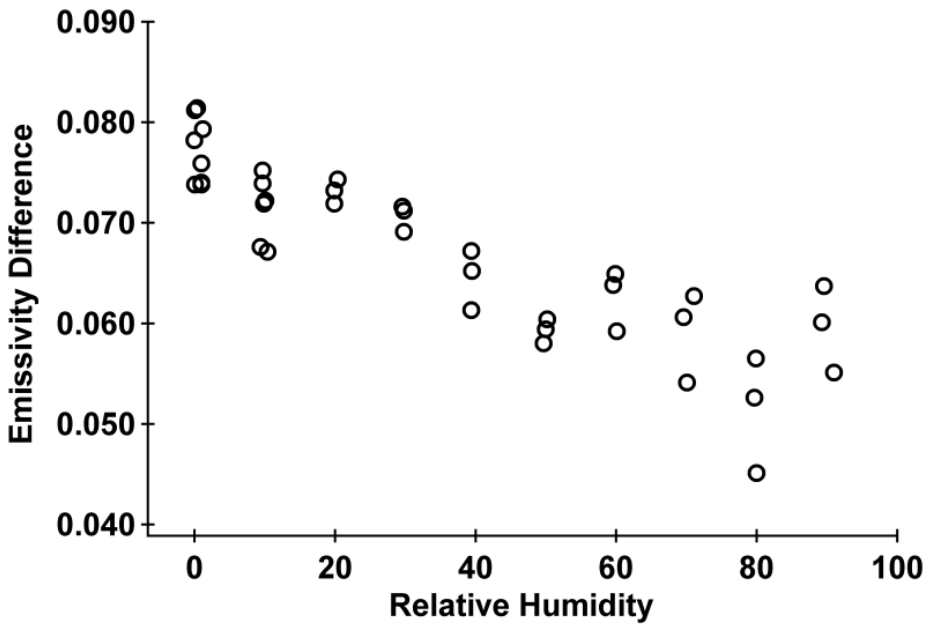

Figure 5.4. Plot of the difference in emissivity of the dried blood stain and blank acrylic 899 fabric areas of the Aged sample.

camera from the blood-coated area of the fabric is not influenced by the acrylic fabric underneath. In other words, the blood-stained areas in the Aged measurement are optically thick. The lower emissivity of the acrylic Ring sample compared to that of the Aged sample indicates that the thickness of the blood coating is not optically thick for the Ring sample, and the emission from the acrylic fabric underneath is still contributing to the observed signal intensity.

5.5 Conclusions

This work is motivated by an interest in a better understanding of the mechanisms of steam thermography. Thermal emissivities of dried blood on cotton, nylon, polyester, and acrylic fabrics at 0% RH are presented, along with measurements of the thermal emissivity of dried blood on acrylic across a range of humidities from 0% to 90% RH. This work provides evidence that the thermal emissivity of blood increases with

increasing RH, and that the change in thermal emissivity of acrylic and blood are different from one another such that the overall difference in the thermal emissivity of the two surfaces decreases with increasing RH. This provides an estimate of the contribution of the differential changes in thermal emissivity to the thermal response observed during a steam thermography measurement.

REFERENCES

1. J. M. Dust, C. M. Grieshop, C. M. Parsons, et al. Chemical composition, protein quality, palatability, and digestibility of alternate protein sources for dogs. *J. Anim. Sci.* 2005; 83: 2414-2422. https://doi.org/10.2527/2005.83102414x

2. N. Laan, F. Smith, C. Nicloux, et al. Morphology of drying blood pools. *Forensic Sci. Int.* 2016; 267: 104-109. https://doi.org/10.1016/j.forsciint.2016.08.005

3. V. Sterzik, M. Bohnert. Reconstruction of crimes by infrared photography. *Int. J. Legal. Med.* 2016; 130: 1437-1596. https://doi.org/10.1007/s00414-016-1343-2

4. J. Finnis, J. Lewis, A. Davidson. Comparison of methods for visualizing blood on dark surfaces. *Sci. Justice* 2013; 53: 178-186. http://dx.doi.org/10.1016/j.scijus.2012.09.001

5. B. Li, P. Beveridge, W. T. O'Hare, et al. The application of visible wavelength reflectance hyperspectral imaging for the detection and identification of blood stains. *Sci. Justice* 2014; 54: 432-438. http://dx.doi.org/10.1016/j.scijus.2014.05.003

6. A. Lin, H. Hsieh, L. Tsai, et al. Forensic applications of infrared imaging for the detection and recording of latent evidence. *J. Forensic Sci*. 2007; 52: 1148-1150. https://doi.org/10.1111/j.1556-4029.2007.00502.x

7. S. J. Seashols, H. D. Cross, D. L. Shrader, et al. A comparison of chemical enhancements for the detection of latent blood. *J. Forensic Sci.* 2013; 58: 130-133. https://doi.org/10.1111/j.1556-4029.2012.02259.x

8. G. E. Miranda, F. B. Prado, F. Delwing, et al. Analysis of the fluorescence of body fluids on different surfaces and times. *Sci. Justice* 2014; 54: 427-431. http://dx.doi.org/10.1016/j.scijus.2014.10.002

9. J. L. Webb, J. I. Creamer, T. I. Quickenden. A comparison of the presumptive luminol test for blood with four non-chemiluminescent forensic techniques. *Lumin.* 2006; 21: 214-220. https://doi.org/10.1002/bio.908

10. K. Virkler, I. K. Lednev. Analysis of body fluids for forensic purposes: From laboratory testing to non-destructive rapid confirmatory identification at a crime scene. *Forensic Sci. Int.* 2009; 118: 1-17. http://dx.doi.org/10.1016/j.forsciint.2009.02.013

11. W. Lalonde, J. S. Millman. Case study: Loss of Kastle-Meyer test specificity on jeans. *Sci. Justice* 2019; 59: 359-361. https://doi.org/10.1016/j.scijus.2018.12.002

12. R. G. Belliveau, S. A. DeJong, B. M. Cassidy, et al. Ridge patterns of blood-transferred simulated fingerprints observed on fabrics via steam thermography. *Forensic Chem.* 2016; 1: 74-77. https://doi.org/10.1016/j.forc.2016.07.005

13. W. L. O'Brien, N. D. Boltin, Z. Lu, et al. Chemical contrast observed in thermal images of blood-stained fabrics exposed to steam. *Analyst* 2015; 140: 6222-6225. https://doi.org/10.1039/C5AN01413A

14. R. G. Belliveau, S. A. DeJong, N. D. Boltin, et al. Mid-infrared emissivity of nylon, cotton, acrylic and polyester fabrics as a function of moisture content. *Text. Res. J.* accepted for publication, 2019.

15. B. M. Cassidy, Z. Lu, J. P. Martin, et al. A quantitative method for determining a representative detection limit of the forensic luminol test for latent bloodstains. *Forensic Sci. Int*. 2017; 278: 396-403. http://dx.doi.org/10.1016/j.forsciint.2017.06.031

16. F. Ramsthaler, J. Schlote, C. Wagner, et al. The ring phenomenon of diluted blood droplets. *Int. J. Legal Med*. 2016; 130: 731-736. http://dx.doi.org/10.1007/s00414-015-1304-1

17. T. C. DeCastro. Forensic interpretation of bloodstains on fabrics, in *Forensic Textile Science* (ed. D. Carr), Cambridge, MA: Woodhead Publishing, 2017, pp 127-167.

18. C. A. S. Hill, A. Norton, G. Newman. The water vapor sorption behavior of natural fibers. *J. Appl. Polym. Sci*. 2009; 112: 1524-1537. https://doi.org/10.1002/app.29725

19. S. J. Gregg, K. S. W. Sing. Adsorption, Surface Area and Porosity. Second ed., London, U. K.: Academic Press, 1982.

20. M. L. Myrick, M. N. Simcock, M. Baranowski, et al. The Kubelka-Munk diffuse reflectance formula revisited. *Appl. Spectrosc. Rev.* 2011; 46: 140-165. http://dx.doi.org/10.1080/05704928.2010.537004

21. M. Mira, E. Valor, R. Boluda, et al. Influence of soil water content on the thermal infrared emissivity of bare soils: Implication for land surface temperature determination. *J. Geophys. Res*. 2007; 112: 1-11. https://doi.org/10.1029/2007JF000749

22. N. Kitamura, S. Ishizaka, H. Kim. Effects of light-scattering coefficient of adsorbent in diffuse reflectance spectroscopy of dye-doped microparticles. *Anal. Sci.* 1997; 13: 791-796. https://doi.org/10.2116/analsci.13.791

23. P. Sopade. Criteria for an appropriate sorption model based on statistical analysis. *Int. J. Food Prop*. 2001; 4: 405-418. https://doi.org/10.1081/JFP-100108642

24. J. Stencl, J. Gotlhardova, P. Homola. Equilibrium moisture content of dried blood flour in the temperature range of 20 – 50 °C. *Drying Technol.* 1998; 16: 1729-1739. http://dx.doi.org/10.1080/07373939808917489

25. R. A. M. Delaney. Protein concentrates from slaughter animal blood. II. Composition and properties of spray dried red blood cell concentrates. *Int. J. Food Sci. Technol.* 1977; 12: 355-368. https://doi.org/10.1111/j.1365-2621.1977.tb00118.x

CHAPTER 6: RIDGE PATTERNS OF BLOOD-TRANSFERRED SIMULATED FINGERPRINTS OBSERVED ON FABRICS VIA STEAM THERMOGRAPHY[c]

6.1 INTRODUCTION

Several reports in the literature describe efforts to detect fingerprints and bloodstains for forensic applications via visible light fluorescence, chemiluminescent tests, alternative light sources, and infrared reflectance.[1-7] Existing methods have difficulties with patterned and colored substrates, or may contaminate the sample, or may fail to render fine detail when it is important, such as in ridge detail of a fingerprint. This laboratory recently demonstrated a new method for thermographic imaging of dried bloodstains on hydrophobic synthetic fabrics exposed to steam or water vapor.[8] The thermal contrast observed is derived mostly from differential adsorption of water with its associated enthalpy (heat) of adsorption, but there are numerous unknowns about the method. Questions arising from Reference 7 that remain unanswered include (1) whether fine detail in a bloodstain could be preserved despite wicking of the stain into the fabric, (2) whether the necessary adsorption of water would obscure any fine detail that might be preserved, and (3) whether the method could be extended to hydrophilic fabrics such as cotton.

[c] Reproduced and modified from R. G. Belliveau, S. A. DeJong, B. M. Cassidy, et al. Ridge patterns of blood-transferred simulated fingerprints observed on fabrics via steam thermography. Forensic Chem. 2016; 1: 74-77. https://doi.org/10.1016/j.forc.2016.07.005 with permission from Elsevier.

To address these questions, we utilized a new infrared camera with higher spatial and temporal resolution than the camera used in Reference 8 and other chapters, and simulated fingerprints with ridge patterns transferred using rat blood. The present report describes these experiments and provides definite answers to the first two of these questions, and insight into the third. Even in conditions where the fingerprints wick into a synthetic fabric, the ridge patterns remain visible in both the initial exposure to steam and repeated exposures, in the heat-up and in the cool-down phases of the experiment. Further, it appears that high-speed micro-imaging may offer a method for suppressing the strong background fabric response observed in cotton by visualizing individual cotton fibers at the surface where ridge patterns may be preserved.

6.2 Materials and Methods

6.2.1 Simulated fingerprint stamp

A custom rubber stamp (Smith Rubber Stamps & Seals, Columbia, SC) was made with which to transfer simulated ridge patterns to any surface of our choice, using any transfer medium compatible with the stamp materials. The stamp was designed by adapting artificial fingerprint artwork (Figure 3.6) that was purchased from shutterstock.com (Image ID: 180872426). The final stamp is 51 x 33 mm in size, which is approximately 50% larger than a natural fingerprint; the size was chosen as the minimum that allowed the rubber stamp to be commercially fabricated with preserved ridge detail. The stamp and its use are described in more detail in Chapter 3. Two transfer prints were placed on the surface of each fabric, one made with undiluted rat blood, and the other made with rat blood diluted 1:10 with water (Figure 6.1). At the time of these experiments the prints had dried and aged in air for approximately eight months.

The visible light images of the transfer prints (Figure 6.1) show that on the right edge of each transfer print, the blood did not maintain the ridge structure after it was stamped. The fused ridges were produced while transferring the blood to the fabric using the stamp, and are not a defect of the stamp itself, nor an artifact of steam thermography.

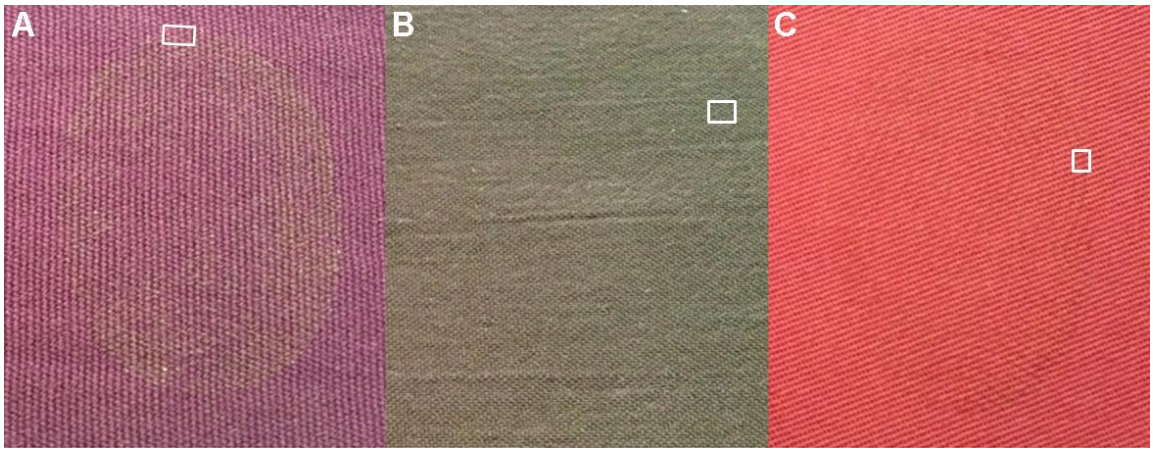

Figure 6.1. Visible light images of the whole blood transfer prints on three fabrics. A) Acrylic. B) Polyester. C) Cotton. Each fabric has two transfer prints, one in whole blood, and the other in ten-fold diluted blood (not shown) as described in the text. White boxes indicate the location of each fabric imaged by microthermography, as shown in Figure 6.3.

6.2.2 FABRICS

Three fabrics are used in this study: the purple acrylic 917 fabric, the brown polyester 905 fabric, and the red cotton 899 fabric, each of which are described in detail Chapter 1. Each fabric was commercially obtained undyed, and subsequently triple-dyed using the dyes in Table 1.1 at North Carolina State University's Wilson College of Textiles in 2004. The properties of the fabrics and the fibers they are composed of are given in the same table, along with references to spectroscopic measurements by this group using these fabrics as samples or sample substrates.

The acrylic fabric is warp-faced, meaning that it is the warp threads that form the most prominent features on the face of the fabric. The polyester fabric is a uniform plain weave, meaning the face of the fabric is composed equally of both the warp and the weft threads. The cotton fabric is a twill, and so it has two distinct faces. One of the faces has warp threads that are the most prominent, while the other is dominated by weft threads. In both cases, however, the two types of threads contribute to the exposed surface. The transfer print was placed onto the warp-dominant side of the fabric.

6.2.3 IMAGING

The samples were thermographically imaged in two ways: imaging an entire print at once using a 50 mm lens, and imaging a single ridge magnified by a 13 mm lens placed backwards from the standard configuration to act as an extreme macro-type lens for microscopic imaging. Both lenses have an *f*/# of *f*/2.5, and a numerical aperture of 0.20. Both data sets were acquired using a FLIR Systems A6751sc SLS thermal imaging camera, using the settings in Table 6.1. The camera was operated using FLIR Systems ResearchIR software.

Table 6.1. Camera settings for the macroscopic imaging of full prints and the microscopic imaging of print areas using the FLIR Systems A6751sc SLS thermal imaging camera.

Settings	Full Print	Magnified Print
Framerate	**30 Hz**	**120 Hz**
Lens	**50 mm**	**13 mm**
Window Resolution	**320x256**	**640x512**
Integration Time	**480 ns**	**480 ns**

Steam was generated as described previously using a hand-held garment steamer.[8] Recordings began prior to the exposure of a fabric to moisture. Steam was directed

toward the fabric from a distance of about 1 foot for approximately 3 seconds, and then the source was removed to allow the adsorbed moisture to begin evaporating. This process was repeated until the end of each recording. Each recording thus begins with the fabric at equilibrium followed by moderately rapid cycles (periods in the range of ~10 seconds) of adsorption and desorption.

6.3 Results and Discussion

Steam thermography images of the undiluted ridge patterns on acrylic, polyester, and

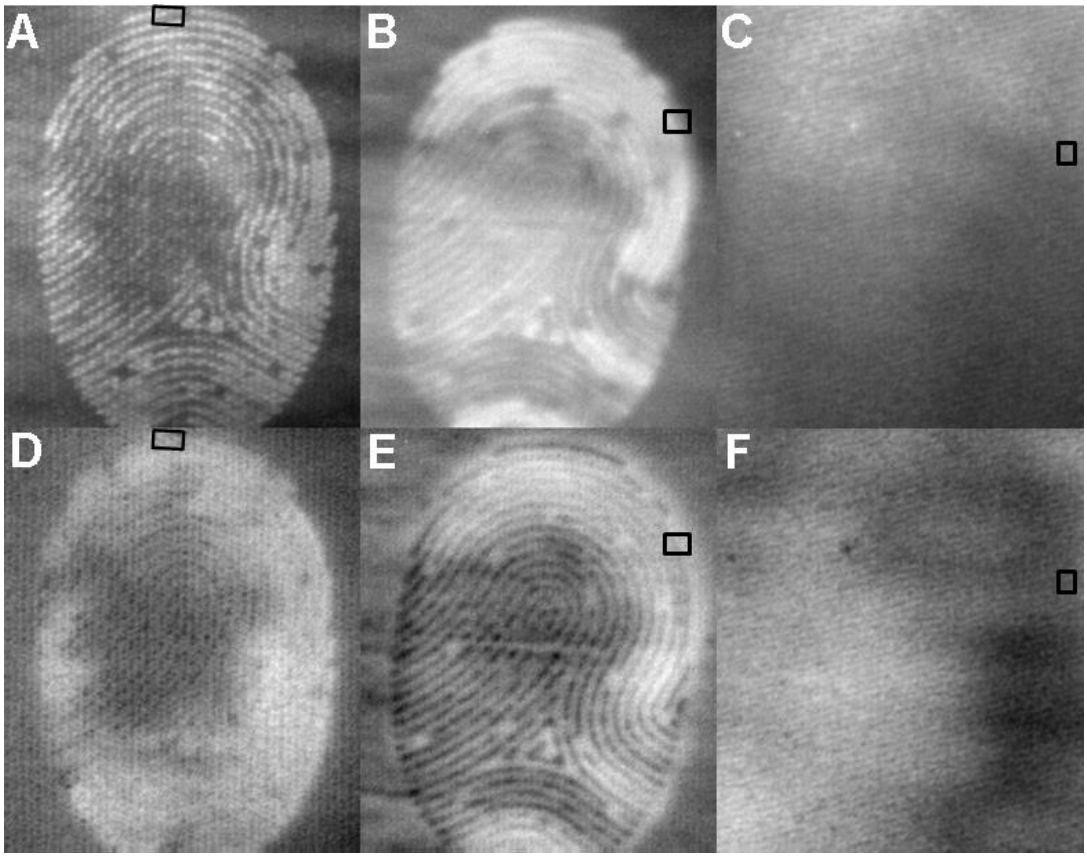

Figure 6.2. Individual frames from 30 s recordings of dried blood transferred prints on the acrylic 917 (A and D), polyester 905 (B and E), and cotton 899 (C and F) fabrics. Black boxes indicate the location of each fabric imaged by microthermography, as shown in Figure 6.3. Details of these images are found in the text.

cotton are shown in Figures 6.2A-6.2F. The images in the figure are extracted from individual frames taken from 30 second recordings at 30 frames per second. Figures 6.2A-6.2C were recorded during a 3 s exposure to water vapor, while frames 6.2D-6.2F were recorded approximately 2 s after the end of the water vapor exposure, during the evaporative cycle. The whole blood patterns on acrylic and polyester "leap out" for the observer immediately on exposure to steam with enough contrast to easily distinguish individual ridges in the transfer print on both fabrics. During the process of the vapor evaporating from the surfaces, the prints cool and again individual ridges of each transfer print are distinguishable, but as darker than the fabric. Prints on cotton however, are not readily observable.

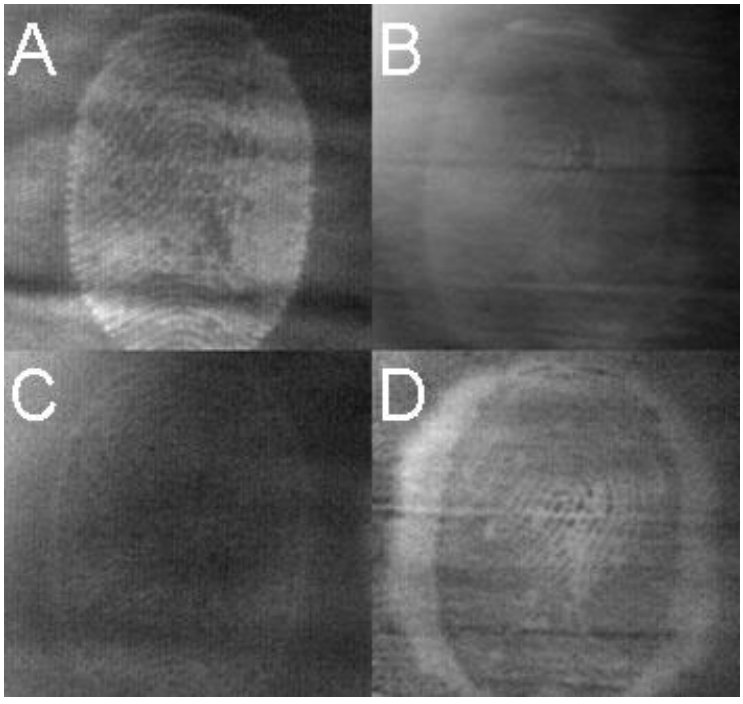

Figure 6.3. Individual frames from 30 s recordings of transfer prints made using 10X diluted blood on the acrylic 917 (A and C) and polyester 905 (B and D) fabrics. The top row shows the transfer prints during exposure to water vapor, and the bottom row shows the transfer prints approximately 2 s after the end of the water vapor exposure during the evaporative cool-down cycle.

Patterns made with blood diluted ten-fold with water, shown in Figures 6.3A-6.3D, were also easily visualized on acrylic and polyester, but not on cotton, with the caveat that on polyester these lower-concentration prints showed a "halo" similar to that reported previously.[8] Despite this effect, the ridge pattern remains clear on two of the three fabrics. We attribute the halo effect observed on polyester to separation of components of the blood when the diluted solution wicks into the fabric. If this is the correct interpretation, at least some blood components that are important to steam thermography observation must remain at the site of initial deposition and resist transport.

A novel observation with the new thermal imaging camera used for this study was made possible by micro-thermographic imaging. Adult fingerprint ridges are approximately 500 µm in breadth.[9] Under the conditions of the measurement of the full prints, the camera has a spatial resolution on the order of 200 µm, which allows the ridges themselves to be distinguished. Accordingly, the images of Figure 6.2 are suitable to show that any preserved ridge-level detail on a fabric is retained in steam thermography. However, the microstructure of the ridge patterns on fabrics is not readily observable in Figure 6.2 or Figure 6.3 for any of the fabrics. By reversing a lens and using the camera in a close-up mode, we were able to produce images showing an area on the fabric that is approximately 3 mm across with a spatial resolution of approximately 5 µm, enough to easily observe fibers and features within a ridge. Figure 6.4 shows these magnified images aligned to match the orientation of the same regions in Figures 6.1 and 6.2. Small boxes drawn in Figures 6.1 and 6.2 for reference show where the magnified

images in Figure 6.4 were acquired. A higher frame rate of 120 frames per second enabled improved temporal resolution at the same time.

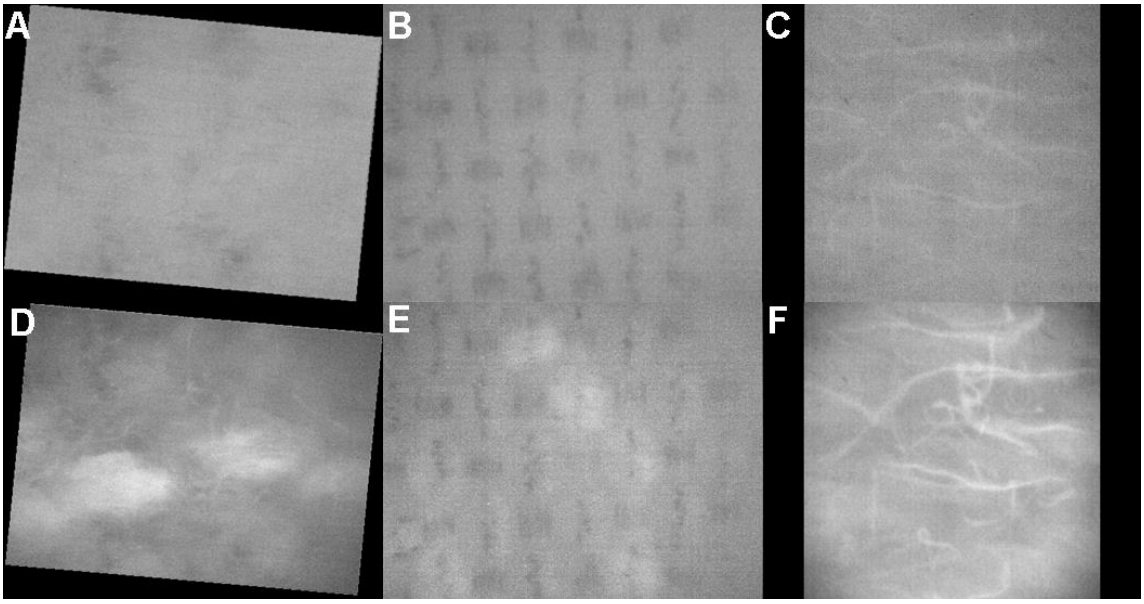

Figure 6.4. Microthermographic images of blood transfer print ridge patterns on the acrylic 917 (A and D), polyester 905 (B and E), and cotton 899 (C and F) fabrics. Each image shows an area of approx. 3 mm. Top row images show fabrics prior to water vapor exposure. Bottom row images show the same areas of each fabric during exposure to water vapor. Images are rotated to the same orientation as the transfer prints in Figures 6.1 and 6.2.

Figure 6.4 shows detail of print ridges on acrylic, polyester and cotton. One problem that is observed in steam thermography is the difficulty of producing an even exposure to moisture. Micro-scale steam thermography, as shown in Figure 6.4, effectively eliminates this problem because the spatial distribution of steam/vapor is uniform on a very small spatial scale.

On acrylic, the print ridge is readily observable on exposure to steam. Literature studies of transfer prints show that the transfer is not even across a woven fabric, but occurs mainly on the top of the weave.[10-12] This phenomenon results in periodic breaks in

the print ridge that are not obvious in the images of Figure 6.2. One of these breaks is visible in the center of the ridge in Figure 6.4D. The break corresponds to a depression in the warp of the fabric due to the presence of a weft thread, which is not visible.

In comparison, the whole blood print ridge on polyester showed less contrast during steam microthermography, possibly due to the same leaching of soluble blood solids into the fabric that results in the "halo" effect. Similar to acrylic, though, it is the raised portions of the fabric weave that preserve evidence of the print ridges (Figure 6.4E). Because of the uniform nature of this fabric, the transfer print appears on both the warp and weft threads.

Figures 6.4C and 6.4F show the most intriguing microthermographic imaging in this study. Cotton, as reported previously and also shown in Figures 6.2C and 6.2F, is a difficult subject fabric for steam thermography due to the hydrophilic nature of cotton itself. While most synthetic fabrics like acrylic and polyester do not adsorb water vapor strongly, dry blood can adsorb around 8% of its weight in water vapor at 50% humidity.[13] Literature studies show that the amount of moisture that cotton can adsorb per gram at any given level of humidity is of the same order as can be adsorbed by blood solids.[14] The enthalpy (heat) of water adsorption is also likely to be of the same order for cotton and blood solids. The images shown in Figure 6.4 suggest an approach to visualizing blood on cotton via fast microthermographic imaging.

The most prominent points on the face of the cotton fabric used for the blood transfer print are warp threads. In Figures 6.2C and 6.2F, the blood transfer print is very faint, so

we did not expect to observe ridge pattern detail on the microthermography analysis. However, some ridge pattern detail was observed.

In the magnified images of cotton (Figure 6.4C and 6.4F), individual threads that are protruding from the bulk of the fabric are visible in the region of a print ridge. These threads are approximately 250 µm wide. The contrast between the protruding fibers in the region of a print ridge is visible only for a very short time, approximately 30 ms in these recordings. Our interpretation is that the protruding loose fibers are the first to be exposed when water vapor is directed at the fabric, and the response is stronger for a coated loose fiber than an uncoated loose fiber. This may not be a result of a stronger adsorption of water per unit mass, but indirectly as a result of the increased thermal mass of a coated fiber compared to a clean fiber. Whatever the origin, the ephemeral nature of the observation is due to the fact that when the bulk of the cotton fabric behind the loose fibers begins adsorbing moisture, the details are lost in the very large response of the bulk of the fabric. This is the first, albeit tentative, evidence that there is a thermal signature for a hydrophilic deposit on cotton, and suggests that further work is needed in this area.

6.4 Conclusions

This work illustrates that fine detail can be resolved via steam thermography of blood stains on some fabrics. Ridge detail in blood transfers can be resolved in at least some cases. These results also suggest a possible method for detecting transferred material on cotton despite its strong inherent response to moisture, based on observations of isolated cotton fibers occurring as a natural feature of the fabric.

REFERENCES

1. K. Virkler, I. K. Lednev. Analysis of body fluids for forensic purposes: from laboratory testing to non-destructive rapid confirmatory identification at a crime scene. *For. Sci. Int.* 2009; 188: 1-17.
2. K. Song, P. Huang, C. Yi, et al. Photoacoustic and colorimetric visualization of latent fingerprints. *ACS Nano*. 2015; 9(12): 12344-12348.
3. G. Kwak, W. Lee, W. Kim, et al. Fluorescence imaging of latent fingerprints on conjugated polymer films with large fractional free volume. *Chem. Commun.* 2009; 2112-2114.
4. T. Chen, Z.D. Schultz, I.W. Levin. Infrared spectroscopic imaging of latent fingerprints and associated forensic evidence. *Analyst* 2009; 134: 1902-1904.
5. X. Jin, L. Dong, X. Di, et al. NIR luminescence for the detection of latent fingerprints based on ESIPT and AIE processes. *RSC Adv*. 2015; 5: 87306-87310.
6. L. van der Mee, E.S.Y. Chow, L.C.P.M. de Smet, et al. Fluorescent polyelectrolyte for the visualization of fingermarks. *Anal. Methods* 2015; 7: 10121-10124.
7. V. Sterzik, M. Bohnert. Reconstruction of crimes by infrared photography. *Int. J. Legal. Med.* 2016; 1437-1596.
8. W.L. O'Brien, N.D. Boltin, Z. Lu, et al. Chemical contrast observed in thermal images of blood-stained fabrics exposed to steam. *Analyst* 2015; 140: 6222-6225.

9. M. Kralik, V. Novotny. Epidermal ridge breadth: an indicator of age and sex in paleodermatoglyphics. *Variability and Evolution* 2003; 11: 5-30.
10. M. Holbrook. Evaluation of blood deposition on fabric: distinguishing spatter and transfer stains. *IABPA News* 2010; 26: 3-12.
11. J. A. Slemko. Bloodstains on fabric: the effects of droplet velocity and fabric composition. *IABPA News* 2003; 19: 3-11.
12. Y. Cho, F. Springer, F.A. Tulleners, et al. Quantitative bloodstain analysis: differentiation of contact transfer patterns versus spatter patterns on fabric via microscopic inspection. *Forensic Sci. Int*.2015; 249: 233-240.
13. J. Stencl, J. Gotlhardova, P. Homola. Equilibrium moisture content of dried blood flour in the temperature range of 20-50 °C. *Drying Technology*. 1998; 16: 1729-1739.
14. C.A.S. Hill, A. Norton, G. Newman. The water vapor sorption behavior of natural fibers. *J. Appl. Polym. Sci*. 2009; 112: 1524-1537.

APPENDIX A: MATLAB CODE USED TO PROCESS THERMOGRAPHIC MEASUREMENTS

Appendix A records code used to process thermographic measurements. Each section is a function or script which is commented to provide the information needed to use the code.

A.1. BINARYMOVIE

```
function [data_final,filename,pathname]=binarymovie
%This function reads binary data into matlab. This function is designed to be used
%when recording the steaming operation. Copied from HB's function / Updated by
%OBrien (1/20/13) / Updated by RGBelliveau (10/8/14)
        [filename,pathname] = uigetfile('*.bin');
        fullname = strcat(pathname,filename);
        fid=fopen(fullname,'r','b');
        introdat=(fread(fid,[200,1],'uint16'));
        fseek(fid,0,'eof');
        n=(ftell(fid))/(2*240*320);%n= the total number of frames.

% This code builds the 3D data array of images.
        fseek(fid,0,'bof'); % Ray - I changed this from (fid,200,'bof') to 0 because we
        %have no header in the current recordings. (Wayne - There are 200 bits of
        %"junk" data that we skip.)
        data=zeros(240, 320, n,'uint16'); % Preallocate for speed
        for i=1:n
           data(:,:,i)=rot90((fread(fid,[240,320],'uint16')),3)';
        end
        fclose('all');
        data_final = double(data);%Ray - I changed this from flipping the image
        %(flipdim, X, 2) to not flipping it. Conversion to Double type of data
```

A.2. MOVIEPLAYER

```
function MoviePlayer(I,pausetime)
```

```
%By Raymond Belliveau, Aug 2014. Reads in an array, and displays each x,y
%matrix as a single movie frame. The number of frames is the length of the 3rd
%dimension of the array. I is the 3d array to be played. Pausetime is the time between
%frames, it is optional.

        Pcheck=exist('pausetime','var');

        if Pcheck==0
           pausetime=0.01;
        end

%Build the display window and style it.
        figure, set(gcf, 'Color','white');

%Plays through the 3rd dimension at a rate determined by the pause  function.
        for i=1:length(I);
           II=rot90(I(:,:,i));
           pcolor(II);shading interp; colormap(gray);
           title(num2str(i));
           drawnow;
           pause(pausetime);
        end;
```

A.3. AVIEXPORTER

```
%Raymond Belliveau, March 2015.
%This makes an avi file from a data array. The file is saved into the active MATLAB
%directory.

function AviExporter(I,framerate)
%Name the array:
        n=input('What is this movie called?','s');

%Create figure
        figure, set(gcf, 'Color','white')
        set(gca, 'nextplot','replacechildren', 'Visible','off');

%Create AVI object
        nFrames = size(I,3);
        vidObj = VideoWriter(n);
        vidObj.Quality = 100;
        vidObj.FrameRate = framerate;
        open(vidObj);
```

```
%Create movie
        for k=1:nFrames;
          pcolor(I(:,:,k)),shading interp,colormap(gray);
          writeVideo(vidObj, getframe(gca));
        end
        close(gcf)

%Save as AVI file, and open it using the default system video player
        close(vidObj);
        winopen(vidObj.Filename)
```

A.4. SensorData

```
%Sensor Data Import and Selection.
%Emissivity measurements recorded temperature and humidity from two sensors into
%a text file during thermal imaging.
%This code pulls data from the tab-deliminated text file, separates it into temperature
%and humidity readings from the sensor, and smooths the data.

function [S1Temperature,S2Temperature,S1RH,S2RH]=SensorData

        [filename,pathname] = uigetfile('*.txt');
        fullname = strcat(pathname,filename);
        sdata=tdfread(fullname);
        ssdata=struct2cell(sdata);
        S1Tr=ssdata{2,:};
        S1RHr=ssdata{4,:};
        S2Tr=ssdata{6,:};
        S2RHr=ssdata{8,:};

%Smooths the sensor data with a Savitzky-Golay filter with a window size of one
%second.

        S1Temperature=sgolayfilt(S1Tr,1,11);
        S2Temperature=sgolayfilt(S2Tr,1,11);
        S1RH=sgolayfilt(S1RHr,1,11);
        S2RH=sgolayfilt(S2RHr,1,11);
```

A.5. VChamberWorkup

```
%This code is used to process all of the recordings from the solvent study at once. It
%requires all of the .bin files to be placed in folder for each solvent (e.g. the folder
%'Water' contains both adsorption and desorption files of the recordings of the water
```

```
%experiments. All of the solvent folders should be placed into a folder which is
%named according to the 'foldername' variable.

function [DataResults]=VChamberWorkup

        foldername='VacuumWork\Array';

        dirr='C:\Users\scott\Documents\RGBelliveau\Data';
        selectiondir=strcat(dirr,'\',foldername);
        foldercheck=exist(selectiondir,'dir');
        if foldercheck==0
           mkdir(dirr,foldername);
        end

        olddir=cd(selectiondir);
        list=dir;

        j=1;
        for i=1:size(list,1)
           if strcmp(list(i,1).name,'.')==0
              if strcmp(list(i,1).name,'..')==0
                 foldernames{j,1}=list(i,1).name;
                 j=j+1;
              end
           end
        end

        path=selectiondir;

        for i=1:length(foldernames)
          L{i}=strcat(path,'\',foldernames{i});
        end

    %Get all filenames.

        for k=1:length(L)
           updir=cd(L{k});
           list=dir;
           j=1;
           for i=1:size(list,1)
              if strcmp(list(i,1).name,'.')==0
                 if strcmp(list(i,1).name,'..')==0
                    filenames{j,k}=list(i,1).name;
                    j=j+1;
                 end
              end
```

```
    end
    cd(updir);
    clearvars -except L olddir filenames
end

y=1;
for i=1:length(L)
    for j=1:size(filenames,1)
        PathList{y}=strcat(L{i},'\',filenames{j,i});
        y=y+1;
    end
end

x=1;
for k=1:length(PathList)

    I=LoadBinMovie(PathList{k});

    PNeat=squeeze(mean(mean(I(171:179,107:113,:))));
    P10X=squeeze(mean(mean(I(115:124,100:109,:))));
    PBlank=squeeze(mean(mean(I(62:71,50:55,:))));
    ANeat=squeeze(mean(mean(I(61:70,98:107,:))));
    A10X=squeeze(mean(mean(I(227:239,45:59,:))));
    ABlank=squeeze(mean(mean(I(116:125,155:165,:))));
    NNeat=squeeze(mean(mean(I(112:121,44:52,:))));
    N10X=squeeze(mean(mean(I(171:186,155:167,:))));
    NBlank=squeeze(mean(mean(I(223:235,104:112,:))));
    CNeat=squeeze(mean(mean(I(226:235,160:167,:))));
    C10X=squeeze(mean(mean(I(69:73,158:159,:))));
    CBlank=squeeze(mean(mean(I(170:179,44:51,:))));


P={PNeat,P10X,PBlank;ANeat,A10X,ABlank;NNeat,N10X,NBlank;CNeat,C
10X,CBlank};
Names={'Polyester','Acrylic','Nylon','Cotton'};


    for j=1:size(P,2);
        for i=1:size(P,1);
            T=(P{i,j});
            Early=mean(T(1:200));
            Later=mean(T(1000:1500));
            Delta(i,j)=Later-Early;
        end
    end
```

```
    y=1;
    for i=1:size(Delta,1)
        for j=1:size(Delta,2)
            Delta2(y)=Delta(i,j);
            y=y+1;
        end
    end

    DataResults{x,1}=PathList{1,k}(70:end);
    DataResults{x,2}=Delta2;
    DataResults{x,3}=P;
    x=x+1;
    clearvars -except filenames PathList DataResults x olddir k
end

%Return directory to where it was before running this.
cd(olddir);
```

A.6. Cotton Silanization Analysis Script

This script was used to extract signal intensity values for calculations in the cotton silanization study.

```
I=binarymovie; %Load in the pre-silanization measurement.
PreImg=I(:,:,450);
PreBlood=I(123:129,167:172,:);
PreFabric=I(123:129,180:184,:);

I=binarymovie; %Load in the post-silanization measurement.
PostBlood=I(122:129,159:165,:);
PostFabric=I(122:129,171:176,:);
PostImg=I(:,:,300);

PreB=squeeze(mean(mean(PreBlood)));
PostB=squeeze(mean(mean(PostBlood)));
PostF=squeeze(mean(mean(PostFabric)));
PreF=squeeze(mean(mean(PreFabric)));

EarlyPreB=mean(PreB(1:200));
EarlyPostB=mean(PostB(1:200));
ZeroedPreB=PreB-EarlyPreB; %Thermal response
ZeroedPostB=PostB-EarlyPostB; %Thermal response

EarlyPreF=mean(PreF(1:200));
EarlyPostF=mean(PostF(1:200));
```

```
ZeroedPreF=PreF-EarlyPreF; %Thermal response
ZeroedPostF=PostF-EarlyPostF; %Thermal response

PreDiff=ZeroedPreB-ZeroedPreF; %Contrast values
PostDiff=ZeroedPostB-ZeroedPostF; %Contrast values
```

APPENDIX B: PERMISSION TO REPRINT

The following is the re-use policy for Sage Publishing. This policy applies to Chapter 4.

Green Open Access: SAGE's Archiving and Sharing Policy

You may share the **Original Submission** or **Accepted Manuscript** at any time and in any format. Your sharing of the **Original Submission** or **Accepted Manuscript** may include posting a downloadable copy on any website, saving a copy in any repository or network, sharing a copy through any social media channel, and distributing print or electronic copies.

For information on use of Institutional Repository (IR) copies by authors and IR users, see Posting to an Institutional Repository - Green Open Access.

You may use the **Final Published PDF** (or **Original Submission** or **Accepted Manuscript**, if preferred) in the following ways:

- in relation to your own teaching, provided that any electronic distribution maintains restricted access
- to share on an individual basis with research colleagues, provided that such sharing is not for commercial purposes
- in your dissertation or thesis, including where the dissertation or thesis will be posted in any electronic Institutional Repository or database
- in a book authored or edited by you, at any time after the Contribution's publication in the journal.

The following is the re-use policy for Elsevier. This policy applies to Chapters 5 and 6.

Personal use

Authors can use their articles, in full or in part, for a wide range of scholarly, non-commercial purposes as outlined below:

- Use by an author in the author's classroom teaching (including distribution of copies, paper or electronic)
- Distribution of copies (including through e-mail) to known research colleagues for their personal use (but not for Commercial Use)
- Inclusion in a thesis or dissertation (provided that this is not to be published commercially)
- Use in a subsequent compilation of the author's works
- Extending the Article to book-length form
- Preparation of other derivative works (but not for Commercial Use)
- Otherwise using or re-using portions or excerpts in other works

These rights apply for all Elsevier authors who publish their article as either a subscription article or an open access article. In all cases we require that all Elsevier authors always include a full acknowledgement and, if appropriate, a link to the final published version hosted on Science Direct.